MODEL FOR QUANTIFICATION AND ANALYSIS OF PULMONARY EMPHYSEMA FROM LOW-DOSE RADIATION CT SCANS

by

SIMINA C. FLUTURE

A dissertation submitted to the Faculty in Computer Science
in partial fulfillment of the requirements for the degree of
Doctor of Philosophy, the City University of New York

2004

INFORMATION TO USERS

The quality of this reproduction is dependent upon the quality of the copy submitted. Broken or indistinct print, colored or poor quality illustrations and photographs, print bleed-through, substandard margins, and improper alignment can adversely affect reproduction.

In the unlikely event that the author did not send a complete manuscript and there are missing pages, these will be noted. Also, if unauthorized copyright material had to be removed, a note will indicate the deletion.

ProQuest Information and Learning Company
300 North Zeeb Road
P.O. Box 1346
Ann Arbor, MI 48106-1346

This manuscript has been read and accepted for the Graduate Faculty in Computer Science in satisfaction of the dissertation requirement for the degree of Doctor of Philosophy.

8/13/2004
Date

Dr. Christina M.D. Zaroliagis
Chair of Examining Committee

8/24/04
Date

Executive Officer

Dr. Gabor Herman, Distinguished Professor

Dr. Ioannis Stamos, Assistant Professor

Dr. David Yankelevitz, MD, Professor

Supervisory Committee

THE CITY UNIVERSITY OF NEW YORK

ABSTRACT

MODEL FOR QUANTIFICATION AND ANALYSYS OF PULMONARY EMPHYSEMA FROM LOW-DOSE RADIATION CT SCANS

by
Simina C. Fluture

Adviser: Dr. Christina M. D. Zamfirescu, Professor

This thesis presents techniques for the automated analysis of low-dose helical CT scans used in the detection of pulmonary emphysema. Our work focused on solving the following problems:

- Determine if existing quantification methods can be successfully used in the detection and quantification of pulmonary emphysema from helical low-radiation CT scans.
- Develop better models for quantifying emphysema based on additional spatial and densitometric information.

The primary contributions of this work are:

The development of an automated *segmentation algorithm* for low-dose lung CT scans. The algorithm is modular, allowing for the removal of surrounding body tissue, vessels, and airways.

The development of the *sliding window method* for quantifying emphysema.

The development of a *graphical display method* of the emphysema index based on slice location. The graphical display will allow radiologists to not only quantify emphysema for the entire lung, but also to understand what regions of the lung are most affected by the disease.

The development of the *spatial adaptive filtering* method necessary for later quantification of pulmonary emphysema. The adaptive filtering method is customized to the noise characteristics present in low-dose chest CT scans.

The development of more accurate *metrics* capable of better quantifying the severity of emphysema.

The development of *metrics* capable of classifying different types of pulmonary emphysema.

ACKNOWLEDGEMENT

To the people who supported and had faith in me along this challenging and exciting road.

TABLE OF CONTENTS

LIST OF TABLES

LIST OF ILLUSTRATIONS

1 RESEARCH SUMMARY AND OVERVIEW

1.1 Motivation

We begin life with a breath and the process continues automatically without a voluntary thought process. It's only when we can't take a deep breath, as in the case of pulmonary emphysema disease, or cannot catch our breath at all without effort, that we become aware of how precious easy breathing really is.

Pulmonary Emphysema is part of a group of lung diseases, referred to as chronic obstructive pulmonary disease (COPD). Nearly three million Americans over the age of 18 have been diagnosed with pulmonary emphysema.

Emphysema is a degenerative disease that creates irreversible lung damage. As a result, the lungs lose their elasticity, and exhaling becomes difficult. The damaged lungs trap air and cannot effectively exchange it for fresh air. As the damage progresses, the effort needed to breathe increases and, ultimately, each breath becomes labored.

There is currently no cure for pulmonary emphysema. It is crucial to identify the disease as early as possible. Methods are being developed continuously to aid physicians in the signs of emphysema at the earliest moment so that preventive and therapeutic measures can be instituted.

The ever growing popularity of screening for lung cancer nowadays, coupled with information (i.e. direct visualization of lungs for emphysema combined with "computer aided volumetric assessment of emphysema"), not only provides a much needed and accurate assessment of the degree of emphysema, but also aids charting the progress and stability of emphysema at regular intervals on CT scans. Radiologists currently can only provide a rough assessment of the severity of emphysema; this is obviously plagued by reader variability and the inability to identify slight changes over time.

Development of volumetric assessment of the lungs is set to change this by making information from CT scans much more useful and accurate. This should enable doctors to tailor the treatment for individual patients. It is likely that it will even reduce the need for further tests to quantify and calculate the progress of emphysema over time; this, in turn, increases the overall cost-effectiveness of using CT scan emphysema detection as well.

1.2 Research

The review of literature given in chapter three describes, in order of computational complexity, different methods currently available in detection and quantification of pulmonary emphysema. The first are automated densitometry methods, which are mainly based on the computation of the percent of low attenuation pixels. These methods proved to be a significant tool in assessing the severity of emphysema. More advanced techniques, based on evolutionary programming or texture analysis, were successful in detecting the disease but not capable of quantifying it.

The reviewed research has one thing in common – all has been done on standard-dose radiation CT scan images. One of the main reasons is that these images are clearer, having far less noise than low-dose radiation CT scans. A lower dose of radiation, however, has always been more beneficial to the patient's health.

The proceeding chapters of the dissertation will describe in detail my work in studying detecting and quantifying pulmonary emphysema using low-dosage CT scan images.

A large database of low-dose radiation (screening) CT scan sets was already available. These images have been collected as part of the ELCAP (Early Lung Cancer Action Program) program at Cornell University's Weill Medical

Center. Studying these cases without additional involvement from patients keeps the research cost low.

Chapter four discusses the techniques involved in the data acquisition process.

Low radiation scans have a high degree of noise. A lung segmentation algorithm had to be developed to counter this special situation. Chapter five gives a detailed description of a modular lung-structure segmentation algorithm for screening CT scans. The algorithm is fully automated and consists of three main steps: segmentation of the lung components, lung segmentation with vessels removal, and lung segmentation with vessels and airway removal.

The remaining chapters describe new methods for quantifying emphysema. Most of the research papers in the study of emphysema use the pixel index[32] as the only significant quantifying parameter. Blechschmidt, et al[7], goes one step further in using the size of emphysematous bullae as criteria in differentiating pulmonary emphysema and pulmonary fibrosis.

We believe that there is much more information about emphysema that can be extracted and analyzed from CT scans. The purpose of our work, described in this paper, is to create a model of emphysema based on additional information given by its spatial and densitometric distribution. The model will allow new methods of emphysema quantification.

As shown in table 1.1, different types of emphysema are situated differently within the lung due to different causes. Information about the spatial distribution,

therefore, is important for emphysema evaluation. Adequate quantification of emphysema could assist others in their research of the disease and the development of specialized cures by the medical community.

Emphysema Type	Spatial Distribution	Associated Cond.
Panlobular	Uniform and diffuse in distribution Predominant in lower lobes	α_1-antitrypsin deficiency
Centrilobular	In the central part of the parenchyma lobule. Usually in upper lung zones.	Smoking
Irregular	Adjacent to localized parenchymal scars.	Pulmonary Fibrosis
Paraseptal	Striking appearance. Subpleural location	Misc. factors

Table 1.1: Types of emphysema and their attributes.

In its final stages, we feel that our software will add accuracy and speed to the currently inexact science of emphysema diagnosis. Its use will assist in bringing comfort to those who are sick by aiding in early detection. Even if one patient can breathe easily again as a result of our work, this research is worth the time and effort.

2 INTRODUCTION

The following chapter provides the necessary foundation for understanding the technology and computer vision methods used in studying pulmonary diseases from CT scan images.

2.1 Computer Vision

2.1.1 What is Computer Vision?

Computer vision represents an exciting and dynamic field of computer science. The goal of computer vision is to create a model of the real world by electronically perceiving and understanding images. The emphasis is on recovering information for the model automatically, with minimal human intervention.

Images are usually two-dimensional (2D) but they can also be three or higher dimensional in nature, and they are acquired by various image sensors (such as TV cameras, ultrasound systems, and computed tomography systems).

Two levels of image processing methods are usually considered: low-level and high level. While high-level methods are heavily based on knowledge, low-

level methods depend on little knowledge regarding the content of the images. Low-level methods include image compression, image sharpening, edge extraction, and pre-processing methods for noise filtering. Output of low-level processing might represent input for high-level processing.

High-level vision begins with a formal model of the application domain. The perceived "reality," in the form of digitized images, is then compared to the model. High-level processing constantly extracts new information from the images and updates the knowledge regarding the content – for example: object size, shape, and texture. There is a continuous feedback from high-level processing to low-level processing.

Figures 2.1 and 2.2 illustrate different representations of the same subject, depending on the type of the information provided. Figure 2.2 shows the relationship between pixel count (y-axis) and intensity (x-axis) of the image.

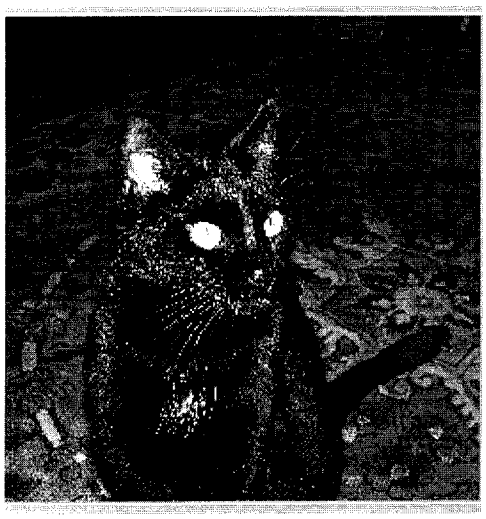

Figure 2.1: Photo of a cat.

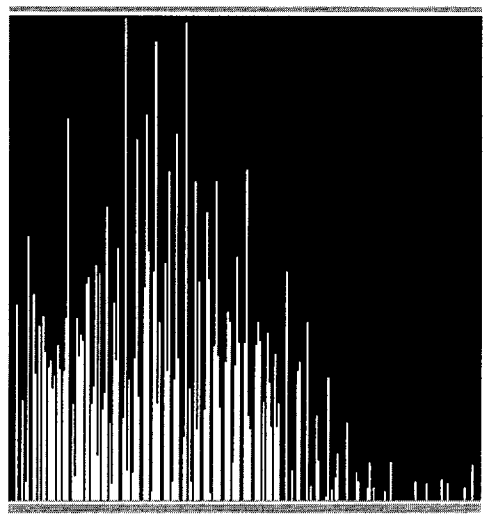

Figure 2.2: Intensity histogram of Figure 2.1

2.1.2 Relationships with Other Scientific Fields

The field of computer vision is closely related to other fields in computer science (see figure 2.3), such as:

- **Image Processing** transforms images into other images.
- **Computer Graphics** generates images from geometric primitives and free-form surfaces. Computer graphics is the synthesis of images, as compared to machine (computer) vision, which is the analysis of images.

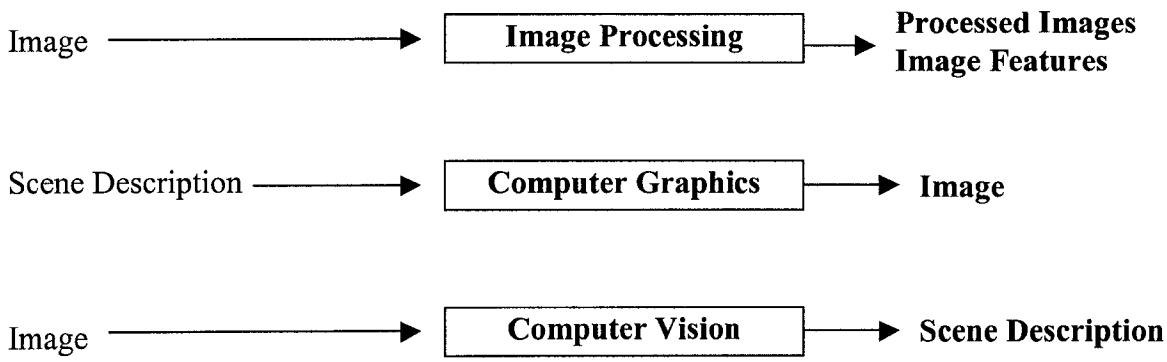

Figure 2.3: Various relationships between computer science and computer vision.

Computer vision also employs techniques from the following areas:

- **Pattern Recognition** classifies numerical and symbolic data.
- **Artificial Intelligence** is concerned with designing systems that are intelligent and with studying computational aspects of intelligence.[30]
- **Neural Networks** are increasingly used to solve some machine vision problems.

- **Psychophysics** prepares computational models of human vision rather than designing machine vision systems.

2.1.3 Computer Vision's Applied Areas

Beside its important applications in the medical imaging field, machine vision also has applications in:

- remote sensing
- industrial inspection
- document processing
- multimedia databases
- robotics
- automobile navigation
- weather forecasting
- photometry
- colorimetry
- 3D modeling

The remaining sections in this introductory chapter dive further into a particular field of machine vision – medical imaging. We will provide some background information concerning pulmonary emphysema, the targeted medical condition of this thesis, and computed tomography (CT), the general process of

creating cross-sectional or tomographic images from projections (line integrals) of the object at multiple angles.

2.2 Medical Imaging

Medical imaging has been heavily influenced by computer vision. Medical imaging is defined as the action or process of producing an image, especially by means other than visible light, of various features of the human body to assist in medical diagnosis.

The progress of medical imaging has been amazing in recent decades. Technical challenges are consistently overcome by more powerful computational techniques.

The role of medical imaging goes beyond just the visualization and inspection of anatomic structures. Medical imaging represents a tool for surgical planning, radiotherapy planning, and tracking the progress of a disease. Medical imaging is also necessary in the diagnosis and treatment of many diseases.

2.2.1 Specific Applications of Computer Vision in Medical Imaging

Many aspects of image generation through different modalities (such as CT, MRI, and Nuclear Medicine) are based on computer vision tools. The following applications in medical imaging rely on computer vision algorithms for image segmentation and (2D or 3D) visualization:

- Noninvasive exploration of body cavities.
- Location, size, and shape of abnormal structures such as lesions and masses can be accurately visualized.
- Reconstruction of the skull surface, and cortical brain surface (via MRIs).
- Understanding neuron physiology and obtaining information about a neuron's shape.
- Lung nodule analysis for visualizing shape and measuring size and dimensions of nodules in a 3D space.
- Assessment of the correlation between the lung nodule growth rate and degree of nodule malignancy.
- Assessment and quantification of coronary artery calcification by means of electron beam CT.
- Evaluation and assessment of different pathologies as well as functional assessment of the heart via ultrasound.
- Evaluation of legs and chest for the presence of deep venous thrombosis and pulmonary emboli, respectively, via computed tomography.

- Detection and quantification of chronic obstructive pulmonary diseases (COPDs).

2.2.2 Algorithms of Computer Vision Used in the Medical Field

The following classes of algorithms are used in medical imaging:

Enhancement algorithms improve the quality of the image, reduce noise, and enhance contrast. Doctors can more accurately make a diagnosis by looking at better pictures. Furthermore, a clearer image constitutes a better input for subsequent automated analyses. The computer vision methods most used for enhancements are filtering, convolutions using different kernels, histogram equalization, noise suppression, and edge enhancement.

Segmentation algorithms separate structures of interest from the rest of the image. Though the human visual system segments automatically, this operation is a considerable challenge using computer vision tools.

Segmentation is important for feature extraction, image measurements, and image pixel classification in anatomical or pathological regions. Some of the computer vision methods used are thresholding, clustering algorithms, region growing, and segmentation using fuzzy clustering, or segmentation with neural networks.

Quantification algorithms extract information about the shape and the size of a considered structure from a segmented image. This gives information

about the severity and the extent of a disease. Quantification can be considered as a next step in analyzing image data.

Some of the computer vision criteria considered for shape quantification are compactness, spatial moments, Fourier descriptors, and densitometric measurement techniques. For texture quantification, one can use statistical moments and spectral measures from Fourier transform.

Visualization renders, displays, manipulates and models multidimensional data. It is designed to facilitate visual inspection of medical and biological data. A three dimensional image of the region of interest provides useful information describing the shape, surface, volume and its transformation in time. For example, if in time most of the growth of a nodule is done on the z-axis, without 3D visualization of the nodule, this growth will not be detected.

The computer vision methods used include surface rendering techniques that characteristically require the extraction of edges. Volume rendering techniques based on ray-casting algorithms have become the method of choice for visualization of 3D biomedical volume images.

2.2.3 Modalities Used in Medical Imaging

Medical images are generated through various modalities. These modalities are based on different physics concepts with varying implementations. We will overview some of the most commonly used techniques in this field. This is by no means an exhaustive list; other techniques such as angiography, and conventional tomography are also applied to highly specific areas.

Radiography exposes the body to a small dose of radiation in order to produce an image of the internal organs. X-rays penetrate many substances that are opaque to light. The x-rays are absorbed in varying amounts by different parts of the anatomy. The image is printed on black and white photographic film.

Fluoroscopy is a common radiological technique that allows real-time visualization of the patient. During fluoroscopy, a continuous beam of x-rays passes through the patient to cast an image on a screen, which is amplified by an electronic image intensifier and viewed on high-resolution monitor.

Computed Tomography obtains a series of different angular x-ray projections that are processed by a computer in order to generate the CT scan image. The concept of computed tomography will be discussed in detail later.

Magnetic Resonance Imaging (MRI) uses nuclear magnetic resonance of atoms within the body induced by application of radio waves to produce computerized images of internal body tissue. It is a noninvasive diagnostic technique.

Ultrasound systems generate images (echograms) based on properties of high-frequency sound waves and their interaction with biological tissue.

Nuclear Imaging injects radioactive isotopes (radionuclide) to visualize particular living organs and tissues.

2.3 Pulmonary Emphysema

Computer vision has a promising role in the diagnosis and treatment of pulmonary emphysema.

2.3.1 Definition

Pulmonary emphysema is part of a group of lung diseases, referred to as chronic obstructive pulmonary diseases (COPD) that can interfere with normal breathing. COPDs are the fourth-ranking cause of death, just behind heart diseases, cancers and strokes.

Emphysema is a pulmonary disease that usually develops after many years of assault on lung tissues from cigarette smoke or other toxins that pollute the air.

In this disease the lung's air sacs themselves, rather than the airways, are either damaged or destroyed. This condition leads to poor exchange of oxygen and carbon dioxide between the air in the lungs and the bloodstream.

2.3.2 Symptoms and Treatment

The prevailing symptoms of emphysema are coughing, shortness of breath, and limited exercise tolerance. As the damage progresses, the effort needed to breathe increases and, ultimately, each breath becomes labored. Wheezing and chronic mucus production, are other common symptoms.

As mentioned in previous section there is no cure for pulmonary emphysema but there are strategies that can be followed in order to slow down, or even stop, the progress of the disease.

The most important step (if it is applicable) is to stop smoking. Stopping smoking when the airflow obstruction is mild or moderate slows the development of disabling shortness of breath.

Other possible treatments also exist including:

- **Oxygen therapy** provides supplemental oxygen to benefit a patient whose lung function is severely impaired and cannot absorb enough oxygen from the air.
- **Lung volume reduction surgery (LVRS)** uses a special stapling device to reduce the volume taken up by the diseased portions of the lungs so that the healthy lung tissues have more room to expand within the chest cavity. In some patients, diseased portions of the lungs may become over inflated, leaving inadequate space for normal aspiration expansion of the healthy tissues. The surgery allows some emphysema sufferers to find relief from

their symptoms. LVRS, however, is not only expensive, but also involves significant risks, including death.

- **Transplant surgery** is a highly invasive, complex procedure that carries substantial risk. Because of the known complications of any organ transplant surgery, this option is only viable for a very small, select group of patients.

2.3.3 Modalities Used in Detection and Quantification of Emphysema

The key to managing emphysema is to **identify the disease as early as possible** so that preventive and therapeutic measures can be instituted.

Different tools are used in detecting and quantifying pulmonary emphysema:

Pulmonary Function Testing (PFT) is one of the basic tools for evaluating a patient's respiratory status. In general the pulmonary function test measures the amount of air taken into the lungs with a deep breath and how quickly the air can be expelled. Different forms of PFTs vary the number, depth and time of the measured inhaled and or expelled breaths. Most pulmonary radiologists consider this method as "the gold standard" approach.

Medical Imaging can be used for generating medical images through different modalities such as radiography and computed tomography. In order to

determine the existence or extent of emphysema, radiologists and pulmonary specialists will subsequently analyze these images.

In diagnosing emphysema, radiologists consider the following types of images:

- **Chest X-ray Images**: The presence of emphysema can be indicated by routine chest radiography but not before the disease is already at an advanced stage.
- **CT Scans Images,** particularly high-resolution CT Images (HRCT), has shown excellent correlation with pathologic studies in detecting and quantifying emphysema.

2.3.4 Why CT-scan Images Represent the Best Modality

On x-ray images, a low-density disease (like emphysema) is less easily identified than a high-density lung disease (for example lung nodules). In addition, a diffuse disease (like emphysema) is less readily detected than focal lung diseases (for example pulmonary masses). In general, pulmonary emphysema cannot be detected in x-ray images at an early stage.

MRI images are not sensitive enough in revealing abnormalities of the lung parenchyma. MRI is appropriate for analyzing the soft tissue of the body and its fluids but is not appropriate for the study of body parts whose density is close to that of air. Emphysema is represented by holes filled with air; and air doesn't contain enough protons for the MRI signal to be created.

Additionally, the motion artifacts in an MRI image of a lung are huge. The acquisition time for an MRI image of the lung will be approximately 10 minutes during which it is impossible for the patient to hold their breath for a stand-still chest image. On the other hand, a complete CT scan of the lung takes only about 30 seconds.

In the last twenty years, with the development of more advanced CT-scanners capable of scanning the human body at a faster rate and with a higher resolution, much research was directed at demonstrating that interpretation of the data obtained from CT scans can represent a more accurate, non-invasive way of detecting and quantifying emphysema than PFTs. CT scans can reliably predict even mild emphysema that escapes detection by pulmonary function testing.

The increase of airspace volume and the destruction of the lung walls will change the density of the lungs. Instead of healthy lung tissue (parenchyma), through which the lung can do air exchange, the lung will contain "holes filled with air" that will reduce its working capacity making breathing difficult. These "holes filled with air" that mark the presence of emphysema, are represented on CT scans as areas of abnormally low attenuation. The attenuation of a normal lung parenchyma varies between approximately –870 hounsfield units (a normalized index of X-ray attenuation used in CT imaging) and -750 hounsfield units. Areas of low attenuation appear dark on CT scans; the lower the attenuation, the darker the image.

There are two broad approaches to the use of CT images in the detection of emphysema:

- Subjective visual assessment done by radiologists.
- Computerized techniques based on low attenuation values detected on the CT scan image (see figure 2.4).

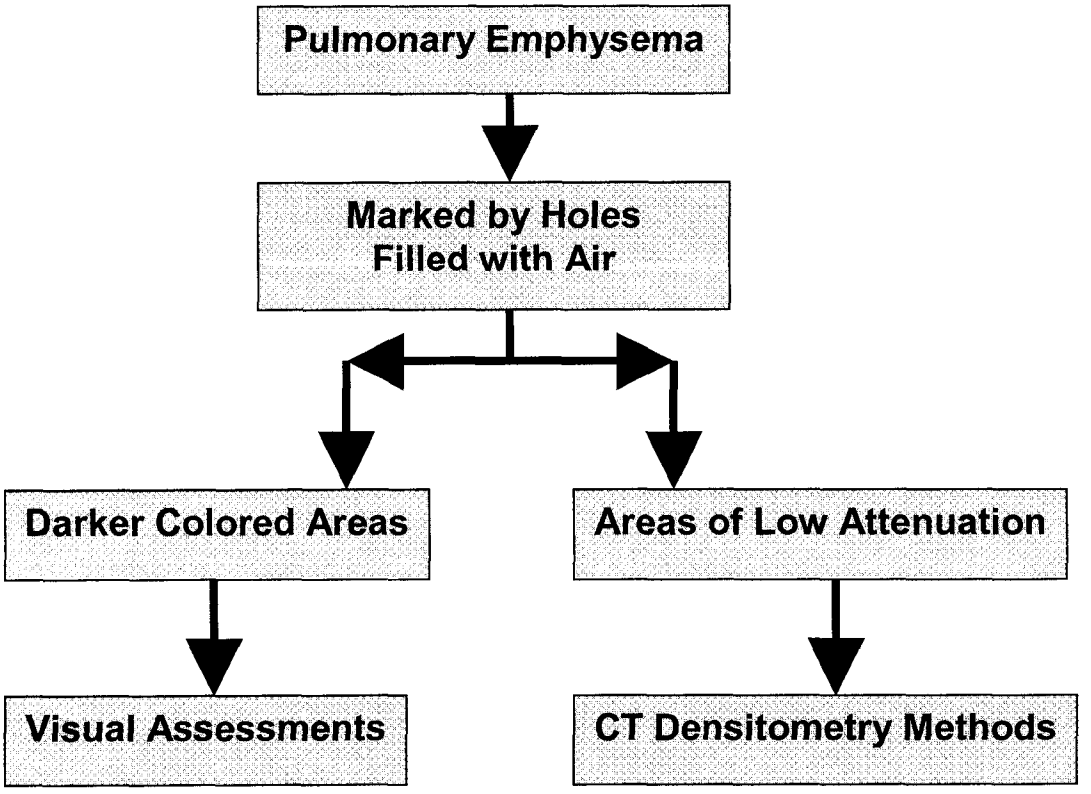

Figure 2.4: Different approaches to the use of CTs in detection of emphysema.

2.4 Computed Tomography

This section provides basic definitions of computed tomography that will be used in the coming chapters.

2.4.1 Computer Axial Tomography Scanner (CAT Scanner)

The CAT scan machine was invented by Godfrey Hounsfield. Sir Godfrey Hounsfield invented the capability for a computer to interpret x-ray signals to form a two-dimensional image of a complex object such as the human head. For his

work, Hounsfield received numerous awards in addition to the Nobel Prize, and he was knighted in 1981.

A CAT scan machine is basically an x-ray tube that rotates in a circle around the patient producing images that closely match the cross sections of the body. The machine looks like a donut standing on its side with a table going through the center of it. The patient lies on the table as it moves slowly through the scanner.

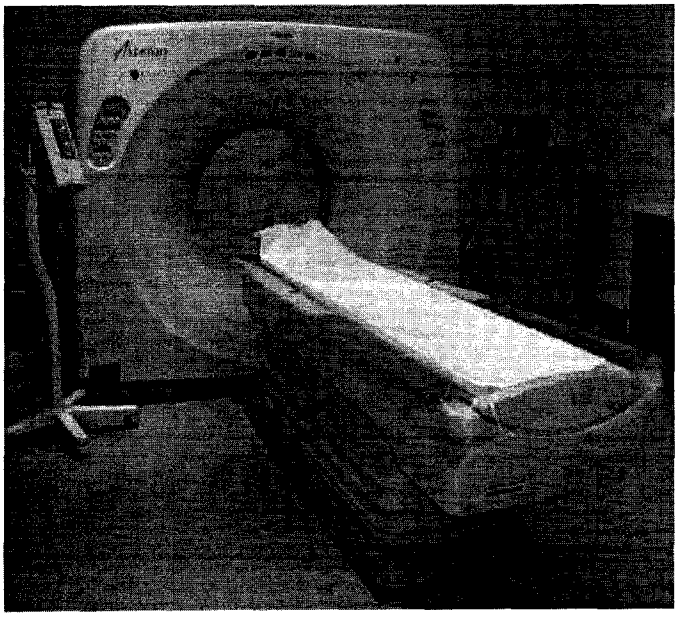

Figure 2.5: CAT scan machine.

2.4.2 Computed Tomography (CT)

Computed tomography (CT) is a specialized x-ray imaging technique that uses the CAT scan machine. The aim of CT is to obtain information regarding the nature

of the tissues inside the body and display the anatomy of a slice of the body. Usually this slice is perpendicular to the axial direction, head to toe.

By spinning the x-ray source and the detectors around the patient, data can be collected from multiple angles (figure 2.6). Computed tomography creates the image by using an array of individual x-ray sensors and a computer.

If we examine images generated by a CAT scan machine we can obtain information about nature, density, position and shape of body tissues.

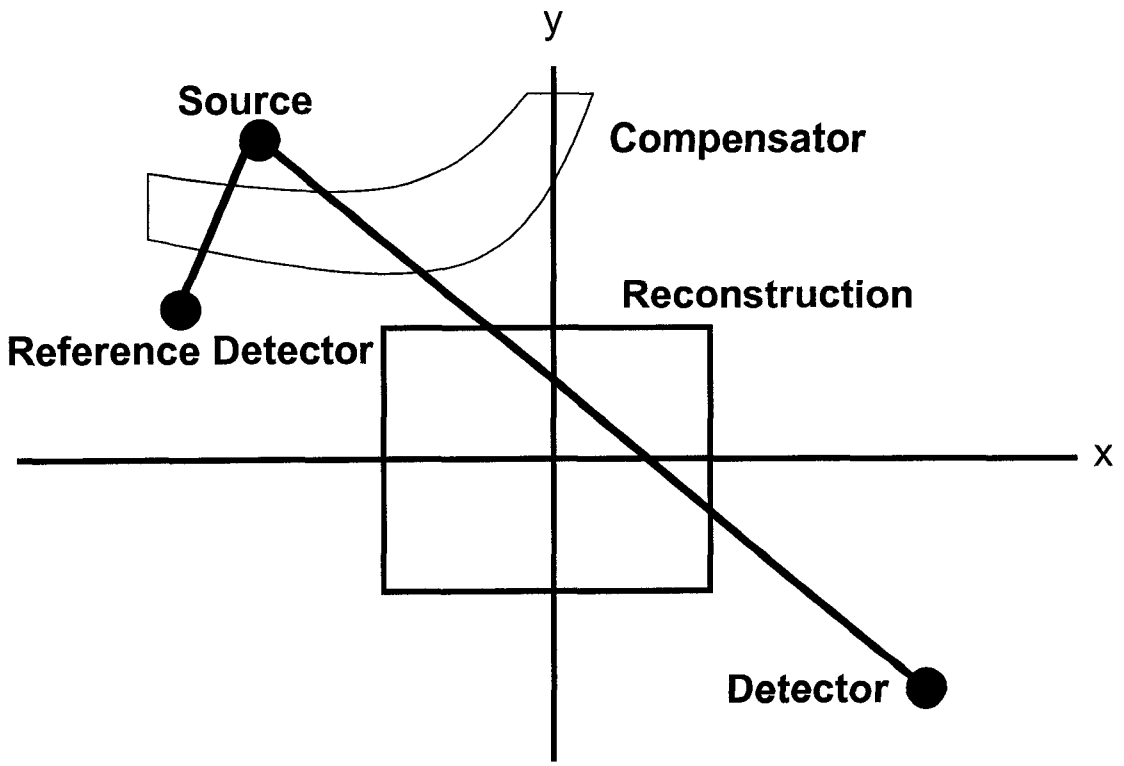

Figure 2.6: Data collection for CT[17].

2.4.3 CT Numbers (Hounsfield Units)[61]

For each combination of source-detector position, two physical measurements have to be taken:

- **Calibration measurement**, which is taken without the object in the path of the x-ray beam.
- **Actual measurement**, during which the object is in the reconstruction region.

When a material is placed between the source and the detector, some of the photons will be removed from the beam. The probability that a photon will be removed depends on the energy of the photon and on the density of the material.

Linear Attenuation Coefficient μ of a tissue t at energy e is

(2.1) $$\mu = - \ln \rho$$

where ρ is the probability that a photon of energy e, that enters a piece of uniform tissue t of unit thickness, will not be absorbed or scattered in the tissue.

More significant for us is the *Relative Linear Attenuation* at energy e.

(2.2) $$\mu^t - \mu^a$$

where t is during the actual measurement

and a is during the calibration measurement

An attenuation number, or CT number, is used to represent the attenuation coefficient measurement obtained in an x-ray computed tomography (CT) reconstruction. CT numbers are proportional to the average relative linear attenuation. The values are in hounsfield units (HU) in honor of Godfrey Hounsfield.

The scale for the CT numbers is set such that the CT number of air is –1000HU and the CT number of water is 0 HU. Depending on its density, bone has values between 1000 and 3000HU.

(2.3) $CT\,Number = K\,(\mu - \mu_w) / \mu_w$

μ_w is the attenuation coefficient of water

μ is the attenuation coefficient of the tissue (considered material)

K is a constant that must be large enough to accommodate the accuracy of the scanner.

2.4.4 CT Densitometry

The term *CT densitometry* is used in many fields of medical imaging. Informally, through CT densitometry techniques, radiologists are able to determine the CT numbers of a specific region (named Region of Interest, ROI) selected on the CT-scan.

CT densitometry measurements take into consideration the CT number of the pixel (or voxel). In much of the literature the two terms *CT densitometry* and *CT densitometric measurements* are used interchangeably.

There are numerous applications of CT densitometry including the detection of osteoporosis, the detection of malignant lung nodules, differentiating adenoma from metastasis, and the detection of fatty liver diseases. However, the most important application for this study is detecting and quantifying pulmonary emphysema.

The next chapter provides an overview of what has been done in the field of quantifying pulmonary emphysema using CT-scans.

3 OVERVIEW OF CURRENT RESEARCH IN QUANTIFYING PULMONARY EMPHYSEMA FROM CT-SCAN IMAGES

Physicians find that it is difficult to accurately diagnose emphysema and almost impossible to quantify it. Before the use of CT scans, emphysema was quantified during autopsy or by examining surgically resected lobes of the lung.

CT assessments can be based on both subjective, as well as, quantitative measurements of CT attenuation values in the lung. Over time, a number of ways of quantifying emphysema using CT images have been developed, starting from visual scores done by radiologists to sophisticated techniques. The latter uses software to distinguish pixels with abnormally low attenuation, associated with presence of emphysema, from those associated with healthy lung tissue. Applied to two-dimensional CT sections, the "density mask" technique was shown to accurately represent the morphologic extent of emphysema. Subsequently, automated techniques have been developed to increase the speed with which emphysema in the whole lung can be quantified, but such software is not yet widely available.

We can classify methods of detecting and quantifying emphysema by taking into consideration their computational complexity:

- Manual, Semi-automated methods
- Automated CT densitometry methods

- Simple CT densitometry methods
- Advanced CT densitometry methods

These approaches are described in detail in the following subchapters.

3.1 Manual, Semi-automated Methods

In this section we review methods of detecting and quantifying emphysema from CT scan images that require minimum use of computation. These methods are usually called "manual" to distinguish them from the highly computerized approaches described later.

3.1.1 Visual Scores

Pulmonary radiologists might suspect emphysema when they see significant areas of dark, gray-colored pixels in the CT scan images of the lung. Through visual scores physicians attempt to quantify the extent and/or severity of emphysema.

The assessment is completely subjective; there is considerable inter-observer and intra-observer variability. The characteristics of the scanner (window levels and widths at which images are analyzed) markedly affect the accuracy of the diagnostic. For their assessment, radiologists are capable of observing only a couple of CT scans of the lung, usually 3–5 images per case. Since a complete scan of the lung typically involves between 70 and 150 images

(depending on the z-axis distance between slices), such a small sampling cannot always provide accurate information.

What is a visual score?

A visual score is a number arrived at by a heuristic approach developed over time by radiologists in order to quantify emphysema in CT scan images.

Examples of Visual Scores

In their paper, Kyung J. Park, et al[43], consider one of the most widely used visual scores, the *severity of emphysema* score, defined by the percentage of the low-attenuation area of the lung on a 0–4 scale (see table 3.1).

0	no emphysema
1	≤ 25% of lung involved
2	26% - 50% of lung involved
3	51% - 75% of lung involved
4	76% - 100% of lung involved

Table 3.1: Emphysema severity scores.

Sakai, et al[50], suggested quantifying the *extent of emphysema* as a function of the Low Attenuation Area diameter (dLAA) (see table 3.2).

0	no emphysema
1	dLAA < 5mm
2	dLAA > 5mm with intervening normal lung
3	diffuse LAA without intervening normal lung

Table 3.2: Emphysema dLAA diameter scores.

One of the emphysema quantification methods described by Blechschmidt, et al[7], uses a combination of the two scores mentioned above: the severity score multiplied by the extent score (see table 3.3).

0	normal
1–3	suspicious on emphysema
4–6	emphysema
7–12	severe bullous emphysema

Table 3.3: Blechschmidt's emphysema quantification method.

3.1.2 Direct Observational Method and the Grid Method

In 1987 Sakai, et al[50], compared two quantification methods that used visual scores. The first method, named "Direct Observational Method" uses the visual score described in table 3.3. The degree of emphysema score (severity score *

extent score) was subsequently divided by 40 to give a numerical score that could be compared with the "Grid Method" described next.

The grid method was introduced in order to reduce the inherent high subjectivity in visual score quantification. An overhead projector places a grid with 1 cm^3 squares on the lung CT scan. Fifty percent of each lung field is then sampled. *Extent of emphysema* is therefore not subjective but fixed as present or absent for a given square. On average, 500 squares are evaluated for each patient.

Severity of emphysema is graded for each square using the same 0 – 4 point scale.

In the grid method, degree of emphysema was defined as

(3.1) $$EmphysemaDegree = \frac{\sum(numSquares * severityGrade)}{numberOfObservations}$$

The authors concluded that computed tomography has demonstrated good sensitivity for detection of emphysema. The results obtained through both methods show high correlation with the pathology and PFTs.

It is somewhat surprising that though the two methods vary in complexity and size of data, both have an extremely high correlation with a coefficient of $r = 0.931$ ($p < 0.001$). No statistical difference between the two methods was found; but, this can be a consequence of the fact that a very small number of patients was considered in the study (N=26).

However, as other methods of quantifying emphysema became available, the limitations of visual scores became more apparent. For example, A.A. Bankier, et al[5], compared visual grading with macroscopic morphometry (obtained through study of resected lobes) and computed tomographic densitometry. In their article, the researchers concluded that, independent of the level of expertise of the individual reader, subjective grading of emphysema (using visual scores) was inferior to both the macroscopic reference standard and the objective method (given by CT densitometry). They subsequently conclude that visual grading is inferior to the aforementioned methods. Subjective grading should be supplemented with objective methods to achieve precise, reader-independent quantification of emphysema.

3.1.3 MLDs, MLDw, AV Number, CT Number

Rosenblum, et al[48], discussed the density pattern of a normal lung. The authors then suggested that variations in these patterns might be useful in diagnosing various lung diseases. For example, the density pattern might increase in case of pneumonia; it might decrease in case of emphysema, or produce variable changes in case of pulmonary thromboembolic disease. These researchers proposed a pattern characterization for a CT image of the normal lung in order to exploit the potential for computed tomography in the early detection of lung disease.

Two points deserve special mention:

1. There is the possibility of gaining insight into the existence of a lung disease by analyzing the density of the lung tissue called parenchyma.
2. Since the density of the parenchyma is directly correlated with its coefficient of low attenuation, we can consider CT numbers instead of physical density values. CT numbers values, for a ROI seen on a CT scan, are generated by the scanner software and are immediately available to radiologists.

Rosenblum, et al, introduce two parameters in order to describe the density patterns of the lung:

- **MLDs**: the mean lung tissue density, or the density of the parenchyma.
- **MLDw**: mean lung density for the whole lung, including the vessels and denser central structures.

The first parameter measures the density of the peripheral-parenchyma, the other determines the density of the whole lung field.

They go on to show that for lung tissue the linear attenuation coefficient is primarily determined by *Compton scattering*. Compton scattering is proportional to the product of the physical density and the electron density. Because the electron density is considered a constant, the approximate equation of the lung density (ρ(lung)) becomes:

(3.2) $\rho(lung) = (AV)/1000 + 1$ expressed in g/cm^3

Instead of standard units for density (g/cm^3), for the rest of the article, authors refer to the density of the lung as the *Attenuation Value* number (AV). The *AV* number or *CT number* is defined in terms of a difference of attenuation coefficients between the material in question and water.

Is "Mean Lung Density" a good parameter in quantifying emphysema?

Kemerink, et al[33], consider that measuring only the mean attenuation of the lung parenchyma is ineffective for assessing the extent of emphysema. One reason is that the extent of emphysema differs from case to case and it is not always directly proportional to the severity of emphysema. Assessment of the mean lung density doesn't give any information about the distribution of emphysema. Nevertheless, it has been shown that mean lung density is lower in emphysematous lungs than in normal lungs, a fact that could be used in future research.

3.2 Simple CT Densitometry Methods

3.2.1 Density Masks

Compared to images of normal healthy lungs, images of emphysematous lungs have higher number of pixels with low attenuation values. Writing a program to provide a "density mask" is relatively straightforward. Such a program highlights only pixels whose density is below a specific threshold value, that of an emphysematous piece of tissue. Most CT-scanners currently provide this functionality. The percentage of pixels with density lower than a set threshold can give information about the degree of emphysema.

Defining the value of the density mask depends on what exactly doctors or researchers are looking for during their emphysema quantification. In Hu, et al[29], an adaptive thresholding method is used to automatically choose a threshold value that will reflect best the characteristics of a subset of different areas of the lung. Hayhurst, et al[25], showed that attenuation values less than –900HU were present exclusively in patients with emphysema and not in patients with normal lungs. In Kenzo Soeijima, et al[54], the following observations were made:

- -900HU, -910HU are considered to be significantly correlated with the morphological destruction of the acinar structure.

- -900HU or –910HU would include areas with partial destruction of the acinar structure in addition to those with complete destruction.
- -950HU: gives the higher correlation coefficient between morphologically detected emphysema and HRCT related emphysema.
- -960HU can be used to solely reflect severe emphysema.

3.2.2 2D Densitometry

Densitometry is a process that uses quantitative computed tomography techniques to evaluate the density or mass of various tissues of the human body. Quantification of emphysema can be done by computing the relative lung area occupied by pixels with low attenuation coefficients, close to the density of air. We will examine some of the methods based on densitometry concepts.

Density mask percent area is the percent of lung area highlighted by a specific density mask. Density mask CT scores[41] can be defined using this measurement. These density mask CT scores have been correlated with visual scores and pathological panel scores for emphysema quantification.

Pixel Index (PI)[32] is another common method of CT image evaluation. It is computed by dividing the number of pixels with lower attenuation than the threshold limit value by the number of pixels of the entire lung.

(3.3) $PI = |\, pix \in CT: pix \in [-1000 \ldots lim\ HU] \,| / ARlung$

where *lim* denotes the upper limit (usually between –950HU and –900HU)

and *ARlung* denotes the set of all pixels of the segmented lung

(3.4) $ARlung = |\, \{pix \in CT: pix \in [-1000 \ldots -200HU]\}|$

3.2.3 3D Densitometry

Because some types of emphysema are predominant only in certain lung regions, 2D densitometry could lead to a false diagnosis. The most accurate method of estimating the percentage of emphysema from CT images is to analyze the whole lung from a 3D perspective.

In 1993 D.C. Archer, et al[2], developed a program that determines *lung volume* and *percentage of emphysema*. The boundaries of the lungs are extracted by using a sub-range filter with a threshold of –400 HU.

(3.5) $Total\ Lung\ Volume = \#\ of\ lung\ pixels * pixel\ size^2 * section\ thickness$

(3.6) $Size\ of\ emphysematous\ area = total\ number\ of\ pixels\ with\ density < -900HU$

(3.7) $\%\ of\ emphysema = \frac{total\_volume\_of\_emphysema}{total\_lung\_volume}$

Likewise, H. Coxson, et al[15], conclude that CT analysis can be used to monitor the progression of emphysematous lung destruction in individual patients and to assess the impact of both surgical and medical treatments for emphysema. A density mask of –910HU had been used. Coxson, et al, discuss the fact that CT data can be used to calculate total lung weight, tissue and airspace volume of the lung. A CT estimate of the surface area provides a tool for tracking the destruction of lung surface area by emphysema. The comparison of CT to morphology in resected lobes confirms that the standard density mask cutoff (-910HU) fails to detect emphysematous lesions less than 5mm in diameter.

3.2.4 Detection of Longitudinal Changes in the Lung

Kenzo Soeijima, et al[54], evaluate the ability of High Resolution Computed Tomography (HRCT) to detect longitudinal changes in structural abnormalities of the lung due to patient's history of smoking. Most of these structural abnormalities are caused by emphysema. The novelty of this study stems from the authors' consideration of a large number of criteria such as: longitudinal position of the CT Scans, patient's age, and the patient's history of smoking. Densitometric measurements are taken from three different regions of each lung: the upper, middle and lower regions. Three parameters are considered in their assessments:

- **MLD**: CT density average of all pixels in a lung region

- **HIST**: CT value with the most frequent appearance in the density histogram constructed for every 10HU
- **%LAA**: percentage of low attenuation area (CT values < -912HU)

Some of the issues addressed are:

- Correlation between PFTs and CT parameters in three different groups of patients: nonsmoking, past smoking, present smoking
- Longitudinal changes in quantitative CT parameters
- Longitudinal changes in PFTs

The authors conclude that in detecting subtle longitudinal changes in acinar structures caused by aging and smoking, HRCTs are superior to PFTs. Aging augments airspace enlargement predominantly in middle and lower lung fields. Continuous smoking worsens emphysematous alterations in upper lung field. Airspace abnormalities may progress even after stopping smoking.

3.3 More Advanced CT Densitometry Methods

3.3.1 Pulmonary Morphology: Possible Criteria

Blechschmidt, et al[7], present a new algorithm of thoracic CT image evaluation based on pulmonary morphology of emphysema. The main feature of their approach is the emphasis on the size of bullous destruction of emphysema rather than the percentage of low attenuation areas. Bullae are continuous, marked low-attenuation areas. The authors introduce a new index, the bullae index (BI) and argue that BI is at least as reliable as PI (pixel index). When both emphysema and pulmonary fibrosis are present, BI can detect the destruction caused by emphysema alone, while PI still indicates normal values for the density of the lung and cannot distinguish between the damage caused by the two diseases.

Bullae are sorted by size into four classes: normal, small, medium and large. The bullae index BI is derived from the percentage of areas covered, respectively by small, medium and large bullae. Additionally, the authors introduce a new measure, that of the emphysema *type*. This score will differentiate between two categories of emphysema: non-bullous and bullous.

These new classification results were compared with visual scores assessments ranging from 0 to 12 given in table 3.3. The authors report that due to the high correlation (r=0.90) between visual scores assessments and their bullae index assessments, the newly introduced method can successfully replace visual

scoring. Blechschmidt concludes that the evidence for bullous emphysema is substantiated, but further studies are needed to confirm its validity in the non-bullous emphysema type.

3.3.2 Texture-Based Adaptive Multiple Feature Method

Uppaluri, et al[58], use a texture-based *adaptive multiple feature method (AMFM)* for evaluating pulmonary parenchyma in CT images. Using a combination of statistical and fractal approaches, AMFM provides information on the texture of parenchyma. During preprocessing (lung segmentation) an edge-segmentation method is used. Feature extraction is then performed on selected regions of interest (ROI). In their paper, the authors consider the following statistical and fractal features:

- **geometric fractal dimension**: It has been previously shown that images of natural surfaces can be modeled using the fractional Brownian motion model. The fractal dimension can provide an estimate of the surface's roughness and smoothness.
- five **first-order texture features** have been derived from the gray-scale frequency histogram: mean, variance, skewness, kurtosis, and gray-level entropy.

- eleven **second-order features** were computed on the ROI of the preprocessed image. These features provide the relationship between pixels and their gray-levels:
    - run-length features: short-run emphasis, long-run emphasis, gray-level non-uniformity, run-length non-uniformity, and run percentage.
    - features based on the co-occurrence matrix: angular second moment, entropy, inertia, contrast, correlation, and inverse difference moment.

The available ROIs were randomly split into a training set and a test set. From the ROIs of the training set an optimal set of features were selected using the divergence measure along with correlation analysis.

The classification was performed using the Bayesian classifier depicted in figure 3.1.

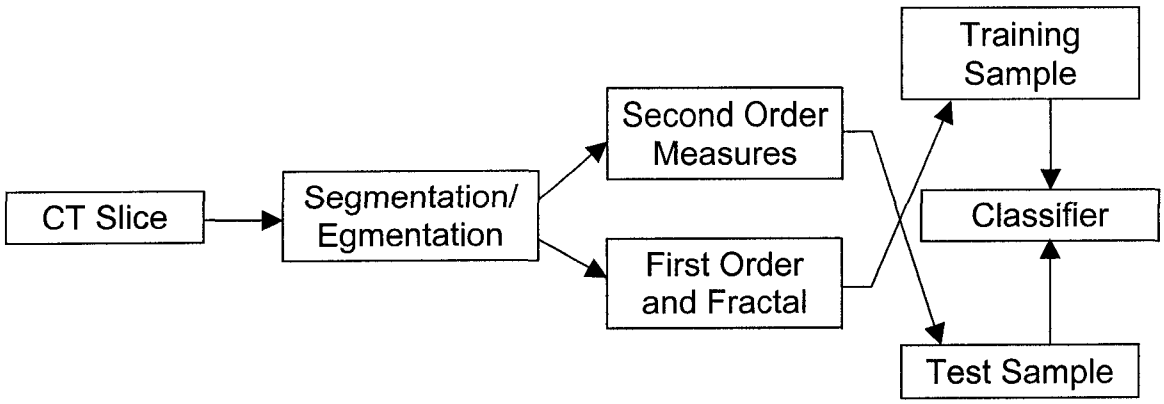

Figure 3.1: Steps of the AMFM method[58].

The new approach was validated against other methods in common use, such as one using the mean lung density (MLD) and one using the lowest fifth

percentile of the density histogram (HIST). The authors conclude that in the detection of emphysema, the AMFM method compares very favorably with MLD and HIST. Several features used in AMFM show significant abnormalities in lungs with emphysema as opposed to healthy lungs. AMFM, with its automatic selection of different features, is better able to discriminate positional changes in the normal lung than MLD or HIST. This new method is sensitive to textural changes and may be more generally applicable to the evaluation of parenchyma diseases. The AMFM method can be used for tissue characterization of the lung, allowing consistent evaluation of parenchymal diseases.

3.3.3 Evolutionary Programming

Madsen, et al[39], discuss the possibility of using *evolutionary programming* in quantifying emphysema. The purpose of their study is to evaluate evolutionary programming for selecting the best features and to build up a useful tissue classifier.

Researchers have compared the performance of an evolutionary programming classifier with that of a Bayesian approach that had been previously validated (AMFM[58]).

In evolutionary programming, algorithmic solutions to the problem are encoded as a list of variables, referred as chromosomes. The fitness of the chromosomes is evaluated via a training set. The fittest chromosomes are allowed

to produce offspring through crossover operations. Offspring with better features will gradually replace the weaker ones. After many generations, a solution evolves. This is analogous to the evolution of an organism under natural selection. Madsen, et al, argue that while there is no guarantee that the final solution is optimal, evolutionary programming often provides a superior solution to detecting emphysema. The result produced by the evolutionary programming, is an executable algorithm that solves the optimization problem on the training set.

In their study, researchers used the three classifiers mentioned in the previously cited article: MLD, HIST, and AMFM. The training set was presented to a commercially available evolution programming software package (Systems Dynamic International, Fenton, Mo). The idea was that evolutionary programming would optimize the training set and a classifier would be obtained. The solution was obtained after running 18,000 generations. Since evolutionary programming does not require any problem-specific modeling for its solution search, it is relatively easy to implement.

The authors conclude that evolutionary programming appears to be an important and useful tool for finding algorithmic solutions to complicated problems where no optimal solution is known. The development of image classifiers demonstrates its ability to derive a useful solution from a complex data set. Not only does the evolutionary programming approach correctly identify all the normal and abnormal lung images, but also it can accomplish this using fewer features than the best statistical method.

3.3.4 Assessments of Pulmonary Emphysema Based on Changes in Structural and Physiological Features of the Lung

Emphysema causes changes in structures and physiological features of the lung. Evaluating the magnitude of these changes allows for the detection and quantification of emphysema. In light of these considerations, some studies quantify pulmonary emphysema through the assessment of related abnormalities of other structures of the lung, besides the parenchyma.

Additionally, the question of whether other lung diseases like asthma might influence the development of emphysema has been addressed. Current research answers this question in the negative.

The structural changes related to emphysema discussed in the literature are as follows:

- **Airwall Thickening**

  Y. Nakano, et al[42], discuss air-wall thickening as an outcome of emphysema. The diameter, surface and volume of the airways are measured using geometrical formulae. Authors consider the airway "wall area percentage" (WA%) a primary measurement of airflow obstruction.

  Their study shows that patients with more emphysema have less severe air-wall thickening than those with less severe emphysema. There is no significant relationship between patient's smoking history and airway

dimensions. Measurement of air-wall dimension can be easily added to the CT assessment of emphysema.

- **Lung Elastic Recoil**

  Baldi, et al[4], study the relationship between the extent of pulmonary emphysema (assessed by CT densitometry) and lung elastic recoil in patients with chronic obstructive pulmonary disease. Lung elastic recoil is a distinctive feature of pulmonary emphysema. They conclude that while HRCT scanning is a reliable, non-evasive method to assess the severity and the extent of macroscopic emphysema, CT scanning is relatively insensitive in detecting emphysematous lesions of less than 0.5 mm. Their study suggests that currently used methods cannot predict the elastic properties of the lung tissue.

- **Distal Airspace Enlargement** – a possible parameter

  Gould, et al[20], consider distal airspace enlargement a possible sign of emphysema. They define emphysema as airspaces with size greater than one mm in diameter. The necessary characteristic for defining emphysema is "an increase in size of airspaces distal to the terminal bronchioles." This implies that the ratio between the surface areas of the walls to the volume of such airspaces is reduced in emphysema. The degree of distal airspace enlargement is consistent with non-evasive CT densitometric measurements. The authors concluded that the exploration of the range of

distal airspace size may eventually lead to a numerical definition of emphysema.

- **Asthma and emphysema** - no correlation

  Mochizuki, et al[40], attempted to determine whether or not asthma affects the development of emphysema. If there were a correlation, the presence of asthma might be a criterion in detecting emphysema. The researchers found no evidence of such an effect. They concluded both that emphysema occurs irrespective of the severity or duration of asthma and that asthma does not lead to emphysema. The authors point out, however, that other researchers have reported that the severity of asthma was significantly correlated with the presence of emphysema. The question remains open.

It is clear from all the above that computer vision techniques provide very powerful tools in the area of medical image processing. It is equally clear that current techniques are still quite limited. Much work remains to be done.

4 DATA ACQUISITION

I am part of a relatively small but very active research group at the Weill Medical College of the Cornell University. The CT scan images used in the research are taken from a teaching repository, which is an online resource that has been IRB approved for use by the academic community as a warehouse for those that have an interest in evaluating this type of data but traditionally had been without access. Images were collected as part of the IRB approved Early Lung Cancer Action Project (ELCAP).

4.1 DICOM[67]

Digital Imaging and Communications in Medicine (DICOM) 3.0, a communication protocol, represents an interface to our system. DICOM is used by medical professionals that utilize medical images (including radiology, radiation therapy, cardiology, pathology, etc.). DICOM is considered the standard for communicating between heterogeneous applications, devices and/or systems.

The DICOM standard uses an ISO OSI network model and provides support for the exchange of information on interchange media. DICOM 3.0 allows transferring of medical images in multi-vendor environment, and facilitates

the development and expansion of Picture Archiving and Communication Systems (PACS).

4.2 VisionX

VisionX system was developed over many years of research at Cornell University.

> It is an extensive flexible software system for image processing and computer vision. It has been used in research projects for a wide range of applications including: multispectral image analysis, 3D object recognition, multiframe image analysis, object tracking, neural networks, biological cell analysis, and 3D CT computer aided diagnosis.[70]

The VisionX system reformats CT scan images from the DICOM format to the VisionX format, which keeps the data anonymous by eliminating the DICOM header that contains patient-identifying information. All CT scan images analyzed in the research are in the VisionX format. The VisionX system forms the basis of most of the software developed in the research.

4.3 CT-Scan Images Specifications

The CT datasets were acquired on a GE LightSpeed QX/i at 120 kVp and 40 mA, using 2.5 mm section thickness, 6:1 pitch (1.5:1 standard pitch), and a bone reconstruction algorithm.

The GE LightSpeed QX/I is a multi-slice helical CT scanner, one of the most advanced CT scanner currently available. Multi-slice CT is a newer technology which allows the scanner to gather a larger number of slices with a single rotation of the scanner gantry (housing for the x-ray tube, filters, and motors). The path of x-ray beam around the patient follows a helical path that eliminates wait in-between slices for table movement. Thinner slices give better z-axis resolution. The multi-slice technology also leads to faster scans – a very important development for lung CT scans since the patients must hold their breath during the scans.

Radiation dose is governed by x-ray beam parameters and image parameters. While a lower radiation dosage is beneficial to the patient, on the other hand it compromises the quality of the scan.

The x-ray beam is defined by the following parameters: *kilovoltage* (kVp) determines the penetration depth of the x-ray; *milliamperage* (mA) determines the quantity of the x-ray; *filtration* can be used to remove the low energy x-rays which can contribute additional radiation to the patient; *collimation* is used to point the x-ray beam to the desired area.

Image parameters include *noise* (due to partial volume error, photon starvation, metal artifacts, patient movement), *spatial resolution*, and *slice thickness*.

Pitch can be defined relative to total x-ray collimation (x) (or individual detector width (d)).

(4.1) $$pitch = \frac{t}{cw}$$

where t is the table travel speed (in mm)
and cw is the collimation width of the x-ray beam (in mm)

For example for a protocol with 15mm/rot table speed and 2.5mm slice width, the pitch is 6:1.

5 AUTOMATED LUNG PARENCHYMA SEGMENTATION ALGORITHM FOR LOW-DOSE CT-SCAN IMAGES

5.1 Introduction

Over the past few years, pulmonary CT images have been used for identifying many pulmonary diseases, for the study of parenchyma density, and for the analysis of the airway structures and other morphological components of the lungs. These studies would be greatly aided by the development of accurate lung segmentation algorithms that would require minimum or no human interaction.

There are a number of manual or semi-automated edge-tracing and pixel-tracing methods for segmenting CT images; these range from manual contouring of objects to techniques that require a single, operator-defined, seed point. Manual segmentation consists of manually tracing on the computer display the boundary of the object of interest using a mouse or light pen. It is a laborious and subjective task. Edge tracking has been applied by Hayhurst, et al[25], to lung segmentation with the operator providing a seed point to initiate the search to desired lung-pleural interface. Another technique often used in semi-automatic segmentation of CT scan images is gray-level thresholding. Because of differing density, different structures can be identified by isolating pixels of a specific gray-level range[43].

Willi A. Kalender, et al[31], developed a semi-automated segmentation for normal-dose radiation CT scan images, that isolates the lung boundaries by fast contour tracking and defines sub-regions by shrinking and radial segmenting.

Matthew S. Brown, et al[10], present an automated, knowledge-based method for segmenting chest computed tomography datasets. They use anatomic knowledge to guide low-level image processing routines.

B. M. Carvalho, et al[11], use a fuzzy connectedness algorithm that effectively segments out objects containing noise and/or shading. For images corrupted by noise, they believe that thresholding might not be an appropriate method of segmentation. The authors use tomographic reconstructions as CT and PET images to evaluate the speed and accuracy of the algorithm.

S. Hu, et al[29], in their paper describe a fully automatic method for identifying the lungs. The lung extraction is done using an adaptive thresholding approach. The authors address the segmentation of the trachea and large airways as well. In their paper, trachea, left, and right main-stem bronchi are identified in the original image using close-space dilation with a unit radius kernel. This method does not seem too promising to us, however. Over the last years of working with CT images it has become clear that, generally, bronchi are not seen as circular areas on the CT scans. Additionally, the right-bronchi often branches from the trachea much earlier than the left bronchi. Thus their method of segmenting the airways will not be accurate enough in many cases.

Since our main research interest is to develop computerized methods for early diagnosis of pulmonary diseases, more precisely for emphysema, we've focused on developing methods to better understand the disease quantitatively and to then develop software for early detection and screening.

We stress the importance of the integrity of the starting data – the preprocessed, segmented lung CT-scan images. The accuracy of this data greatly affects the quality of the final analysis. Preprocessing consists of noise filtering, image sharpening, edge extraction, and enhancement algorithms that improve the quality of the image, reduce noise, and enhance contrast. A clearer image is a better input for subsequent automated analysis.

More difficult, and perhaps more crucial, is the segmentation from the CT-scan image of the morphological components of the lung that will be subsequently analyzed: lung nodules, trachea, bronchi and lung tissue (parenchyma). Segmentation is the process by which structures of interest are separated from the rest of the image. It is important for feature extraction, image measurements, and to classify image pixels in anatomical or pathological regions.

The current study will only consider low-dose radiation CT scans taken from the Cornell ELCAP screening database. All research done to date in the area was performed on CT scans with standard radiation. Since low-dose CT scans are far less invasive for the patient, they present an important clinical advantage. The development of an effective and efficient segmentation program of the lung from low-dose CT scans will allow for the concurrent evaluation of pulmonary diseases

in the context of screening for other diseases, yielding additional diagnostic information with no additional radiation exposure.

5.2 Overview of the New Automated Segmentation Program[35]

Most current segmentation algorithms lack accurate segmentation of the main airways (trachea and bronchi). Most deal only with the delineation of the lung boundaries from the original CT scan. This limited information might not be sufficient for many studies of the pulmonary diseases.

The difficulty of lung segmentation of low-dose helical CT scans is increased if we use parameters designed to reduce radiation exposure to the minimum, since this leads to increased presence of noise in the scans acquired.

Our new algorithm is modular, allowing for any or all of the following processes to be specified by the user:

- Lung components segmentation
- Vascular removal
- Airways removal

During **Lung segmentation**, the lung volume boundaries are delineated. Areas of the body's tissue irrelevant to the lungs such as the rib cage and the mediastinum are removed from the image.

Vascular removal allows for the removal of blood vessels that are embedded in the parenchyma's tissue. This process involves locating and then carefully cropping these areas without damaging the data held in the adjacent tissue.

Airways removal starts with the removal of the trachea followed by the removal of the two bronchi. During trachea removal, the start of the trachea is located and traced downwards. This stage terminates when the trachea branches off into the two main tubes of the lung, the left and right bronchi. The bronchi branch again, into secondary and tertiary bronchi, then smaller bronchioles, and finally terminal bronchioles.

The airways removal step segments out the lung airways starting with the trachea and continuing all the way down to the level of small bronchioles. At this final level most of the bronchioles merge into the parenchyma tissue, and, therefore are, all but undetectable by current CT scans.

The flowchart in figure 5.1 gives an outline and highlights of encountered problems, as well as the Computer Vision techniques that are likely to be employed:

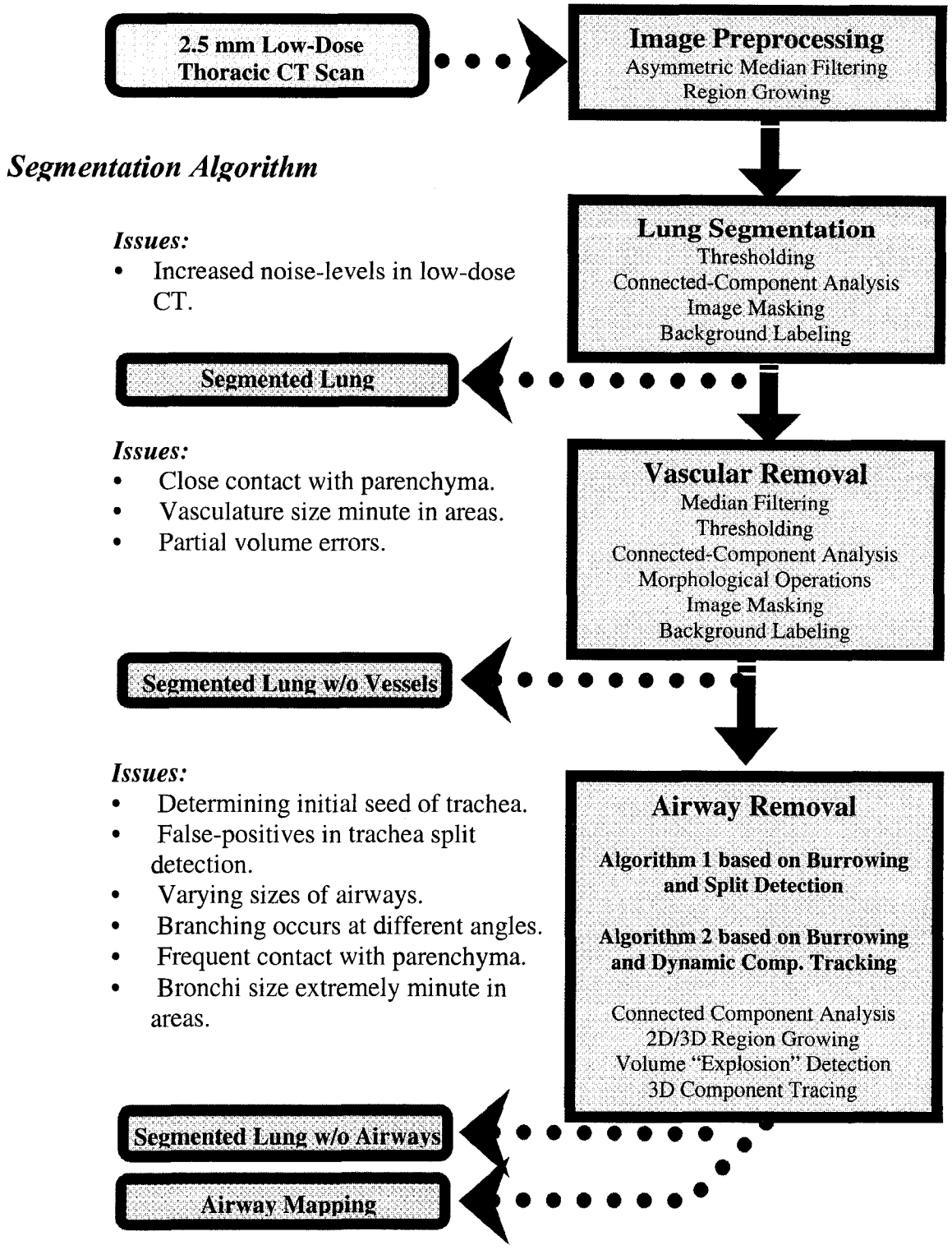

Figure 5.1: Steps of the lung segmentation algorithm.

5.3 Tools and Techniques

A large set of low-dose CT screening examinations, performed in the 2001 calendar year in our lung cancer-screening program, was used as input image data. Each of these CT datasets was acquired on a GE LightSpeed QX/i at 120 kVp and 40 mA, using a 2.5 mm section thickness, 6:1 pitch (1.5:1 standard pitch), and a bone reconstruction algorithm. Each of the CT exams will be further evaluated for the presence of artifacts that might prevent acceptable segmentation of the lungs.

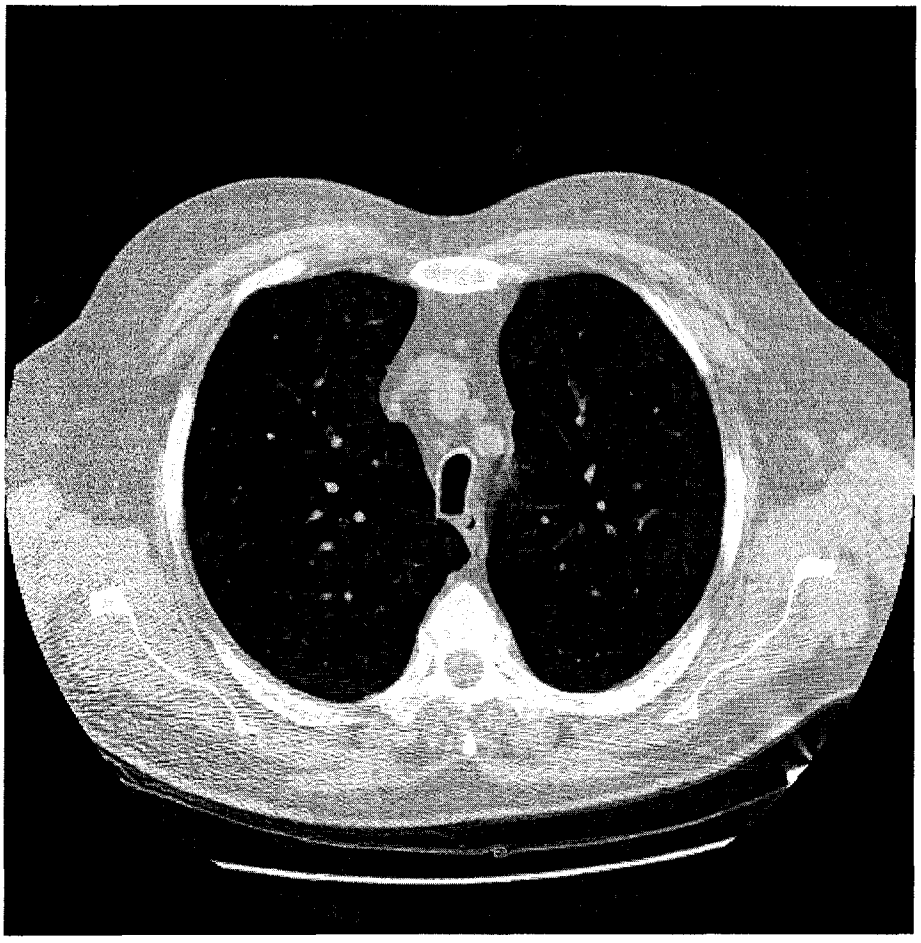

Figure 5.2: Sample of a low dose radiation CT-Scan image slice.

The algorithms we developed include shell scripts that make use of our custom-developed C-language programs and the VisionX system developed at Cornell University.

Storage

The research has necessitated large data storage. Each CT-scan image is a raw three-dimensional image, packed with much information. A typical image that covers the lung with a z-resolution of 2.5mm will contain approximately 140 slices. The size of a CT scan slice is 512x512 pixels. A single pixel's intensity is represented by a short integer, or 2 bytes. The total for a single test case:

(5.1) $$CT\text{-}scan\ image\ size_{bytes} = p * b * s$$

where p is the number of pixels per slice.

b is the number of bytes per pixel

and s is the number of slices.

(5.2) By formula 5.1, we determine our space requirements:

p = 512 * 512 pixels

b = 2 bytes per pixel

s = 140 slices

$$CT\ scan\ image\ size_{bytes} = (512 * 512) * 2 * 140 \approx 70\ MB$$

To properly evaluate the algorithm, we ran it against many cases. Our testing database is a set of approximately eighty CT scan images. Add to this the intermediate files generated for each case. In total, the machine generated 28 GB of hard data through the segmentation and analysis algorithms. Our primary research machine was a Dell PowerEdge server with a hard drive capacity of 250 GB.

5.3.1 Segmentation of the Lung Components

The original CT scan image presents a high degree of noise and horizontal streaking artifacts, particularly in the lung apices. As part of the preprocessing image step, filtering is necessary. However, to keep the original image information as intact as possible, noise filtering was applied solely to images that will generate the mask of the segmented lung. The filtering consisted of a median filter followed by a mean filter. Through a median filter, the gray filter level of each pixel placed in the center of the kernel is replaced by the median of the gray levels of the pixels covered by the kernel. The method is particularly effective when noise consists of strong, spike-like components and we aim to preserve the sharpness.

The design and performance of the median filter will be discussed in more detail in chapter seven, which focuses on emphysema segmentation. A mean filter implemented using a convolution operation with a vertical kernel was applied as

next step. An asymmetric vertical kernel is appropriate, since the remaining streaking artifacts are horizontal.

Using a recursive "3D-filling" algorithm, region growing is used to identify the boundaries of the lung and isolate the rib cage.

In order to generate the segmented lung image, the next step is to create a lung image mask that, subsequently, will be applied to the original image. The lung segmentation itself is based on thresholding, combined with shape and connectivity constraints. 3D connected components analysis will detect the largest 3D component in the image that doesn't touch the boundaries of the image – in this case, a lung component. A morphological closing operation (dilation followed by erosion), was performed to include in the mask the higher attenuation voxels corresponding to the lung vasculature and to fill up any other holes created throughout previous steps by noise presence. An additional threshold operation sets the voxels of the lung to 1. Everything else is considered background and set to value 0. A binary multiplication between the lung mask and the original image generates the final image of the segmented lung.

Background re-labeling of voxels values outside the range of lung data makes possible future analysis of the segmented region. Since, by default, the background is labeled with same intensity values as the air present inside the lungs, this step is necessary for later quantification of pulmonary emphysema.

The following is a formal presentation of the two algorithms.

Guide to Style

Keywords are in **bold**.

Method names are in SMALL-CAPS.

Variables are in *italics*.

Constants are in the Arial fontface.

Individual voxels can be addressed as *image[z][y][x]* where x, y, z are integer numbers or *image.p* where p is a triplet representing the pixel's address.

Common Routines

These methods are used in multiple phases of the segmentation algorithm.

```
MASKING ( img1, img2, operation ) {
   for i,j,k ← 0 to Max-Dimension
        v-result[i][j][k] = OPERATION ( img1[i][j][k] , img2[i][j][k] );
        return v-result;
}

BACKGROUND-CORRECTION ( image ) {

        m ← generate mask background: –2000, foreground: 0
        MASKING( image, m, "+" );

}
```

Algorithm 5.1: Lung Segmentation

```
LUNG-SEGMENTATION ( image ) {
// Initially the main structures appearing are: ribcage (white),
// lung with vessels and airways (grey), air outside the human body (grey).

        preprocessed-image  ← PREPROCESSING( image );
        no-ribcage          ← RIBCAGE-ELIMINATION( preprocessed-image );
        mask                ← LUNG-MASK-GENERATION( no-ribcage );
        segmented-lung      ← MASKING( image, mask, "*" );
        return BACKGROUND-CORRECTION( segmented-lung );

}
PREPROCESSING ( image ) {
        image1 ← apply a median filter with a kernel of 2x2 on image;
        image2 ← apply a mean filter with a kernel of 1x3 on image1;
        return image2;
}

RIBCAGE-ELIMINATION ( image ) {

        change the image's border color: background → white;
        V3BFILL( image );       // fills region connected to border with background
        negate the image;
        threshold the image;

}

LUNG-MASK-GENERATION ( image ) {

        ccSet ← perform 3D connected components analysis

        // Keep only the lung
        for each component c in ccSet {
                if      c != largest || c adjacent to edge of image
                then    ERASE-COMPONENT( c );
                        ccSet -= c;
        }

        // Create mask
        perform a closing operation on ccSet
        threshold ccSet

}
```

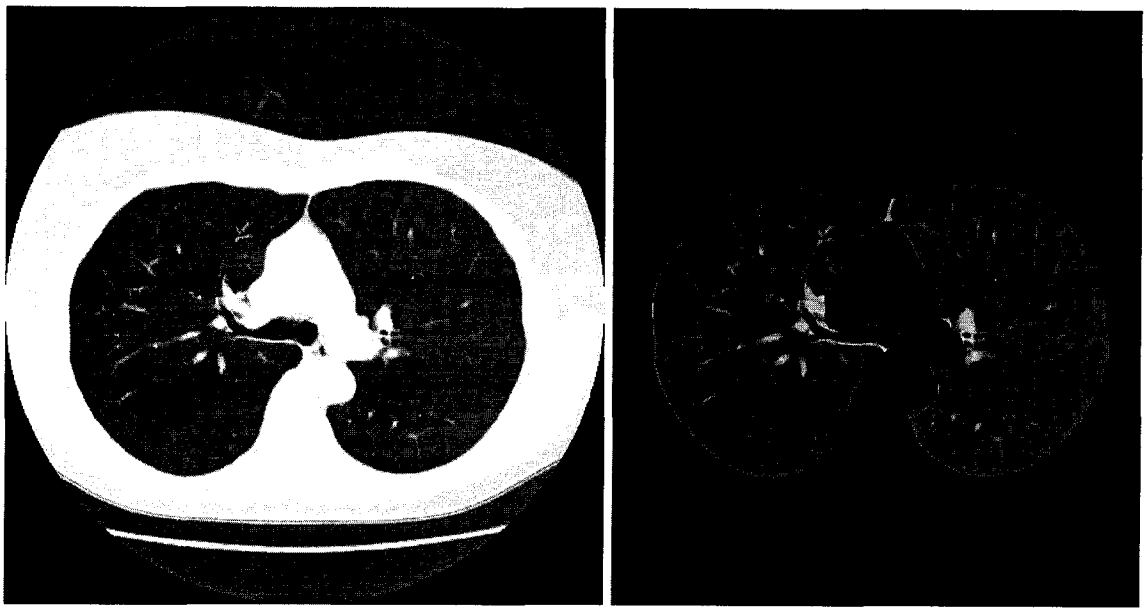

Figure 5.3: A view of the lung before *(left)* and after *(right)* segmentation.

5.3.2 Segmentation of the Lung with Vessels Removal

The segmentation continues with the removal of the vasculature. The vascular removal starts with a noise reduction step implemented with a symmetric median filter.

Most of the vasculature appears in a much brighter gray level than the rest of the lung. An appropriate thresholding operation will be able to identify most of the vasculature. Connected components analysis is used to detect and keep only those components larger than a specific volume. The very small components that are eliminated are a result of noise and do not represent vessels. However, because the threshold used in the previous step was intentionally chosen at a somewhat high level, the next step will consist of a series of morphological

operations. These operations are able to extend and refine the boundaries of the identified vessels.

As final step, the segmented lung volume will be masked using the results of the vascular removal algorithm. A background re-labeling with voxels values outside of the range of data can be performed.

Algorithm 5.2: Lung Segmentation with Vascular Removal

```
VASCULAR-SEGMENTATION ( image ) {
// The input image is the segmented lung. The result of this step is the segmented lung
// without vessels.

    PREPROCESSING();

    // Process large vessels
    mask1              ← VASCULATURE-MASK-GEN( th1, size1, image );
    lung-without-vessels1 ← MASKING( image, mask, "&" );
    processed1         ← BACKGROUND-CORRECTION( lung-without-vessels1 );

    // Process small vessels
    mask2              ← VASCULATURE-MASK-GEN( th2, size2, processed1 );
    lung-without-vessels2 ← MASKING( processed1, mask2, "&" );
    processed2         ← BACKGROUND-CORRECTION( lung-without-vessels2 );

    return processed2;

}

PREPROCESSING ( image ) {

    apply a median filter with a kernel of 2x2 on image

}
```

```
VASCULATURE-MASK-GEN ( image ) {

        threshold image
        ccSet ← perform 3D connected components analysis

        // eliminate small components corresponding to noise
        for each component c in ccSet
                if      c < size
                then    ERASE-COMPONENT( c );
                        ccSet -= c;

}
```

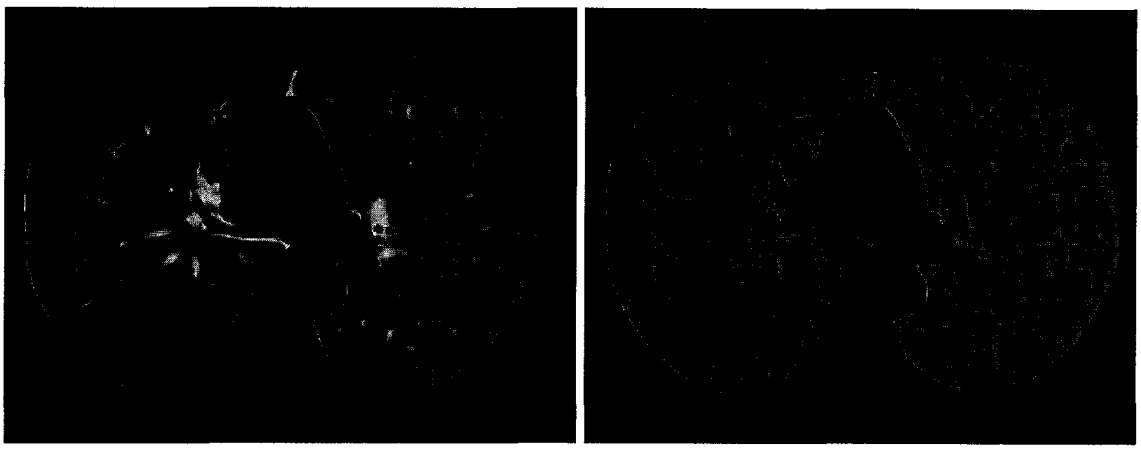

Figure 5.4: 2D image from a segmented lung volume *(left)*;corresponding image from the segmented parenchymal volume following vascular removal *(right)*.

5.3.3 Segmentation of the Lung with Airways Removal

As previously stated, most of the existing lung segmentation algorithms do not remove the airways present inside the lungs, but for us this process is very necessary. Trachea and bronchi contain air. Emphysematous areas also contain air. However due to partial volume errors the intensity of these structures do not consist of a fixed value (such as 0 for the air) but rather belong to a larger intensity range, close to the value for air. In a CT scan image, most of the time, the airways

appear slightly darker than the emphysematous areas. One reason is that the trachea and the bronchi are larger than most of the LAA areas, and unlike parenchyma, do not contain other structures that might vary the intensity values. Partial volume errors are diminished toward the center of the area and affect a smaller percent of pixels out of the total area. However this is not always the rule, thus, differentiation between emphysematous areas and airways purely based on the intensity range is not possible. In quantifying emphysema, the affected lung areas have to be distinguished from other areas. As a start, the implementation of an algorithm that will segment the airways from the segmented parenchyma is essential.

Besides its importance for the current work, an algorithm that correctly generates an image of the lung airways will create input image for future research in lung airways or in quantification of other COPD diseases. Even in quantification of pulmonary emphysema, a different approach than the one taken in this work, can be the study of the degree distal airspace enlargement. Gould, et al[20], consider distal airspace enlargement a possible sign of emphysema. The necessary characteristic defining emphysema: "an increase in size of airspaces distal to the terminal bronchioles," implies that the ratio between the surface areas of their walls to the volume of such airspaces is reduced in emphysema.

The privilege of having a large database of CT scan images allowed us to spend many hours observing how airways and lungs expand throughout the body (along the z-axis), and to understand the morphological properties that can be

generalized across patients as well as the ones that differ from one patient to another, thus requiring a heuristic analysis.

A few morphological properties that have to be considered:

1. Lungs are positioned inside the rib cage. Even if the rib cage has been eliminated in the previous segmentation step, the image of the apices of the lung suffers from noise and streaking artifacts. Problems created by noise pixels are addressed by using an adaptive neighborhood in the seed selection algorithm.

2. The relative 2D transversal position of the lungs and trachea is important information. In most of the cases, the CT scan starts well above the lung; thus the trachea will be the first structure that will appear in the CT data set. Yet, this is not always the case. The fact that the trachea is always located in the center of the images, the apices of the lungs are located in the lower right and left regions of the scan, and that right lung is larger and taller than the left will be used in choosing the appropriate search for trachea seed.

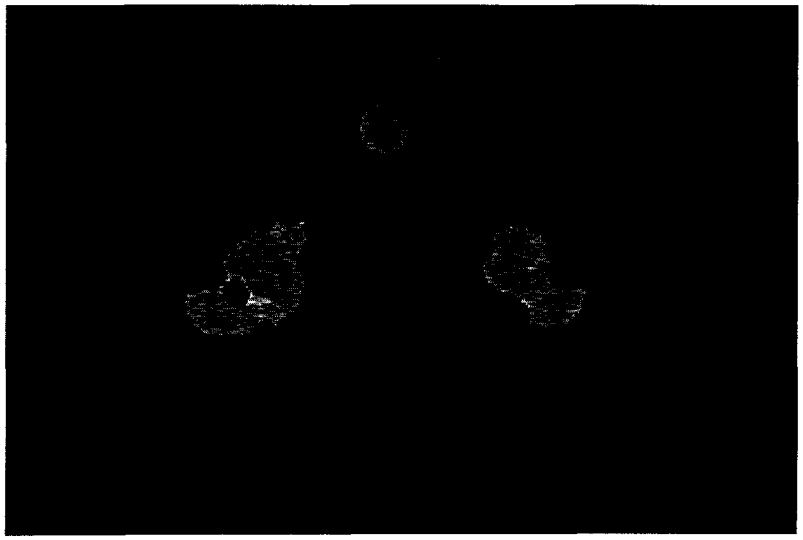

Figure 5.5: The usual spatial distribution of the lung and trachea near the apex.

3. The trachea doesn't always split evenly into the two main bronchi. After the split, the main bronchi branch into secondary and tertiary bronchi that will expand in different angles. This is also illustrated by figure 5.4.

4. Lung airways have a tree-like structure. After each branching, the size of the airway branches decrease.

5. Airways contain air. Emphysematous areas of parenchyma are also marked by holes filled with air. The intensity range of airways and some parenchyma areas might overlap to a very large extent.

6. The leaves of the airway tree do not merge into the lung parenchyma simultaneously. Furthermore, some might just graze the parenchyma at some point, but afterwards continue expanding before a final merge.

The next two sections will present two different approaches to segmenting trachea and bronchi. There will be the burrowing approach and component tracking approach.

5.3.3.1 Segmentation of Trachea and Bronchi with Split-Detection and Downward Growth Using Burrowing

This algorithm breaks the airways tracing process into three distinct steps without the need for human interaction: trachea, bronchi, and bronchiole segmentation. After the first stage, components of the left and right airway network are kept track of as a group. A mask of the airways inside the lung is generated. The mask

will have different labels for the trachea (L1), left (L2) and right bronchi (L3); this makes it possible to segment only one of the mentioned airway structures.

The initial design for tracing the airways used simple region growing and 3D connected components analysis. Briefly, we find a single seed that belongs to trachea, copy and label the seed and all its neighbors in 3D within a certain intensity range into the new image. We repeat the process until the trachea splits. This will mark the beginning of the bronchi. From this point, grow the region into the new image using different labels to represent the right and left bronchi.

While our initial approach may be suitable for regular image processing use, it doesn't fair well when faced with the irregularities of the human body. Left to its own devices, the first approach easily mistakes parenchyma for airway and small branches for the major bifurcations. Our two major contributions to the solution of these problems are heuristic split-detection and burrowing with backtracking. The former performs a multi-slice analysis on branches to determine their true nature. The latter departs from traditional 3D region growing, replacing it with copying and 2D expansion, backing up and correcting itself with limited growth when parenchyma is encountered.

In the development of our approach, a number of issues and problems needed to be addressed and overcome.

The first issue that we addressed was how to pick the correct set of seeds corresponding to the trachea. A seed is chosen by recognizing the gray-level range corresponding to trachea. Since the first slices that are close to the apices of

the lung suffer from noise and streaking artifacts (property 1), the search for only one seed or even a few might not be sufficient for the 3D region growing process in the next step. This problem is intensified when the seed is surrounded by noise pixels. Here the construction of an adaptive neighborhood with enough redundant seeds is appropriate. The lung parenchyma often has pixels in the same range as the trachea. If an inappropriate scanning order for the seed is made, parenchyma might be chosen in the seed selection stage. This issue is further exacerbated because of our need to choose multiple redundant seeds. Based on the second property, the scan for seeds on each slice has been done vertically ($y_{hi} \rightarrow y_{lo}$) starting from the top and working right to left ($x_{hi} \rightarrow x_{lo}$). This gives preference to the trachea. Also, since most components were taller vertically than they were wide horizontally, this increased the chance that all seeds being picked were in the trachea, as opposed to picking some from the trachea and some from the parenchyma. Finally, size checks were added to discard the initial seed set if its 2D growth resulted in a too large region, indicating parenchyma.

Once the correct seed set is selected, 3D region growing based on intensity range properties, and connected component analysis is performed until the trachea splits into right and left bronchi. Voxels corresponding to the trachea in the original image are copied and labeled (L1) into the new image that will generate the airways mask.

Simple detection of a split can be done by comparing the size of the region obtained through 3D growth with the size of any chosen 2D component within the

same slice. It is clear that if the sizes are much different then the component doesn't encapsulate the entire region, and there must be a satellite that split from it. Small differences are not considered splits, as it is possible for noise to isolate small areas. An allowance of one hundred pixels was found to be optimal during experimentation.

Alas, simple detection results in many false-positives. Based on morphological property 3, our research showed that during some splits while one of the components still represented the trachea, the other is due to a small upward expansion of the right bronchi, as opposed to the main bronchi bifurcations. Thus, detecting a single region split doesn't necessarily mean that it was the trachea split. We can only be convinced that it is a complete trachea to bronchi split after seeing it carried across a couple of slices. Not only do multiple slices need to have splits, the split must be in the same general area. Of further concern here was that several consecutive slices may have these upwards growths in different areas that are unrelated to one another, thus "tricking" the algorithm. Split continuity detection, by checking their juxtaposition, was added. This allowed 3D connected component analysis to determine that two "split" regions were later reconnected. This methodology is illustrated in figure 5.6.

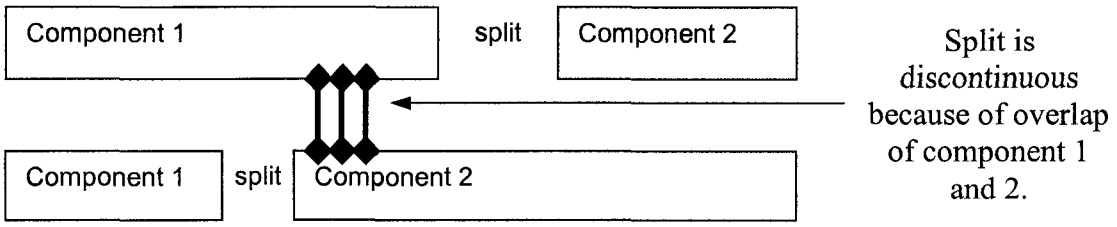

Figure 5.6: Split detection in the airways segmentation algorithm.

After the split, the algorithm begins the sensitive process of tracing the bronchi. At any slice there is the chance of airways colliding with parenchyma. It therefore became crucial to regularly check the slices during a run.

We examined statistical characteristics (such as variance) of the unwanted components. However, there was no discernable correlation between any statistical measure and areas of the traced image that contained parenchyma. Drawing on the lesson learned from the size solution to choosing non-parenchyma seeds during the tracing, we were able to solve our problem by removing components that had gotten either too large or too small. Massive components were clearly lung. Miniscule components were often unrelated noise or small lung fragments. On the off-chance case that they represented airways, their loss would hardly affect the computation.

Undesirable components were eliminated, but only after carrying their error to the previous and next slices. This is due to the nature of the standard 3D growing algorithm. To prevent the cascading of errors, we developed the "burrowing" technique. Think of image burrowing like a gopher that digs a long

hole directly down in the soil. With this, the progression involves expanding components only in 2D, cleaning up based on size, and then copying (as opposed to 3D region growing) selected pixels to the next slice where the destination pixels are within the specified threshold range. Any undesirable components are eliminated long before they are transferred to the next slice, thus the error propagation is stopped immediately.

To deal with the continually shrinking trachea, bronchi, and bronchioles, the algorithm needed to adapt its criteria. As it descended lower into the lung, the acceptable threshold range narrowed. Also, the region size range and growth was tightened using an adaptive setting based on the branching level. Furthermore, when it came to the bronchioles, instead of eliminating components that have grown to encapsulate lung mass, these components were simply burrowed but no 2D growth was performed. While this caused the loss of airways as they bend slightly, it gave better results than stopping the process on earlier slices.

The output of the airways tracing process is a labeled mask of the airways. By masking the airways out of the segmented lung, an image of the segmented lung with airway removal is generated. The process starts with noise filtering of the airways mask followed by a thresholding operation. A dilation operation is applied to compensate for subtle difference between the shape of trachea mask and the original image. The 3D growing of the trachea might have left out some of the voxels belonging to the trachea border, since, due to partial volume errors, the voxels may have been outside of the considered intensity range. A second

thresholding operation sets the airways voxels to 0 and 1 otherwise. The final image of the segmented lung with airways removal will be the result of a binary multiplication between the last and the original image.

Algorithm 5.3: First Lung Segmentation with Airways Removal

5.3a Airways Tracing

```
AIRWAY-TRACE ( im ) {
// From a segmented lung image a mask of the airways is generated.

    AirwayIntensityRange ← { bimin:0...bimax:180 }

    nim ← create new blank image of equal size

    // populate adaptive neighborhood
    start-slice ← find slice of im
    do      find pixel im[slice].p where slice >= start-slice
            if      im.p ∈ AirwayIntensityRange
            then    nim.p ← seed-label
                    seed-count++;
    until seed-count = redundantSeedNumber

    // Grow in 3D and label trachea
    slice ← 0
    do      3D-REGION-GROWING( slice );
            label trachea region on nim
            slice++;
    until   SPLIT-DETECTED( slice )
    split-slice ← slice

    // the Burrowing Technique
    label left bronchi region on nim
    label right bronchi region on nim

    for each slice > split-slice
            for region-label ← { left, right }
                    ELIMINATEUNDESIRED( region-label, slice );
                    BURROWDOWN( region-label, slice, slice + 1, allowGrowth );
```

```
            // Detect region merging into lung parenchyma caused
            // by burrow & growth
            if      REGION-SIZE-2D( region-label, slice + 1) >
                    growthFactor * REGION-SIZE-2D( region-label, slice )
            then    clear pixels created by burrowing
                    BURROWDOWN( region-label, slice, slice + 1, noGrowth );

}


ELIMINATEUNDESIRED ( region, slice ) {

    for each component c ∈ slice where c = region
            // Noise components that will not affect computation
            if      c < minRegionSize
            then    clear c
            // Regions that have significantly expanded from the previous slice contain
            // parenchyma
            if      c > growthFactor * region ∈ slice – 1
            then    clear c
}

BURROWDOWN( region-label, source, destination, growth_requested ) {

    for each im[destination].p ∈ AirwayIntensityRange
            copy labeled pixels: nim[source].p → nim[destination].p

    if      growth_requested = allowGrowth
    then    2D-REGION-GROWING( slice );

}


COMPONENT-SIZE-2D( slice ) {
// Selects any one non-background component it can find on a slice and sizes it.

}


REGION-SIZE-2D( region-label, slice ) {
// Counts the number of pixels on a slice with the specified label.

}
```

```
SPLIT-DETECTED ( slice ) {
// Determines whether or not the trachea has divided into the left and right bronchi.

        // Find a split
        if      REGION-SIZE-2D( slice ) – COMPONENT-SIZE-2D( slice ) < sizeDifference
        then    return no split detected

        // Extend split to next slice
        label two components with region1-label and region2-label
        3D-REGION-GROWING( region1-label );
        3D-REGION-GROWING( region2-label );

        // Determines legitimacy
        return ( IS3DCONNECTED( region1-label, slice, region2-label, slice + 1 ) |
                 IS3DCONNECTED( region2-label, slice, region1-label, slice + 1 ) );

}
```

5.3.b Airway Removal

```
AIRWAY-REMOVAL( segmented-lung, airway-mask ) {
// Given a lung and a mask of its airway, produces lung image without airways.

        // Preprocess the airway-mask, remove noise, remove holes, and reset mask values
        filtered    ← perform a median filter with a kernel of 1x3 on airway-mask
        thres1      ← threshold filtered with a value of th1

        // Compensate for subtle difference between shape of trachea mask and original
image
        dilated     ← perform a dilation operation on thres1
        new-airMask ← threshold dilated with a value of th2

        return MASKING( segmented-lung, new-airMask, "&" );

}
```

Algorithm 5.3 was relatively successful up until the bronchiole stage. In this last stage the segmentation stopped early since the burrowing technique would usually yield lung tissue. The algorithm could not be made precise enough to

function at that level. This is because although the left and right airways split into many independent components, the algorithm considers two complete regions. This means that if a single bronchiole hits the lung, the entire side is no longer considered. Furthermore, this algorithmic vagueness forced us to set arbitrary limits on minimum and maximum sizes. These estimates, such as a maximum size allowance of ten-thousand pixels, were based on trial-and-error and never worked unilaterally across the cases. Instead the specific growth, the question of whether or not an individual component (not region) has doubled or tripled in size needed to be taken into account.

5.3.3.2 Segmentation of Trachea and Bronchi with Individual Component Tracking

In the previous algorithm, the left and right airways split into many components, yet are considered one group each to our algorithm. We soon realized that the key to increasing the accuracy is to study the specific growth of individual components. Because there was no support for this, the algorithm was rewritten from scratch. The second program keeps track of every component created and destroyed through splitting and merging; they are no longer lumped into just left and right regions. While our second approach incorporated the important insights of our first method, the new algorithm no longer has distinct stages; one methodology was applied from trachea to bronchioles. Each component is assigned its own label. A table tracks the size of the components during the

movement from slice to slice. During the process, size and threshold criteria were adjusted automatically to compensate for the airway type.

The component-tracking table is dynamic. It is shrunk and grown to deal with the number of active components on each slice. Moreover, components that split are relabeled with a new value, but are still associated with their ancestors so that the size of the component over its life can be monitored for abnormal changes due to lung contact. The same is true of merging components. With this table, the algorithm was able to overcome the two biggest limitations of its predecessor. The first is ability to track airways that branch upwards. The second is the ability to precisely deal with the smallest of airways through relative growth checks, instead of hard-coded size ranges.

The airway removal routine is improved from the first algorithm. This is done by incorporating the possibility of choosing the type of output image, depending on future needs. Either the segmented lung airways image, or the image of the segmented lung without the airways can be gotten.

The second algorithm proved superior on all tests. Its single stage process was faster and more robust in anomalous cases. Its individualized component tracking allowed it to follow airways for a greater distance and with more accuracy, therefore resulting in a deeper and cleaner segmentation.

Algorithm 5.4: Second Lung Segmentation with Airways Removal

5.4a Airways Tracing

```
AIRWAY-TRACE ( im ) {
// From a segmented lung image a mask of the airways is generated.

    AirwayIntensityRange ← { bimin:0...bimax:180 }

    nim ← create new blank image of equal size

    // populate adaptive neighborhood
    start-slice ← find slice of im
    do      find pixel im[slice].p where slice >= start-slice
            if      im.p ∈ AirwayIntensityRange
            then    nim.p ← seed-label
                    seed-count++;
    until seed-count = redundantSeedNumber

    // storage to keep track of found components
    integer componentSize[max_#_components][#_of_slices][ancestors];
    2D-COMPONENT-GROWING( seed-label, start-slice );
    #-components ← 1;

    // downwards then upwards growth
    for direction ← { downwards, upwards }
            BURROWDOWN( previous_slice, current_slice );

            // grows within the appropriate threshold range
            for component_label ← 1 to #_components
                    2D-COMPONENT-GROWING( component_label, current_slice );

            #_components, componentSize[current_slice]
                                            ← SIZECOMPONENTS(current_slice);

            ELIMINATEUNDESIRED( current_slice );

            // Adaptive Thresholding based on morphological properties
            if      slice = bronchiStart & direction = downwards
            then    bimax -= thresholdAdjust;

            if      slice = bronchiStart & direction = upwards
            then    bimax += thresholdAdjust;

}
```

```
BURROWDOWN( source, destination, growth_requested ) {

        for each pixel p
                if      im[destination].p ∈ AirwayIntensityRange &
                        nim[source].p is labelled
                then    nim[source].p → nim[destination].p

}


2D-COMPONENT-GROWING( component_label, slice ) {
// Grows components in 2D

        for each pixel im.p ∈ slice
                if      nim.p = component_label
                then    for each 2D neighbor im.n of im.p
                                if      im.n ∈ AcceptableBronchiIntensityRange
                                then    nim.n ← component_color

}
SIZECOMPONENTS( slice ) {
// Computes the current and ancestor size of each component on a slice.

        for each component ∈ nim[slice]
                // Airway merging
                if      a connected component has multiple label colors
                then    relabel with smallest label value
                        set ancestor size is a fraction of ancestor

        // Airway splitting
        if      multiple components have same label
        then    relabel each with new value
                set ancestor size is sum of ancestors

        return count and size of components

}


ELIMINATEUNDESIRED( slice ) {

        if      slice >= bronchioleStart
        then    growthFactor ← 1.4
        else    growthFactor ← 3.1
```

```
        clear components ∈ nim[slice] < minComponentSize;
        clear components ∈ nim[slice] > maxComponentSize;
        clear components ∈ nim[slice] > growthFactor * componentSize[ancestor];

}
```

5.4b Airway Removal

```
AIRWAY-REMOVAL( segmented-lung, airway-mask ) {
// Given a lung and a mask of its airway, produces either lung image without airways or
an
// airway image.

        // Preprocess the airway-mask, remove noise, remove holes, and reset mask values
        filtered      ← perform a median filter with a kernel of 1x3 on airway-mask
        thres1        ← threshold filtered with a value of th1

        // Compensate for subtle difference between shape of trachea mask
        // and original image
        dilated       ← perform a dilation operation on thres1
        new-airMask   ← threshold dilated with a value of th2

        if    we want airway removal
        then  new-lungMask ← threshold segmented-lung th1
              sub-image    ← MASKING( new-lungMask, new-airMask, "-" );
              output       ← MASKING( segmented-lung, sub-image, "*" );


        // Generate image of airway
        else  output       ← MASKING( segmented-lung, new-airMask, "*" );

        return BACKGROUND-CORRECTION( output );

}
```

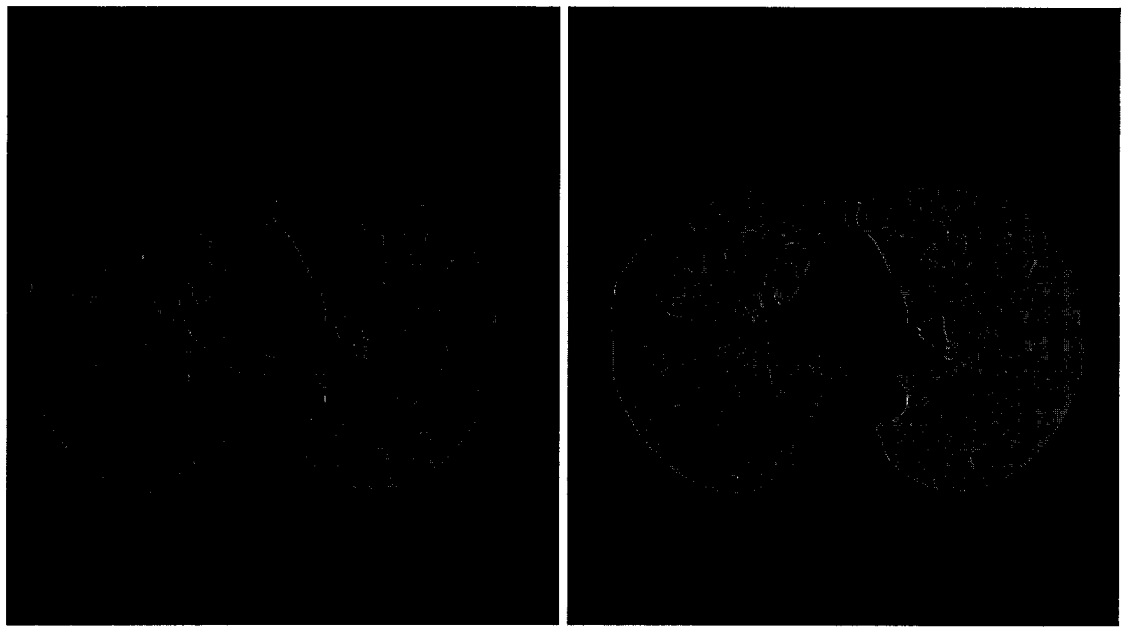

Figure 5.7: An image of a segmented lung before and after airways removal.

5.4 Evaluation of the Segmentation Algorithm on Low-Dose CT-Scan Images

The segmentation algorithms were able to automatically segment the vast majority of the low-dose CT scans considered for the study. There were originally 86 cases that were evaluated in the selection process; four cases had to be excluded due to artifacts that were sufficiently severe to prevent accurate segmentation. The eliminated CT scan sets were highly corrupted as a result of patient movement and presence of a pacemaker. The remaining cases were reviewed by an experienced thoracic radiologist to determine the correctness of the segmentation. Overall, the

algorithms produced "correct" segmentations in 94% (77/82) of the considered CT scan sets.

The evaluation process performed by pulmonary radiologist using visual scores on a 1-3 scale (table 5.1) consists of three independent steps:

1. evaluation of the lung segmentation
2. evaluation of the lung segmentation with vessels removal
3. evaluation of the lung segmentation with airways removal

Visual Score Scale:	**1**	very good (correct) segmentation
	2	good with slight imperfection segmentation
	3	unacceptable segmentation

Table 5.1: Visual scores for lung segmentation algorithm.

Seventy-seven cases have been found correct throughout all three validation-steps.

Two cases were graded as 2, in the evaluation of the lung segmentation with vessels removal. The vessels in the apices of the lung are estimated to be larger then their correct volume. This is a direct consequence of the high noise present in that area.

Another three cases showed minor imperfection in the lung segmentation with airways removal; the algorithm failed to remove in one of the slices a region of the left bronchi upwards expansion.

The results of the evaluation are summarized in table 5.2

Score / Algorithm	Very Good (1)	Good (2)	Unacceptable (3)
Selection	-	-	4
Segmentation			
Step 1	82	0	0
Step 2	78	2	0
Step 3	77	3	0

Table 5.2: Evaluation of segmentation algorithm.

Of the cases that were deemed to be correctly segmented by the radiologist, the quality of the segmentation of the lung volumes and the removal of the majority of pulmonary vasculature and airways was generally uniform. In some especially noisy images, the quality of the segmentation was somewhat reduced in the lung apices and, more rarely, in regions of dependent changes in the posterior portions of the lung bases; though the extent of the errors was sufficiently minor to be disregarded by the radiologist in his assessment.

A good lung segmentation program from low-dose CT scans would allow for the concurrent evaluation of emphysema in the context of screening for other diseases, yielding additional diagnostic information with no additional radiation exposure. Note that the quality of low-dose radiation images is noticeably reduced from that which is typical of standard-dose clinical scans, and we would therefore expect these new algorithms to achieve even better performance in standard-dose settings.

The next subchapters will analyze in more detail the behavior of the segmentation algorithms in scans with different noise degrees.

5.5 Noise Sensitivity Analysis[64]

The performance of any segmentation algorithm may vary depending on the degree of noise present. We begin with a look at types of noise in CT images. The later sections discuss the effects of a higher or lower noise level than the one present in our initial low-dose radiation dataset. For our study, twenty cases were randomly chosen from the "very good" segmentation cases previously evaluated.

5.5.1 An Overview of Types and Reasons of the Noise Presence

Images are degraded by random errors that are usually called noise. Noise can occur during any step of image handling, starting with image capture and ending with image reconstruction and processing. Noise can be dependent or not on image content.

Quantum noise consists of randomness in the reconstructed CT image attenuation values. X-ray photon production, interaction with tissues, and detection has a statistical nature that results in error in the projection measurements. Quantum noise can be diminished by increasing the radiation dose; however this might not always be in the best interest of the patient.

One essential physical artifact is beam hardening. X-ray beams reaching a specific location inside the body, coming from different directions, and passing different density tissues do not have same spectra and thus they will be attenuated differently at the destination. Beam hardening is the phenomenon that a

polychromatic x-ray beam as the one use in CT scans becomes more penetrating or harder as it traverses the body. "For any fixed initial x-ray spectrum and tissue type, the process of beam hardening represents a monotonic increase in beam hardness as a function of thickness traversed". As result the effective attenuation coefficient is higher for beams that penetrate through the edge of the object.[64]

A common artifact in computed tomography is the streak artifact. There are different reasons that streak artifacts can be created. It can occur due to inconsistent attenuation measurements, the presence of a highly attenuating object as a piece of metal, as well as sharp edge transition in the human body. The last type is present in all segmented CT scans and is triggered by the sharp edge transition from high density ribcage bones to low density soft tissues of the lungs.

"Motion artifacts happen whenever image acquisition time takes longer than the time over which physiological motion occurs in the body region of interest".[64] Motion artifacts are usually not a problem in scanning body extremities or the brain but represent an important issue in the case of thorax CT scans. During the chest scan the patient must hold his/her breath to minimize the motion artifacts. This becomes very difficult especially if the patient suffers from respiratory pulmonary diseases as emphysema or asthma. Motion artifacts might be generated by respiratory and/or cardiac movements. Small range movements will have a blurring effect in the CT scan image. In my study, motion artifacts due to large range movement have been eliminated in the selection process.

5.5.2 Algorithm Performance in Scans with Lower Degree of Noise

The degree of noise in the original image has been reduced by applying a median filter with a 3x3 kernel. This decreased part of the impulse noise and streaking artifacts.

Out of the total number of examined cases, the pulmonary expert evaluated eighteen cases as "very good" in all the three steps of segmentation. The remaining two cases received a "good" segmentation score. Each of these faulted images had problems toward the end of the CT scan. The lower portion of the lungs exhibited some components (one component for one of the cases, and two components from the second) that allowed their growth into the parenchyma tissue by a small amount of pixels (less than 15 pixels). This is a consequence of the smoothing process of the image. When the airways become small, their range intensity greatly overlaps that of the parenchymal tissue. We were able to correct these two segmentation cases by interactively providing the program a higher value than the default one for the starting adaptive threshold at the level of tertiary bronchi.

5.5.3 Algorithm Performance in Scans with Higher Degree of Noise

In order to increase the degree of noise in the original scans, an algorithm for noise enhancement[55] has been applied to a randomly subset of the previously selected cases. The algorithm will generate zero mean additive Gaussian noise.

Roughly, the noise algorithm builds a Gaussian curve. For every pixel of the original, points of the curve are added or subtracted from the original values. The extremities are corrected so that each doesn't go beyond the maximum or minimum value in the image prior to noise addition.[55]

In the third phase of the algorithm, noise pixels are not taken in consideration during the size computation of an individual component, but are considered in the CCA done at the level of vessels detection. Understanding this, we accordingly adjusted the size of minimum component size allowed prior to testing the segmentation. We increased the minimum area size of the accepted 2D connected component in the process of vascular removal and decreased the size of a 2D connected component in the process of airways removal. The radiologist determined that the outputted images were at the same level of quality as before.

5.5.4 Aspects of Segmentation Algorithm Sensitive to Noise

The presence of noise has been taken in consideration in many steps of the algorithm's implementation. Most of the preprocessing steps use some type of filtering with kernels of a specific size. The filtering method is chosen based on the type and degree of the noise present on the image. A radical decrease in the noise degree might require a smaller kernel as well as fewer filtering passes; similarly, a higher degree of noise will call for a higher number of filtering passes with larger kernel sizes. Filtering is applied during all of the main parts of the segmentation algorithm: the preprocessing step of lung segmentation, segmentation with vascular removal, and airways removal.

The number of selected seeds for trachea tracing depends on the noise level. A low degree of noise will require a fewer number of seeds, since the probability is low for an initial seed to be surrounded by noise pixels; and, as it is expected; the converse is true for a higher noise degree.

Counting the number of pixels within a specific intensity range of interest is often done throughout the algorithm; this is necessary in setting the limits on specific component sizes. Here, noise pixels are not considered in the counting. A decrease in the degree of noise will move some pixel values from outside the range into the range of interest. The number of noise pixels will decrease while the number of the pixels in the range will rise. As result the benchmarks for component size will have to change.

6 QUANTIFICATION ANALYSIS BASED ON THE EMPHYSEMA INDEX

Over the last few years the analysis of emphysema in CT scans has developed into an active area in computer-aided diagnosis. The literature review chapter presented an overview of the research that has been done toward the development and improvement of automated methods for detecting emphysema and quantifying its extent and severity. Most of the cited papers indicate that there is a high correlation between emphysema assessments obtained with CT densitometry methods and emphysema assessments done by visual scores. One of the studies[5] concluded that the CT densitometry methods were in fact superior to visual grading methods.

The current study extends the work reviewed to automated analysis of *low-dose* helical CT scans. This represents a challenge since in such CT scans, the reduced signal-to-noise ratio (SNR), due to quantum noise, compromises the ability of detecting subtle variations in the attenuation of the lung tissue.

The first set of quantification analysis is based on current methods and uses the fully automated lung segmentation software described previously in chapter five.

There are several goals achieved by this work:

- In the reviewed literature, quantification of emphysema has been done solely on standard – radiation CT scan images. This work will investigate the extent to which automated computer analysis of low-dose helical CT scans can accurately estimate the severity of emphysema.
- A good validation of the preliminary quantitative results with visual scores assessment will enhance the credibility of the segmentation algorithm.
- The quantitative results generated by the current methods may be used in future comparison with results of newly developed methods.

6.1 Quantitative Results Based on Currently Used Methods

We applied two currently used methods for quantifying emphysema, to a large CT scan database. We then assessed the severity on low dose helical CT scans, through the computation of an emphysema index.

6.1.1 Case Selection

Cases have been from a database of low-dose CT screening exams acquired in the calendar year 2001. The scans were reviewed by experienced thoracic radiologists and given a severity score on a four-point scale (normal, mild, moderate, severe). The final set of cases considered included twenty cases from each of the mentioned categories. Our goal was to study the relationship between the automated metrics and the visual assessments made by the radiologists. Metrics were obtained using two different methods: the four-slice method and the total volumetric evaluation method.

6.1.2 The Four-Slice Method and the Total Volumetric Evaluation Method

Each of the two studied methods was based on quantifying the relative percentage of emphysematous tissue within a portion of the segmented lung volume, and thus were derivatives of the percent of low attenuation area (LAA%) method. The LAA% method computes the relative area of low attenuation within one or more 2D CT slices or within the entire lung volume.

In order to determine which voxels are contained in the low attenuation areas, typically a single or dual threshold operation is applied. The attenuation values used for these thresholds vary in the reported literature, depending on the particular research objective; the upper threshold is typically set between –960 and

–910HU while the lower threshold typically ranges from –1024 to –980HU. In our case, the lower and upper thresholds were determined using a series of preliminary experiments within a sample set of eight cases exhibiting different degrees of emphysema (two in each category defined by visual scores). We considered voxels with attenuation between -1024 and -950 HU as members in the set of LAA voxels. These specific threshold values yielded the wider difference between each pair of cases with different emphysema scores.

Using an emphysema index as the basis for quantifying the degree of emphysema, we have studied two methods of emphysema assessment:

- average emphysema index computed in four CT slices
- emphysema index computed in overall lung volume

The first method is the simplest and most traditional. Given a thoracic CT scan, four 2D axial images (slices) are selected. These images are uniformly spread throughout the lung volume. The lung regions in each of these images were already segmented by our lung segmentation algorithm. Be aware, this is not always the case; usually researchers do not have the possibility of accessing a complete CT-scan set that will cover the entire lung. In that case, after the four slices are selected, the segmentation process is applied separately on each of the slices. An emphysema index is computed for each slice. The average of the four index values will represent an estimate of the overall extent of emphysema in the total lung volume.

For this method we defined the emphysema index, $E_{4\text{-}slice}$, as:

(6.1) $$E_{4-slice} = (\sum_{i=1}^{4} E_{slice(i)})/4$$

where the emphysema index is computed for each slice as:

(6.2) $$E_{slice(i)} = \frac{|\{v(x,y,z) \mid -1024HU \le H(v(x,y,z)) \le -950HU\}|}{|\{v(x,y,z) \mid v(x,y,z) \in segmented\_parenchymal\_volume_{slice}\}|}$$

where $H(v(x,y,z))$ represents the intensity in hounsfield units of the voxel with coordinates x, y, z.

The second method, the total volumetric method, requires the segmentation of the entire 3D CT-dataset. The emphysema index is then computed as the percentage of LAA in the total lung parenchymal volume. Here we define the emphysema index, as:

(6.3) $$E_{volume} = \frac{|\{v(x,y,z) \mid -1024HU \le H(v(x,y,z)) \le -950HU\}|}{|\{v(x,y,z) \mid v(x,y,z) \in segmented\_parenchymal\_volume\}|}$$

The value of the emphysema index E was computed from segmented lung images with:

- the total segmented lung volume
- segmented parenchyma volume after the vascular removal
- segmented parenchyma volume after the vascular and airways removal

6.1.3 Current Methods' Results

We examined the correlation between the four-slice results, the total lung volume results, and the emphysema score determined by the radiologists. While there was certainly overlap between the distributions of E values for each category, it appears that there is a promising correspondence between the values of emphysema parameter E and the emphysema assessments done through visual scores.

Statistical analysis of the quantification methods results on each segmentation sets (lung, lung with vessel removal, lung with vessels and airways removal) has been done. For each set we computed the mean, standard error of mean, standard deviation and variance. The standard error of the mean represents a measure of the variability of the mean of the sample as an estimate of the true value of the population mean. Standard deviation is a measure of variability, quantifying how much the values vary from each other. Variance is also considered a measure of variability; numerically it is the square of the standard deviation.

To determine if there is a significant difference on the emphysema index between different categories (normal, mild, moderate, severe) and if there is an increasing trend in the emphysema index proportional to the increase of its severity, we determined the *p-value.* This represents the probability that an indicated relationship between variables is due to sampling error, the measured

probability of a finding occurring, by chance alone, given that the null hypothesis is actually true.

To check if there are significant differences between categories we defined the null hypothesis as:

(6.4) H_{01}: *meanE_mild* = *meanE_normal*

H_{02}: *meanE_moderate* = *meanE_mild*

H_{03}: *meanE_severe* = *meanE_moderate*

meaning that there is no difference in the emphysema index between different severity categories evaluated by radiologists through visual scores.

To determine if there is an increasing trend in the emphysema index with the increase of severity we defined the alternative hypothesis as:

(6.5) H_{11}: *meanE_mild* > *meanE_normal*

H_{12}: *meanE_moderate* > *meanE_mild*

H_{13}: *meanE_severe* > *meanE_moderate*

meaning that there is an increasing trend in the emphysema index with increase of emphysema severity.

In most clinical trials[65] "statistical significance means the likelihood that the difference found between groups could have occurred by chance alone is less than 1 in 100. This is expressed as a *p value* < 0.01. A *p value* < 0.01 is often

considered significant, since there is less than a 1% probability that the findings were due to chance alone".

Our statistical results show a *p-value* < 0.01 which corresponds to a Z_{right} > 2.34 or T_{right} > 2.42.

Tables 6.1 through 6.6 show the numeric results of our analysis.[66]

Category / E index	normal (0)	mild (1)	moderate (2)	severe (3)
Mean	9.231428	12.115714	19.820625	29.627220
sem.	0.899887	0.713675	1.311513	1.994180
std.dev.	4.123800	3.776414	5.246051	8.460590
var.	17.005732	14.261306	27.521060	71.581590
Z > 2.34		2.511276	5.160285	4.108677
p* from *Z		0.006	0.00005	0.00005
Stat.sign.		**YES**	**YES**	**YES**
***T* > 2.42**		2.490528	5.498634608	3.883086
p* from *T		0.008	0.00005	0.00005
Stat. sign.		**YES**	**YES**	**YES**

Table 6.1: Distribution of emphysema index using the volumetric method on segmented lung images.

Category / E index	normal (0)	mild(1)	moderate (2)	severe (3)
mean	9.918571	13.061786	21.178750	31.220000
sem.	0.925303	0.726663	1.342455	1.917850
std.dev.	4.240272	3.845142	5.369820	8.136749
var.	17.979900	14.785119	28.834971	66.206680
Z > 2.34		2.671594	5.317342	4.289278
P* from *Z		0.004	0.00005	0.00005
Stat.sign.		**YES**	**YES**	**YES**
***T* > 2.42**		2.653208	5.673379	4.066049
P* from *Z		0.005	0.00005	0.00005
Stat.sign.		**YES**	**YES**	**YES**

Table 6.2: Distribution of emphysema index using the volumetric method on segmented lung with vessels removal images.

Category / E index	normal (0)	mild (1)	moderate (2)	severe (3)
mean	9.456666	12.597500	20.826875	30.942222
sem	0.937886	0.738196	1.360675	1.937595
std.dev	4.297934	3.906169	5.442703	8.220523
var	18.472243	15.258160	29.623023	67.577006
Z > 2.34		2.631502	5.316056	4.272334
p* from *Z		0.004	0.00005	0.00005
Stat.sign.		**YES**	**YES**	**YES**
***T* > 2.42**		2.612563	5.668841	4.050640
p* from *T		0.006	0.00005	0.00015
Stat.sign.		**YES**	**YES**	**YES**

Table 6.3: Distribution of emphysema index using the volumetric method on segmented lung with vessels and airways removal images.

Category / E index	normal (0)	mild (1)	moderate (2)	severe (3)
mean	10.028333	13.271161	20.163281	28.503750
sem.	0.522921	0.536053	1.889041	1.643871
std.dev.	4.792657	5.673060	8.909464	13.948710
var.	22.969563	32.183618	79.378556	194.566400
$Z > 2.34$		4.330314	5.576244	4.200481
p* from *Z		0.00005	0.00005	0.00005
Stat.sign.		**YES**	**YES**	**YES**
$T > 2.42$		4.206544	6.225732	4.067597
p* from *T		0.00005	0.00005	0.00005
Stat.sign.		**YES**	**YES**	**YES**

Table 6.4: Distribution of emphysema index using the four-slice method on segmented lung images.

Category / E index	normal (0)	mild (1)	moderate (2)	severe (3)
mean	10.695833	14.132767	21.347969	29.856670
sem.	0.533509	0.537467	1.890652	1.645542
std.dev.	4.889691	5.688026	8.947646	13.962890
var.	23.909084	32.353643	80.060372	194.962300
$Z > 2.34$		4.538403	5.814523	4.276455
p* from *Z		0.00005	0.00005	0.00005
Stat.sign.		**YES**	**YES**	**YES**
$T > 2.42$		4.419392	6.494181	4.141823
p* from *T		0.00005	0.00005	0.00005
Stat.sign.		**YES**	**YES**	**YES**

Table 6.5: Distribution of emphysema index using the four-slice method on segmented lung with vessels removal images.

Category / E index	normal (0)	mild (1)	Moderate (2)	severe (3)
mean	10.232024	13.711875	21.020938	29.634310
Sem.	0.533700	0.527545	1.918259	1.633361
std.dev.	4.891447	5.583017	8.825189	13.859520
var.	23.926260	31.170084	77.883974	192.086400
$Z > 2.34$		4.637161	5.977313	4.370070
p* from *Z		0.00005	0.00005	0.00005
Stat.sign.		**YES**	**YES**	**YES**
$T > 2.42$		4.527590	6.683333	4.231189
p* from *T		0.00005	0.00005	0.00005
Stat.sign.		**YES**	**YES**	**YES**

Table 6.6: Distribution of emphysema index using the four-slice method on segmented lung with vessels and airways removal images.

The statistical analysis of all our cases shows the *p-value* < 0.01. Between the four categories of emphysema there was a statistically significant difference in their emphysema index values. In conclusion, all null hypotheses H_0 are rejected.

The largest *p-values* were found in differences between normal and mild categories. It is concluded that stronger differences are seen between mild and moderate categories, or moderate and severe categories compared to normal and mild.

There was a trend of larger mean differences between mild versus moderate, moderate versus severe compared to normal versus mild severity. This is also reflected by larger corresponding Z and T values.

Comparing the emphysema index E values determined using the four-slice method and the total lung parenchyma volume, we concluded that there was a high correlation between the emphysema indices computed by each method (0.98). While examination of emphysema index in an individual case can reveal considerable variability, in most of the cases, the mean value of the four-slices estimates seem to characterize the average for the whole volume. Surprisingly, these results indicate that, in many instances, the four-slice method may be sufficient in quantification of the degree of emphysema present in the lung. On the other hand it makes us question whether the emphysema index is a sufficient and reliable enough parameter in quantifying the pulmonary disease. Since emphysema is not homogenously distributed throughout the lung we were expecting to see differences in the results of the two methods and the total volumetric method to be superior.

The results indicate that it is possible to quantify emphysema from low-dose radiation screening CT scans. The analysis of emphysema may be used in conjunction with data acquired in the screening setting and it will not represent any additional radiation exposure to the patient. The segmentation algorithms proved their capabilities in generating reasonable segmentations for the vast majority of screening studies; these segmentations were reliable in providing a database for testing the emphysema quantification methods.

6.2 Method for Quantification of Emphysema and Display of its Spatial Distribution[34]

This section explains the implementation of a new method to quantify the severity of emphysema and describe its spatial distribution based on the emphysema index. The two methods described in 6.1 are special cases of the new *sliding-window method*. In addition, the information provided by the new method can be displayed in a graphical format. This display may provide doctors with a concise depiction of the severity and distribution of emphysema in a particular subject.

6.2.1 Previous Use of Graphical Display in Emphysema Quantification

A number of histogram-based methods have been used in the quantification of emphysema. Coxson, et al[15], used histograms that display the frequency distribution of the CT voxels expressed as gas volume per gram of tissue. The histograms were generated for each different emphysema degree group (control or no-emphysema, mild emphysema and severe-emphysema). The authors concluded that the frequency distribution curves are different between the three groups. Park, et al[43], used histograms from CT scans with standard radiation dose to examine the frequency distribution of voxels with specific attenuation numbers that correlate with the presence of pulmonary emphysema. They concluded that throughout their histogram-based model, the proportion of voxels with attenuation

values within the emphysema range was readily determined by thresholding the voxels frequency distribution. Uppaluri[57] used the HIST metric to compare the emphysema detection with their new method based on fractal analysis and statistical methods. Soejima, et al[54], compared three popular methods MLD (mean lung density), LAA (low attenuation area) and HIST (histogram) for quantifying emphysema. They concluded that the HIST method reflects "the densities of peripheral lung regions with normal acini and those with incomplete destruction of the acinar structure." In their study, longitudinal changes as measured by the HIST method become more positive in the middle and lower lung.

6.2.2 Outline of the Sliding-Window Method

The sliding-window method allows for assessment of emphysema burden within each lung zone along the longitudinal axis of the human body.

In the "sliding window" method, a window of "width" w is used to compute the emphysema index of the w slices covered by the window. This window can travel the lung along the z-axis at different speeds. The speed of the window is determined by its "jump" j.

The next two examples depict two out of the three possibilities of covering the lungs:

Example 1 (non-overlapping windows):

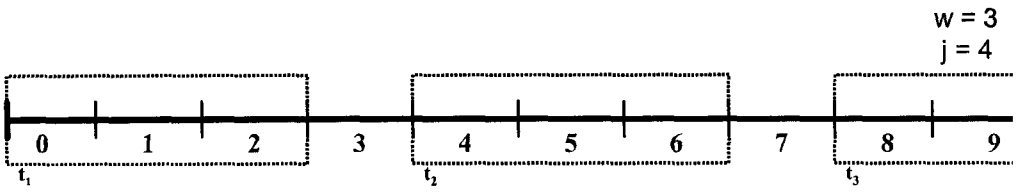

Figure 6.1: Distribution of non-overlapping windows.

At t_1 the window covers slices s_0 to s_2; at t_2 the window covers slices s_4 to s_6; at t_3 the window covers s_8 to s_{10}; the trend continues. For a lung covered by 100 slices (from z_0 to z_{99}), with a window of width $w = 3$ and jump $j = 4$ the emphysema index will be computed in 25 non-overlapping windows.

A particular case of the non-overlapping windows example is when **w = j**. In this case, no slice will be skipped in the computation of the emphysema index.

Example 2 (overlapping windows):

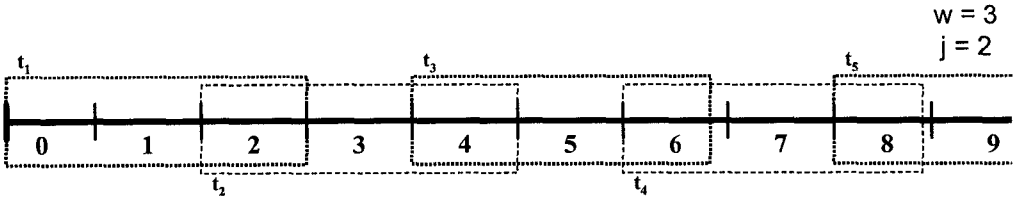

Figure 6.2: Distribution of overlapping windows.

At t_1 the window covers slices s_0 to s_3, at t_2 the window covers slices s_2 to s_4 at t_3 the window covers s_4 to s_6 and so on. Again for a lung covered by 100 slices (from z_0 to z_{99}), with a window of width $w = 3$ and jump $j = 2$, the emphysema index will be computed in 50 overlapping windows.

For different pairs of values *(w, j)*, we computed the emphysema index of each set of slices covered by the sliding window at a given time. The result is an array of measurements that captures the severity of emphysema as a function of vertical (upper-lower) position within the lungs.

We define the emphysema index ***E*** at vertical displacement ***i*** as a function of the voxel values in the following slices by

(6.6) $$E_i = f(S_{ij},\ldots,S_{ij+w})$$

For arbitrary values of w and j, there are three possible scenarios:

- **j < w: overlapping sliding window** (case 1)
- **j = w: multiple segments that cover the entire lung** (case 2)
- **j > w: non-overlapping samplings of the volume** (case 3)

It can be seen that the four-slice method is an instance of case 3, in which w is equal to N/4 where N is the number of slices in the CT dataset. Similarly, in the total volume method, w and j are both equal to N, and it is therefore an instance of case 2.

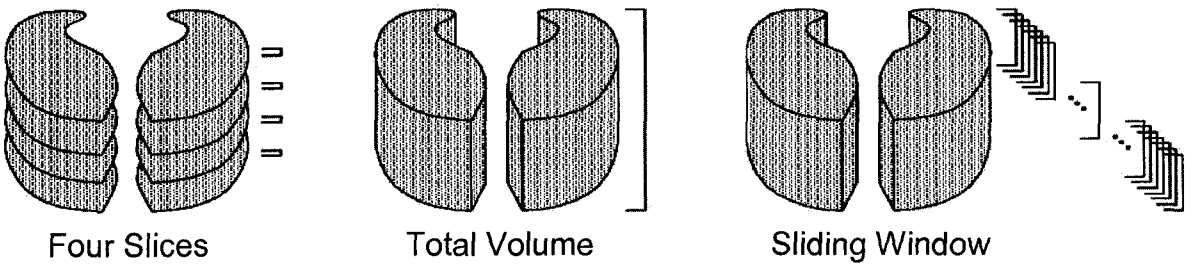

Figure 6.3: Illustration of the three quantification methods.

Following preliminary experiments, we selected the value of 5 for w, and 1 for j (case 1). These values produce a reasonably noise-free series at the maximum spatial resolution available in the original data. Larger values of j could be used to reduce the amount of information recorded per case, but that would not typically be a priority, as the maximum vector length is bounded by the number of slices in the original dataset.

A formal outline of the sliding window method is provided by algorithm 6.1.

Algorithm 6.1: Sliding Window Analysis

```
ANALYSIS ( image, options ) {
        Intensity-Vector    ← CREATE-VECTOR ( image, {parameters} )
        E-Set               ← E-INDEX ( Intensity-Vector, options )
        if      OMode ∈ options
        then    GENERATE-HISTOGRAM( E-Set )
}
```

6.1a. Intensity Vector Creation

```
CREATE-VECTOR ( image, pda[], p, width, jump ) {
// Takes in a segmented lung image, pixel density array,
// slice number from which the window starts,
// width of the slice-window, jump (speed) of the slice-window
//
// Outputs pixel intensity vectors


        // Go throughout entire lung, window-by-window
        for k ← p to (k < p + width) && (p+width <= (image.zmax + 1)
                for each pixel pix ∈ image[k]
                        // store in the pixel density array the intensity of each
                        // pixel not in the background
                        if      pix ∉ background
                        then    pda[count] = image.pix
                                count += 1
                                num++

                // Advance to next window
                p ← p + jump

        return pda;
}
```

6.1b. Emphysema Index Computation

```
E-INDEX ( iarr[], mode ) {
// Takes in an array of one or more vectors containing pixel intensity values.
// Returns one of the following:
//      mode = Overall    → overall percentage of emphysema
//      mode = OMode      → generates vector output for histogram
//                              (one vector per case)
//      mode = SMode      → generates percent index of selected slices
//                              (for example four slice method)
//      mode = IMode      → generate percent index of every individual slice

      parr ← create an array the same size of varr

      for each vector v ∈ iarr
            for each intensity i ∈ v
                  if    i ∈ Emphysema-Range
                  then  compute:    min, max, range, rangecount,
                                    percent, sum, pind   // percent index

                  // store percent into parr[ ] array
                  if    OMode | SMode | IMode
                  then  parr[++pind] ← percent;
                  if    OMode
                  then  return parr

                  // depending on the number of samples compute the location
                  // of selected slices
                  // soff : offset inside the lung from its top and bottom
                  // sdivs: number of selected slices (divisions)
                  if    SMode
                  then
                     sind[0] ← soff - 1;
                     sind[1] ← (((pind - soff) – (soff - 1)) / (sdivs - 1)) + soff
                     sind[2] ← (pind-soff) – (((pind - soff)-(soff-1)) / (sdivs - 1))
                     sind[3] ← pind - soff

                  // store and output the percent index of the selected
                  //  slices into ps[] array
                   ps[0] = parr[sind[0]]
                   ps[1] = parr[sind[1]]
                   ps[2] = parr[sind[2]]
                   ps[3] = parr[sind[3]]
```

```
        // Store and output the overall percent index
        if      lMode
        then    for each j ∈ parr < pind
                ps[0] += j
}
```

6.2.3 Graphical Display of Emphysema Spatial Distribution

A method for graphical representation of the emphysema index as a function of slice axial position within the lungs has been developed. The data for this representation was derived using the sliding window method that helped mitigate the signal-to-noise issues of low-dose CT scans. These problems were particularly present in the lung apices.

For implementing the graphical display, algorithm 6.1, described in previous section, has been used. Throughout the algorithm, intensity information covered by each window had been stored in a separate vector. These vectors were plotted into an application capable of generating a graphical display of emphysema as a function of the slice axial position throughout the lung.

Figure 6.4 is a sample graphical representation for one analyzed case in each of the four categories (chosen by emphysema score). In these cases, the emphysema is of relatively constant severity throughout the lung volume. However, this is not always the case.

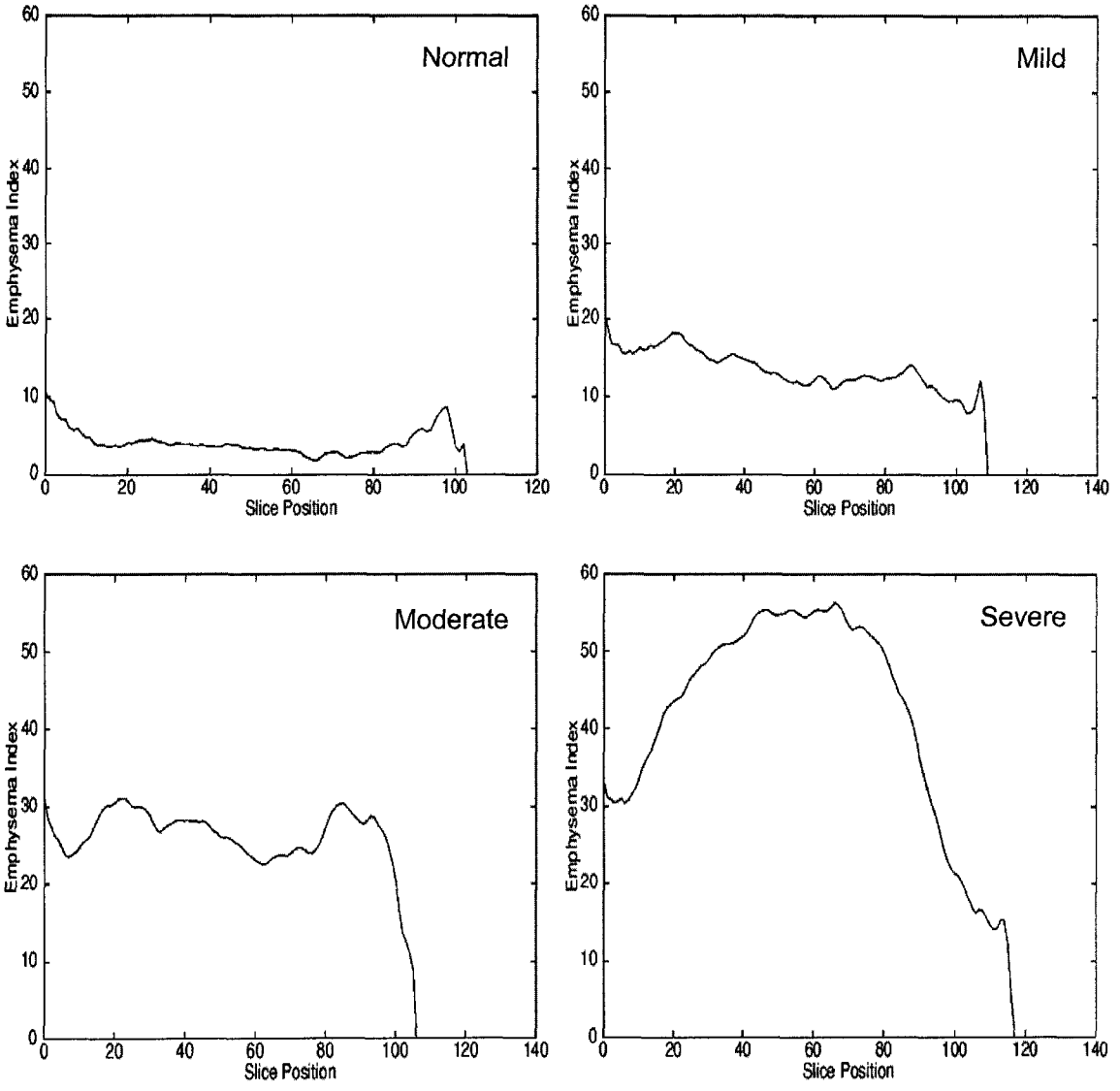

Figure 6.4: Graphical representation of emphysema as a function of axial slice position using the sliding window method in our cases by radiologist's emphysema score: normal *(top left)*, mild *(top right)*, moderate *(bottom left)*, severe *(bottom right)*.

Figure 6.5 shows the results for two cases, one in which the severity of emphysema decreases nearly linearly with increasing axial position (toward the inferior direction), and one in which there is severe emphysema that is mostly limited to the lung apex.

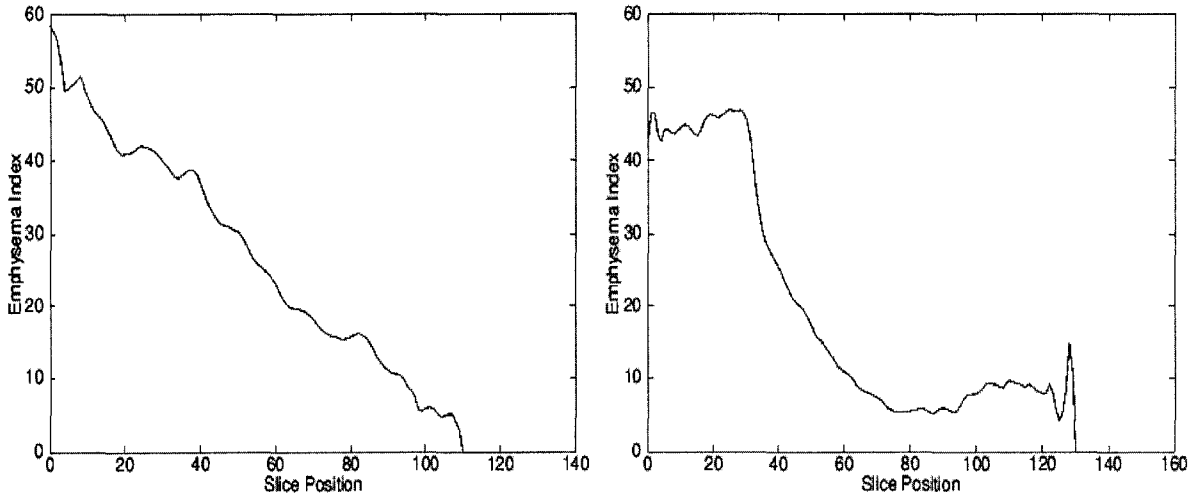

Figure 6.5: Graphical representation of emphysema, as a function of axial slice. Two of the possible spatial distributions of disease: linearly decreasing *(left)* and apical *(right)* are shown.

We presented our results to a group of radiologists for medical interpretation. The linear decrease in severity of emphysema seen in the first case is common to *smoking-induced* emphysema, where more damage is typically done to the parenchyma toward the superior portion of the lungs. In contrast, a subject with α_1-*antitrypsin* deficiency might have a linear increase in the severity of emphysema toward the lung bases. Thus the display may provide useful information that might be used in the determination of the type of emphysema in a particular subject.

6.2.4 Conclusion

The graphical display will allow radiologists to not only quantify emphysema for the entire lung, but also to understand what regions of the lung are most affected by the disease. This may allow them to make the most appropriate follow-up and diagnostic decisions. In addition, new methods of analysis that build upon this notion may be developed.

The next chapter will discuss analysis methods based on additional information brought by the spatial and densitometric distribution of the low attenuation regions. These methods will define a new emphysema model. Such classification algorithms will help in characterizing the pulmonary disease and distinguish some of its various types.

7 EMPHYSEMA MODEL BASED ON SPATIAL AND DENSITOMETRIC DISTRIBUTIONS

One goal of my research is to understand what additional information can be used in detecting and quantifying emphysema. While some of the spatial and/or densitometric properties of the affected areas might not be relevant in quantifying emphysema on low dose CT scans, others might be useful in creating a more accurate model of the disease.

Section 7.1 defines the properties of our regions of interest. In order to correctly and completely identify our ROIs, a preliminary image pre-processing step will reduce noise. Section 7.2 describes a spatial – adaptive filtering method to be used specifically on lung CT scans. Then, an overview of the main spatial and densitometric information is covered in section 7.3. Once all the information has been automatically gathered, the last step is to analyze its importance and usefulness in developing a better emphysema model. These models are presented in sections 7.4.1 and 7.4.2.

7.1 Basic Model for Emphysema

Processing proceeds from the raw image to the segmented image, to region description and on to image recognition and classification. In order to be able to analyze the characteristics of the emphysematous regions, we must specify to the computer a rudimentary description of the areas of interest. We will discuss appropriate values for the density range (thresholds) and minimum size of low attenuation areas in order to be considered emphysematous areas.

What is the best threshold?

We can think of emphysema as a condition in which the lung contains "holes filled with air". These holes, that signify the presence of emphysema, are represented on CT scans as areas of abnormally low attenuation. The attenuation of a normal lung parenchyma varies between -870HU and -750HU. The attenuation of the air is -1024HU.

Due to partial volume error and other factors, emphysematous areas on CT scan images do not have a constant density value (-1024HU), the attenuation of their voxels is, rather, spread over a large range. Voxels located in the interior of an object have a better approximation of the CT attenuation value. On the other hand, voxels that are at the boundary of an object will have an attenuation value that roughly equals to the average of the attenuation of voxels inside the object and attenuation value of voxels outside the object. In detection of emphysematous

areas, the issue becomes even more difficult due to the fact that the areas have an irregular shape.

One of the main issues is finding the value of the threshold value that will best correlate with the degree of emphysema. There are many suggestions in the literature. Some researchers use only one threshold value (sometimes called *density mask*) in their quantification, others use two, and still others, three. The following is a list of common choices for the threshold values:

-900HU[2]

-900HU, -960HU[18]

-920HU, -910HU, -900HU[41]

-950HU, -910HU, -900HU[5]

Hofman, et al[29] use an *adaptive thresholding* method to automatically choose a threshold value that will best reflect the characteristics of different areas of the lung.

For our model, we have used a simple dual-thresholding technique. A few threshold-pair values were tested on the segmented image. The thresholds selected are those that yielded the largest difference between cases with different emphysema scores in previously used quantification methods. Voxels are considered to be part of an LAA region in the segmented volume if their attenuation is between –1024 HU and –950HU.

We define the set of voxels ***S***:

(7.1) $$S = \{v(x,y,z) | - 1024HU \leq H(v(x,y,z)) \leq -950HU \}$$

Note that some voxels in ***S*** might be included as result of partial volume error or noise, and are not a result of emphysema presence in that immediate area.

How do we bound emphysematous areas?

A voxel $v(x,y,z)$ is a 3D cube. We define two voxels as being *adjacent* when they have a face, side or vertex in common. Thus any voxel has 26 voxels adjacent to it. A *path* is defined as a sequence of voxels $v_1, v_2, \ldots v_n$ such that v_{i+1} is adjacent to v_i for all i, $1 \leq i \leq n-1$. We define the *connected component* $C(v)$ of a voxel v, as the set of all voxels that can be connected to v through a path of voxels belonging to S.

Some connected components might be a result of partial volume error or noise, and are not created by the emphysema disease. Therefore, we will consider as emphysematous areas, only components of size (number of voxels) greater or equal to minimum value S_{min}.

(7.2) $$| C(v) | \geq S_{min} \qquad S_{min} > 1$$

The optimal value for S_{min} has been determined by a number of experiments. We ran connected component analysis on a sample set of cases with

different severity assessments. We analyzed the number of low attenuation connected components and their size for each case. We concluded that we would consider as significant emphysematous area any 3D-connected component of size greater or equal to 100 voxels. For the basic model of emphysema, we consider fixed minimum component size for all categories of severity. On the assumption that the refined segmentation algorithm successfully removed the two bronchi, other restrictions have not been imposed.

Based on the characteristics described above, we will collect additional information related to location and densitometric distribution of the disease.

7.2 Data Preprocessing: Noise Filtering

Our desire is to keep the CT scan information as intact as possible. Thus until this point, the segmentation algorithm has only applied filtering to the masked image. The final segmented lung image contains the same high degree of noise as the input scan. Future studies of segmentation algorithms may choose a different route and apply noise reduction in the preprocessing step. It is important to note that noise filtering should be customized to goals of specific radiological studies.

In order to analyze the characteristics and distribution of the low attenuation areas corresponding to pulmonary emphysema, segmentation of the

regions of interest (areas in the emphysema intensity range) is necessary. Unfortunately, the noise causes adverse effects in the generation of segmented regions. Contiguous regions are divided into smaller groups by noise that registers in the healthy tissue range; this case gives rise to the impression that there is healthy parenchyma within the emphysema areas.

The presence of noise will alter our capability to accurately analyze the low attenuation areas. Therefore a gray-level filtering of the segmented lung prior to the emphysematous regions segmentation is, therefore, deemed highly desirable.

7.2.1 Nature of the Noise and its Appearance

The most common types of noise present in our low dose CT scans are impulse noise and streaking artifacts. Impulse noise, which appears as white speckles, is present all over the CT images with a relatively homogenous spatial distribution in the x-y plane. It is very hard to spot it visually in the original image but it becomes readily apparent in the segmented emphysematous regions.

Streaking artifacts are mainly caused by inconsistent attenuation measurements, the presence of a highly attenuating object such as bones, or the sharp edge transitions in the human body. Among these, the sharp edge transitions contribute, by far, the most artifacts. Since the lung is encased in the ribcage, the bone to soft tissue transition is unavoidable. Furthermore, under close observation we discovered that the noise streaks and actual tissue pixels are interlaced. This

means that in the especially noisy regions around the ribcage, a noise pixel often interleaves two good pixels along the y-axis. The streaking artifacts are present in a higher degree along the top, bottom, and posterior sides of the lungs. (See figure 7.1.)

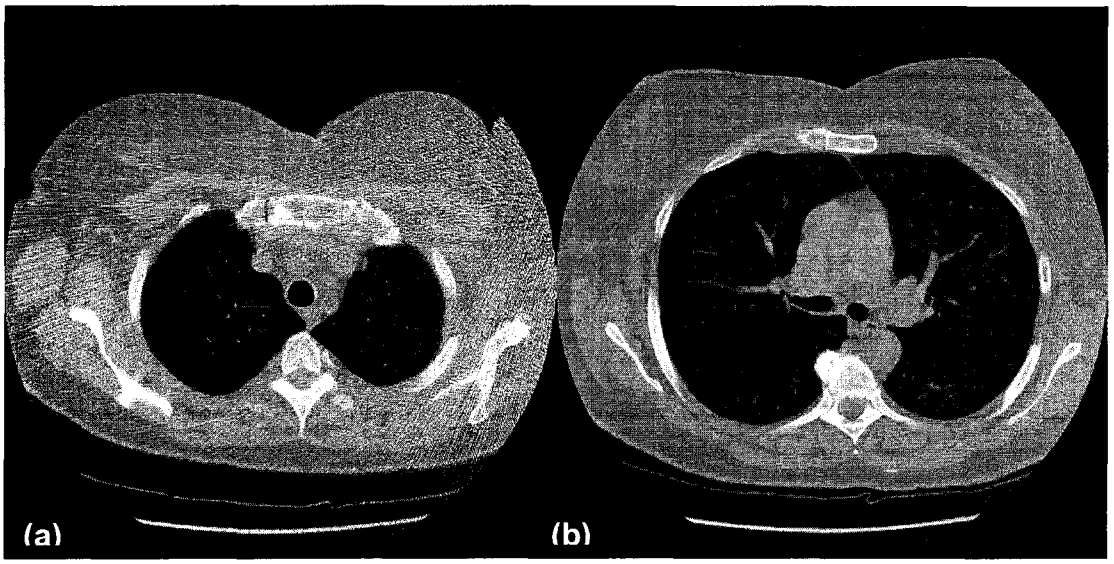

Figure 7.1: Noise distribution in lungs. *(a)* A slice from the apices of the lung. An increased presence of noise is visible over the entire image. *(b)* A slice from the middle of the lung. There is a higher presence of noise in the posterior region and around the ribcage.

7.2.2 Designing a Filtering Method

Due to the nature of the noise the use of median filters in our adaptive filtering method was determined to be the most suitable choice. Median filtering is highly effective in removing the peppery impulse noise. A two (three) dimensional filter can be represented by a two (three) dimensional array of pixels. The basic concept of median filtering is quite simple: center a filter (often referred to as the kernel) of a certain size (3-by-3 being the most common) over the pixel that needs

processing; sort all the pixel intensity values within the filter; replace the intensity value of the center pixel with the median value of the sorted list. Unlike other common filtering techniques, such as a mean filter, the median filter has the advantage of preserving the sharpness and contrast of the edges and keeping the intensity information within the initial range. Furthermore, median filters can be applied sequentially without repetitive information loss.

There are, however, several issues that still need addressing:

7.2.2.1 Filtered Area

Unlike most low-quality images, CT scans have a noise boundary with fairly well defined intensity values. In our study we have the advantage of being able to reasonably approximate the intensity range of the noise, as well as, the intensity range of the parenchyma. We consider the parenchyma to be in the range of -1024 – -750HU, and the remaining fine vessels to have a lighter appearance around –700HU. The noise pixels, on the other hand, are in a range decidedly higher than -700HU. Targeting specific pixels that are deemed to be noisy not only reduces the chance of replacing signal with noise but also improves the overall filtering performance. Since most of the noise is caused by sharp edge transitions, it is reasonable to assume that the noisiest portions of the images are along the edges of the lungs, and the noise level would fall off gradually for the interior pixels. This assumption held true in all our examined cases. Our initial attempt was to locate the border of the lung with an edge detection algorithm and begin filtering inwards

until the noise levels sharply dropped off. This turned out to be insufficient since while the noise level does decrease overall nearer to the center, there are still fluctuations beyond the noisiest portions.

We designed two new variations of the traditional median filter:

Generic-Ignore-Noise median filter: This is a median filter that is applied to all pixels in the image except the background. However, if noise pixels lay within the kernel, they are not taken into consideration when determining the median.

Noise-Only median filter: This is a more selective filter that gets applied only to pixels having intensity values within the specified noise range. Again, the noise pixels within the kernel do not contribute to the median value computation.

7.2.2.2 Number of Filtering Passes

Multiple passes are the more desirable option. Instead of trying to do all the work at once, it is simpler to focus on different areas during different stages of noise reduction. A first run would help to further reduce the overall noise level and create larger and contiguous noise-free regions. Subsequent passes then can focus more on the noise pixels without disturbing pixels in the parenchyma range.

Our filtering method uses three main passes. The first filter pass is meant to eliminate most of the impulse noise throughout the entire image. The subsequent two stages target the remaining streaking artifacts. These stages do not overlap in area of the lung processed.

7.2.2.3 Spatial Distribution Considerations

As mentioned before, the impulse noise is present all over the images while the streaking artifacts are situated in the top, bottom and posterior sides of the lungs. In first step, therefore, we apply the *generic-ignore-noise filter* for all pixels to eliminate the impulse noise.

The next two passes target the streaking artifacts based on their locations. To analyze the spatial distribution we plotted the noise with respect to the z- and y-axes. The z-axis percent graph shows that roughly the first and the last twenty or so slices have a much higher percentage (>20%) of noise than the slices in the middle of the lung. Outside that range, the noise percentage drops drastically, to around 2%. We decided that the most reasonable approach was to apply noise-only filtering in the second pass to the top and the bottom slices up to the point where noise percentage drops under 2%.

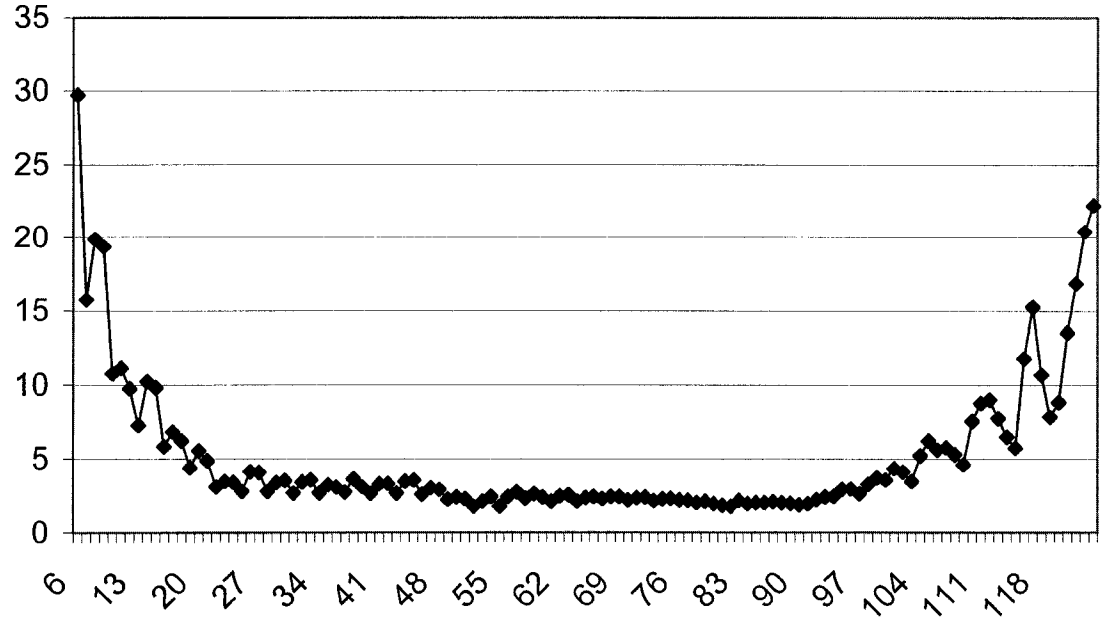

Figure 7.2: A graphical depiction of the percentage of noise as function of slice position (z).

The histograms, taken with respect to the z-axis, help us in defining the boundaries of the third filtering pass, again using the noise-only method, along the z-axis. The third pass is applied in the x-y plane to all slices that were not considered during the second filtering pass.

7.2.2.4 Kernel Size

Since the first pass addresses the homogenous distribution of noise, we found a square filter to be the appropriate choice. Larger kernel sizes, while greatly reducing the chance of replacing signal with noise, leads to increased data loss. Also, since the median value within the filter could be quite distant from the actual

pixel value, the image is softened in the process. After some empirical testing, a kernel size of 3-by-3 was decided on.

For the following two passes, the narrow horizontal bands of streaking noise naturally lead to a vertically oriented filter. Such an arrangement ensures the replacement of a noise pixel with a parenchyma-ranged pixel. Since the subsequent passes are more restricted, covering the areas already processed by the first pass, a filter with a small vertical kernel of size 1-by-3 is selected as the most appropriate with data preservation in mind.

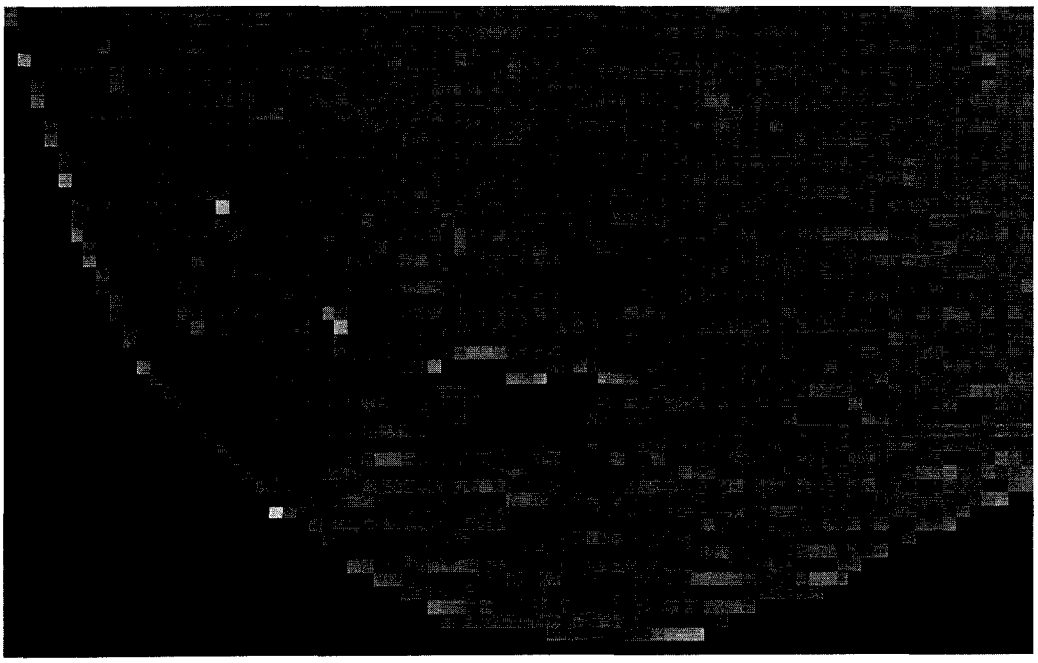

Figure 7.3: A magnified (5.9x) image of the lung. Streaking noise caused by lung proximity to the ribcage appears as lighter-gray horizontal lines.

7.2.3 Spatial-Adaptive Filtering Method

In conclusion, the segmented lung images were put through a median spatial-adaptive filtering method, consisting of three passes. The first pass is a symmetric filter that handles impulse noise present throughout the entire image. The second pass alleviates the streaking artifacts present in the apices of the lung through a vertical kernel. The third pass, also using a vertical kernel, addresses the noise present in the posterior part of the lungs. The method is described by the pseudo-code shown in algorithm 7.1.

Algorithm 7.1 Adaptive Lung Filter

```
ADAPTIVE-LUNG-FILTER ( im ) {
// Takes a picture representing a lung and returns the image having undergone 3 filter
passes.

    // Phase 1: General Pass over all pixels
    nim1 ← exact copy of im
    for z,y ∈ im
        MEDIAN-FILTER( image, nim1, z, y, NOISE-LEVEL-1, ALL-PIXELS );

    // Phase 2: Apex Filtering
    nim2 ← exact copy of nim1

    for z ∈ im
        if    PERCENT-NOISE( z slice ) > 1%
              && slice is near top or bottom of lung
        then  MEDIAN-FILTER( nim1, nim2, z, y, NOISE-LEVEL-2, NOISE-ONLY );

    // Phase 3: Rear-of-Body Filtering
    nim3 ← exact copy of nim2
    for z,y ∈ im
        if    PERCENT-NOISE( y row in z slice ) > 1%
              & & row is near bottom of lung
        then  MEDIAN-FILTER( nim1, nim2, z, y, NOISE-LEVEL-3, NOISE-ONLY );

}
```

```
MEDIAN-FILTER ( image, new-image, z, y, noise-minimum, noise-selected ) {
// Performs an adaptive median filter on pixels in a horizontal row.
        if      noise-selected = NOISE-ONLY
        then    P ← {∀x / image[z][y][x] > noise-minimum } // noise pixels only
        else    P ← {∀x / image[z][y][x]}

        for each pixel p ∈ P
                N ← neighbors of p ∈ image within the kernel
                new-image.p ← FIND-MEDIAN( N );
        return new-image;
}

PERCENT-NOISE ( image, z-hi, y-hi, x-hi, z-lo, y-lo, x-lo ) {
// Determines the percentage of noise to non-background
}
```

The output-images of the adaptive median filter are shown in shown in figure 7.4.

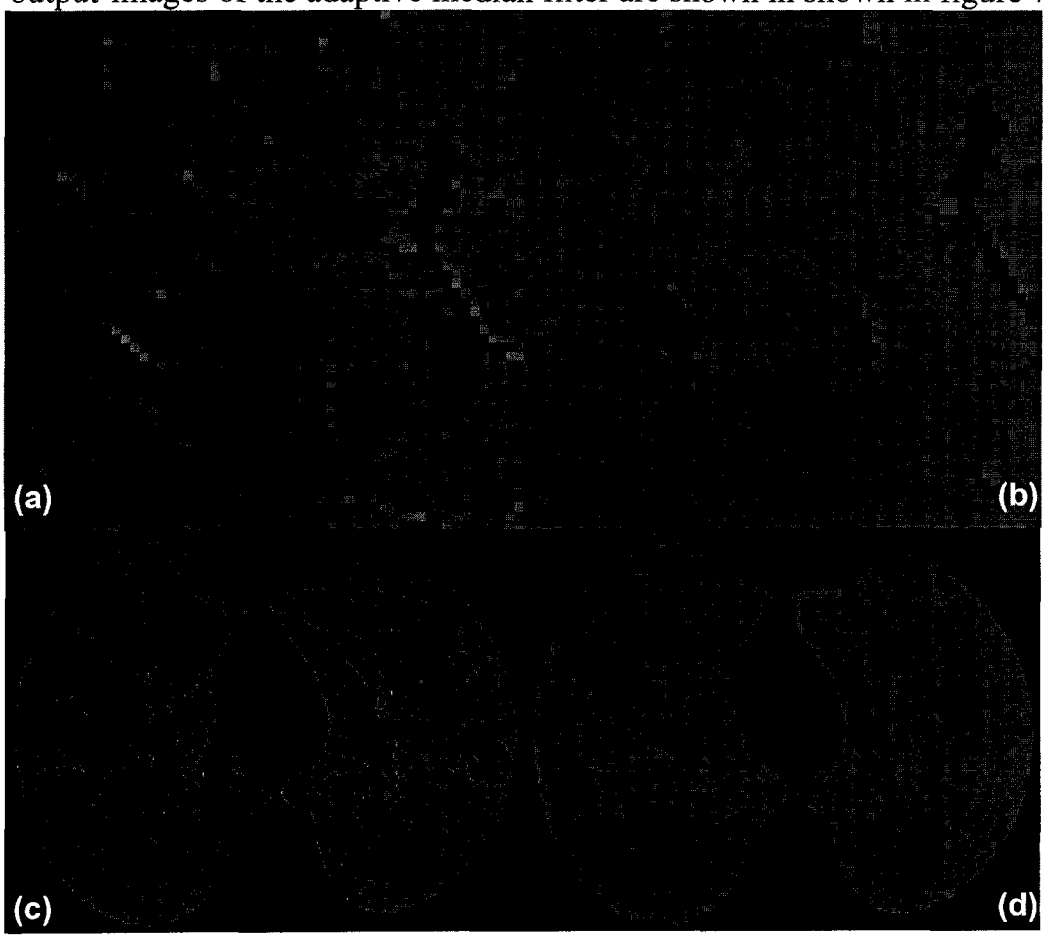

Figure 7.4: Images of the lung before *(a,c)* and after the filtering *(b,d)* show a reduction in noise.

7.2.4 Other Effects of Image Filtering

Beside the positive outcome of noise reduction, a side effect of this filtering technique is a slightly decreased contrast between different structures. The filtered image is slightly blurrier than the original. Considering that emphysematous areas do not show visible margins and are not homogeneous, this side effect does not impede future analysis.

The filtering also changes the density range of the pixels, most importantly the density range of the pixels identifying the emphysematous areas. This aspect will be discussed in more detail in the following chapter which deals with the emphysematous areas model.

7.3 Morphological Information

In this section we present a number of size and shape descriptors as well as spatial and density distribution descriptors useful in performing morphological analysis of the emphysematous areas. The analysis of these descriptors will lead to the final emphysema model's specifications. These descriptors will be computed at two different levels:

- in a 3D space, as an aggregate of the entire lung volume. The emphysematous areas are seen as one large component region.

- in a 3D space, considering each emphysematous connected component separately. The emphysematous areas consist of a multitude of connected components; each connected component is described separately.

7.3.1 Size and Shape Descriptors

We now examine the commonly used statistical measures of size and shape.

7.3.1.1 Primary Metrics

Volume and *area* calculations are straightforward; nevertheless, they constitute important parameters in current methods for quantification of emphysema.

Area

The simplest property of a region is its area given by the number of pixels of which the region consists. A simple counting of the region's pixels in a 2D space, can provide the area of the region.

The literature review shows that the size of the emphysematous areas is often considered a criterion in quantifying the degree of emphysema in terms of its *extent.* For example, Sakai, et al[50], suggested quantifying the degree of emphysema (on a four point scale) as a function of the *low attenuation area diameter* (dLAA).

- no emphysema
- dLAA < 5mm emphysema

- dLAA > 5mm emphysema with intervening normal lung
- diffuse LAA emphysema without intervening normal lung

Volume

The volume of low attenuation areas is considered one of the main criteria in quantifying emphysema. Because some types of emphysema predominate only in certain lung regions, 2D densitometry would lead to false diagnosis. A more accurate method of estimating the degree of emphysema from CT images is to analyze the whole lung from a 3D perspective. Severity of emphysema, an important parameter in quantifying emphysema, can be determined using manual methods as visual scores, or 3D densitometry methods. As described in 3.1.1 one of the most widely used visual scores evaluates the percentage of the low-attenuation volume of the lung on a 0-4 scale. The percentage of low attenuation regions over the entire lung volume can also be determined through 3D densitometry methods, as described in section 6.1.2.

7.3.1.2 Secondary Metrics

Secondary metrics can be derived from primary metrics, rather than directly from the image. **x/y, y/z, x/z extent ratios** might be useful in describing the shape of the emphysematous areas.

Elongatedness is a ratio between the length and width of the rectangle bounding the region. Elongatedness can also be evaluated as a ratio of the region area and the square of its thickness.

7.3.1.3 Geometric Moments

A technique in region description is to establish a standard set of moments that can uniquely describe the object. Papoulis in his uniqueness theorem states the one-to-one correspondence between a 2D continuous function *f(x,y)* and the moment sequence of order $p+q$, m_{pq}:

if *f(x,y)* is piecewise continuous with nonzero values, moments of all orders exist and the moment sequence m_{pq} is uniquely determined by *f(x,y)*. On the other hand, (m_{pq}) uniquely determines *f(x,y)*.

A moment of order $(p+q)$ is dependent on scaling, translation, and rotation and is defined as:

$$m_{pq} = \sum_{x=0}^{m-1} \sum_{y=0}^{n-1} x^p y^q f(x,y) \tag{7.3}$$

In a 2D representation $m_{0,0}$ provides the area of the region.

Moment sets of order 3 to5 are sufficient for classification of most three-dimensional objects. Region moment representation interprets a normalized gray-level image function as a probability density of a random variable. Moment

characteristics are dependent on the linear gray-level transformations of the region; in the description of region shape properties, in order to eliminate the dependence on the linear gray-level transform, binary image data should be considered. In computing the geometric moments of the emphysematous regions, the value of $f(x,y,z)$ is set to 1.

For a digital image of size $(m * n * l)$ the moment set is given by:

(7.4) $$m_{pqr} = \sum_{x=0}^{m-1} \sum_{y=0}^{n-1} \sum_{z=0}^{r-1} x^p y^q z^r f(x,y,z)$$

In a 3D representation $m_{o,o,o}$ represents the volume of the region.

Translation invariance can be obtained if we use the central moments:

(7.5) $$u_{pqr} = \sum_i \sum_j \sum_k (i - x_c)^p (j - y_c)^q (k - z_c)^r f(x,y,z)$$

where x_c, y_c, z_c are the coordinates of the region's center of mass, which can be obtained using the relations in formula 7.6.

(7.6) $$x_c = m_{100} / m_{000}$$

$$y_c = m_{010} / m_{000}$$

$$z_c = m_{001} / m_{000}$$

7.3.2 Density Distribution Descriptors

The descriptors mentioned in previous sections, will provide the necessary information for the spatial distribution analysis of the emphysema. Densitometric measurements are an important tool in analyzing the density distribution of the emphysematous areas. For the computation of the densitometric parameters, the value of each pixel ($v(x,y,z)$) is defined by its attenuation value.

7.3.2.1 Voxel Attenuation Value (Brightness)

(7.7) $$H(v(x,y,z) = v(x,y,z) - 1024$$

where $v(x,y,z)$ represents the low attenuation value of the voxel with coordinates x,y,z.

and $H(v(x,y,z))$ represents the intensity in hounsfield units (brightness) of the voxel with coordinates x, y, z.

7.3.2.2 Densitometric Moments

An important set of metrics is the densitometric moments. Statistical analysis will be used to obtain information about the densitometric distribution of emphysema. Moments computation is derived from:

(7.8) $$\mu_p = \sum_{0}^{N-1} \left(v(x,y,z) - \mu\right)^p$$

Mean voxel density represents the arithmetic mean of all density values in the segmented region. Mean voxel density can be used as a measure of the average brightness.

(7.9) $$\mu = \frac{1}{N}\sum_{0}^{N-1} v(x, y, z)$$

Variance represents a measure of the variability of density values. Variance is given by:

(7.10) $$variance = \mu_2 / \mu_0$$

The **standard deviation** can measure the variation in values from the mean. It is defined as the square root of the variance.

(7.11) $$\sigma = \sqrt{\text{variance}}$$

To quantify the shape of the density distribution another two parameters can be discussed:

Skewness measures the shift of the distribution.

(7.12) $$skewness = \mu_3 / \sigma^3$$

Kurtosis measures the peakness of the distribution.

(7.13) $$kurtosis = \mu_4 / \sigma^4$$

The metrics mentioned above are not a complete list. Additional metrics and parameters may be considered.

7.3.3 Location Descriptors

The previous two sections gave an overview of descriptors that are widely used in computer vision research. However, beside spatial and densitometric parameters, we took in consideration location parameters. These, while not as common, are specifically related to our research.

7.3.3.1 Location within the Lung Component

When describing the location of components within the lung mass, we worked relative to a set of center points of the image.

Center of a lung (right or left) / both lungs

While any fixed point of the image could be considered a "center", it makes the most sense to choose points relative to the lungs. In doing so, our calculations remain consistent despite lung sizes and slight differences in their position inside the CT-scan image. Three relative center points, as seen in figure 7.5, can be found: center of the lung pair, center of the left lung and center of the right lung individually.

(7.14) $$(x, y, z)_{center} = (\lfloor mean(z_{lo}, z_{hi}) \rfloor, \lfloor mean(y_{lo}, y_{hi}) \rfloor, \lfloor mean(x_{lo}, x_{hi}) \rfloor)$$

where x_{lo}, x_{hi}, y_{lo}, y_{hi}, z_{lo}, and z_{hi} represent the boundaries of the lung(s) of interest.

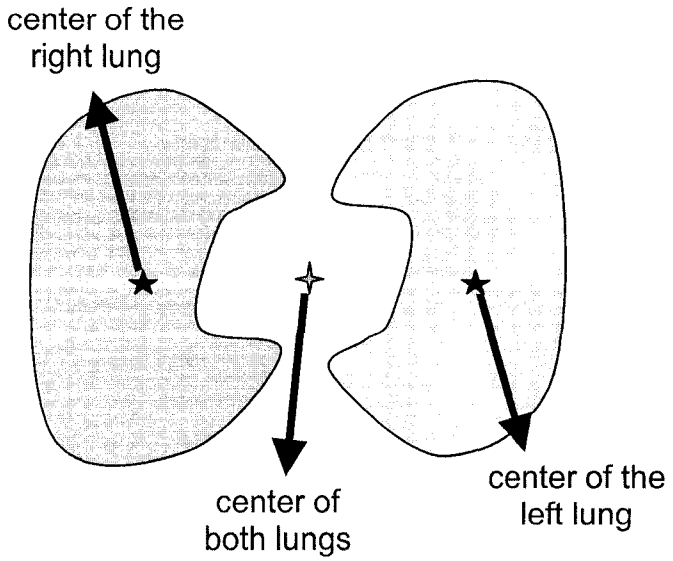

Figure 7.5: The set of center points considered for the relative location of a component.

Spherical Coordinates

A 3D spherical coordinate consists of three components: ρ, the distance from the origin, and θ and φ the angles offset from a vertical axis. They can be defined in terms of *(x,y,z)* distances in a Cartesian plane[63].

(7.15) $$\rho = \sqrt{x^2 + y^2 + z^2}$$

$$\theta = \arcsin(y / \sqrt{x^2 + y^2})$$

$$\varphi = \arccos(z / \rho)$$

The measurements for the center of mass, in turn, allow for the distance and angle of a component to be computed from the center of both lungs and from the center of the lung in which it resides for each emphysematous component.

7.3.4 Automated Information Gathering Algorithm

Up until now we've considered some of the difficulties that go into creating a clean image for data collection. But, the heart of our analysis comes from the raw data generated by our *Automated Information Gathering* program. Figure 7.6 details all the steps involved in our probing process.

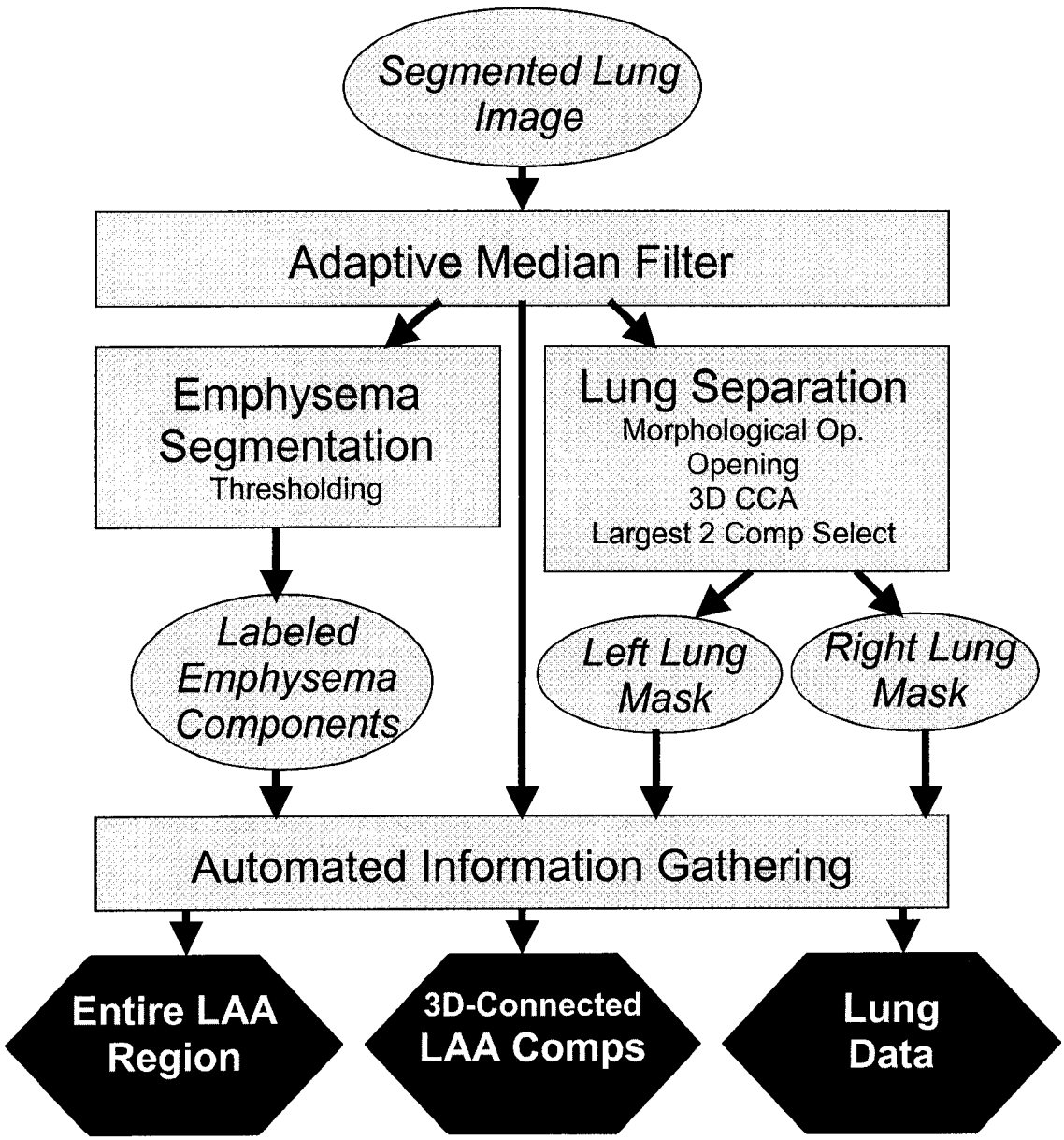

Figure 7.6: The information gathering process.

The terminal stage of the algorithm yields data in three categories: about the lungs in general, about the entire LAA region and about individual 3D-Connected LAA Components.

We start the collection of data with four images: a labeled set of emphysematous components, masks of the left and right lungs independently, plus a noise-filtered version of the image generated by the lung segmentation algorithm. The labeled emphysematous components allow us to easily find our regions of interest. The lung masks images are used to locate the lung in which components belong as well as information about the size and extent of the lung, the coordinates of its physical center. The segmented image gives us an accurate view of the attenuation values as well as the size and center of both lungs taken together.

7.4 Analysis Results

This section presents the results of analyzing the densitometric and spatial information of the low attenuation components of the segmented lung images. The goal is to determine which parameters are able to correlate best with different emphysema severity categories and different emphysema types.

7.4.1 Analysis of the Entire Emphysematous Region

We started with the study of the low attenuation 3D regions seen as one big component scattered throughout the entire lung volume. This is the practice of current work in the field. In section 6.1, severity of emphysema is assessed by the emphysema index E over the entire lung volume. In our research we study additional parameters that can measure the emphysema present more accurately then the existing methods.

7.4.1.1 Brightness: Parameter for Severity Assessments[1]

For evaluating the severity of emphysema, rather than looking at the number of voxels in a specific intensity range, we introduced a new metric based on the attenuation characteristics of the lung CT scan image (its brightness). The brightness of body tissues and regions is the primary aspect that a radiologist takes into consideration during visual assessments. Brightness of the region represents a primary parameter for assessing the CT scan readings.

Our database consisted of eighty scans with 2.5mm sections acquired using low-dose parameters (120kVp, 40mA, 1.5:1pitch). Experienced thoracic radiologists reviewed each scan for the presence of emphysema. The severity of the disease was assessed using a four-point scale into four categories: normal, mild, moderate, and severe. The distribution of cases by emphysema score was: 18 normal cases, 28 mild, 16 moderate and 18 severe.

[1] Abstract submitted for RSNA Conference, November 2004.

A preprocessing step consisted in segmenting and noise-filtering the lung parenchyma using the algorithms described in chapter 5 and section 7.2.

Brightness of the Entire Lung Region

The first approach was to discuss the brightness of the overall region of the lung. We analyzed how useful and efficient the brightness parameter is in quantifying the emphysema severity. Does the lung overall brightness differ between different severity categories? Is this difference statistically significant? Does the new parameter give a more accurate severity-model than the most currently used methods (e.g.: the LAA percentage method)?

We define *brightness index of a region*, as the mean of the brightness of the voxels contained in that region.

(7.16) $$B_{lung\_region} = mean(H(v(x,y,z))$$

where $v(x,y,z) \in lung\_region$

The fact that the brightness parameter is independent of the emphysema intensity bounds presents an advantage. The E index is based on the emphysema range. As mentioned in previous chapters, the literature review gives different upper bounds for the disease intensity range, and there is no common agreement on a predefined value for it. In order to test the effectiveness of brightness as a

discriminator for emphysema, we set up an experiment with the null hypothesis defined as follows:

(7.17) H_{01}: *meanB_mild* = *meanB_normal*

H_{02}: *meanB_moderate* = *meanB_mild*

H_{03}: *meanB_severe* = *meanB_moderate*

The null hypothesis means that there is no difference in the brightness index B, between different severity categories as evaluated by radiologists throughout visual scores.

Emphysematous areas are manifested in scan images as gray-color areas that are darker than the rest of the parenchyma tissue. The lower the intensity of the region the lower is its brightness. We conjectured that with an increase in the severity of the disease there is also an overall decrease in the brightness of the entire lung image. To determine if there is an increasing trend in the brightness index with the decrease of severity we define the alternative hypothesis as:

(7.18) H_{11}: *meanB_mild* < *meanB_normal*

H_{12}: *meanB_moderate* < *meanB_mild*

H_{13}: *meanB_severe* < *meanB_moderate*

Table 7.1 shows the numerical results for the statistical analysis of the brightness index over the entire lung region.

Category / B_{lung_region}	normal	mild	moderate	severe
N	18	28	16	18
Min	-882.060	-904.62	-916.25	-956.480
Max	-824.280	-845.95	-872.45	-885.970
Mean	-858.723	-872.853	-892.763	-909.958
Std.dev.	17.697	15.640	13.040	16.483
var.	313.168	244.604	170.053	271.683
***Z* <- 2.34**		-2.764	-4.525	-3.390
p* from *Z		0.00290	0.000003	0.00030
Stat. sign.		**YES**	**YES**	**YES**

Table 7.1: Distribution of the brightness parameter B_{lung_region} for different categories of emphysema severity.

Overall, the *p-value* clearly shows that for all category-pairs, there is a statistically significant difference. The largest *p-value* of 0.00290, is seen in the difference between the normal and mild categories.

To compare the new severity quantification with assessments done using previous methods we applied the traditional volumetric percentage of low attenuation areas on the same set of data (as presented in section 6.1.3). Using the volumetric method the largest obtained *p-value* is 0.00480. Comparing the *p-values* obtained in the computation of the *E* index with the ones obtained throughout the computation of the *B* index, we may conclude that emphysema quantification based on region brightness is at least as accurate as the one based on emphysema index. In fact we will argue in the rest of the section that this metric allows for finer or more accurate discrimination then current methods.

Brightness of Selected Regions of the Lung

All our cases are selected from a database of low-dose CT screening exams used in the Early Lung Cancer Action Program at Cornell Medical Center. Patients enrolled in the program are long-term smokers, at least one pack a day for least ten years. Thus we can assume that for the vast majority of the patients that might suffer of emphysema, smoking was the main cause in developing the disease. In these cases the apical segments of the upper lobes are affected first.

We assessed the severity of emphysema based on the brightness of the lung in its upper regions, by computing $B_{upper30\%}$:

(7.19) $$B_{upper30\%} = mean(H(v(x,y,z))$$

where $v(x,y,z) \in$ *upper 30% of lung volume*

The results of our statistical analysis are shown in table 7.2.

Category / $B_{upper30\%}$	normal	mild	moderate	severe
N	18	28	16	18
Min	-878.660	-907.270	-929.250	-950.060
Max	-828.330	-845.820	-883.480	-900.280
Mean	-858.388	-877.568	-904.507	-926.959
std.dev.	15.939	16.633	15.044	13.437
var.	254.059	276.654	226.316	180.541
***Z* <- 2.34**		-3.915	-5.496	-4.566
p* from *Z		0.00005	0.00000	0.00003
Stat. sign.		**YES**	**YES**	**YES**

Table 7.2: Distribution of the brightness parameter $B_{upper30\%}$ in different categories of emphysema severity.

The differences between categories of emphysema based on $B_{upper30\%}$ are statistically more significant than the ones based on B_{lung_region}. The p-values tend to 0, all being smaller than $5 * 10^{-5}$.

The quantification based on the brightness index of the upper lung zones, gives better statistical results than all the quantifications discussed in the literature. The new quantification results in higher differences between all category-pairs, especially between the not so easily identifiable mild versus normal cases.

Upper and lower regions of the lung suffer from a high degree of noise. To be sure that our upper regions results are not caused by the high noise presence in the lung apices, we computed the brightness index on the lower regions of the lung as well.

(7.20) $$B_{lower30\%} = mean(H(v(x,y,z))$$

$$\text{where } v(x,y,z) \in \textit{lower 30\% of lung volume}$$

The results for the brightness index in the lower regions of the lung are not statistically significant, and do not show any steady pattern. This fact makes us more confident that $B_{upper30\%}$ represents a reliable parameter in quantifying the severity of emphysema and it is not due to the high noise present at the upper and lower areas of the lungs.

The fact that severity of emphysema can be assessed based on information gathered from CT-scans of limited areas, more exactly the upper region of the lung, is advantageous. Localized CT-scans mean lower radiation exposure than a complete lung CT-scan; this is beneficial to the patient. Even more, the scanning will take a shorter time, diminishing the motion artifacts caused by the patient's breathing during the scanning session.

Relative Brightness Index

Even if the same scanner has taken all the CT scan images, it is possible that due to small variations in the scanner parameters, images would present slight variations in their overall brightness. We define a new brightness parameter that is more independent of small fluctuations of the overall brightness of the CT scan images, the *relative brightness index* of a specific region (BR_{region}):

(7.21) $$BR_{lung} = B_{lung\_region} - B_{normal\_parenchyma}$$

$$B_{normal\_parenchyma} = mean(H(v(x,y,z))$$

$$\text{where } v(x,y,z) \in lung\_region \;\&\&\; H(v(x,y,z)) > -950\ HU$$

This parameter also reflects the weight that the considered emphysema brightness range (-1024 to –950HU) has on the overall brightness index of a region. *BR* is based on the contrast between overall attenuation and that in the presumptively normal parenchyma.

Category / BR_{lung}	normal	mild	moderate	severe
N	18	28	16	18
Min	-4.100	-9.760	-23.500	-39.170
Max	-0.560	-0.760	-5.050	-11.610
Mean	-1.668	-3.991	-11.926	-22.326
std.dev.	0.977	2.039	5.750	6.327
var.	0.955	4.157	33.064	40.025
$Z <$ **-2.34**		-5.174	-5.331	-5.021
p* from *Z		0.00000	0.00000	0.00000
Stat. sign.		**YES**	**YES**	**YES**

Table 7.3: Distribution of the relative-brightness parameter BR_{lung} in different categories of emphysema severity.

The new parameter BR_{lung} differentiates the best the four categories of emphysema severity. The results of the statistical analysis are significant. It yields a *p-value* close to zero even for the normal – mild pair that is the hardest to differentiate using automated methods.

We can define a new emphysema severity-model as shown in table 7.4.

normal: if $BR_{lung} > -2.0$

mild: if $-2.0 \geq BR_{lung} > -6.0$

moderate: if $-6.0 \geq BR_{lung} > -16.0$

severe: if $BR_{lung} \leq -16.0$

Table 7.4: Emphysema severity model based on relative brightness.

The exceptions, as a rule, are due to the "scanning errors". For our low-dose CT-scan database, the BR index proved to be the best parameter in quantifying the severity of emphysema so far.

7.4.1.2 Emphysema Type Classification

Classifying emphysema by type is far trivial task. The medical literature distinguishes between four main types of emphysema:

- *centrilobular* will affect the center of the secondary pulmonary lobule
- *panlobular* affects the entire pulmonary lobule, producing diffuse destruction
- *paraseptal* or localized emphysema involves the distal portion of the lobule
- *paracicatricial* refers to lung destruction from adjacent pulmonary fibrosis

A pulmonary lobule can be considered the pathological and radiological unit of the lung tissue. The parenchyma of the lung is composed of secondary lobules so small that cannot be individually distinguished visually. Thus the emphysema type cannot be visualized or detected on CT-scans, solely based on the above definitions.

More over in many cases, as the disease progresses, different types of emphysema co-exist. There are cases that present centrilobular emphysema in upper areas of the lung, as well as panlobular emphysema in lower areas. As the severity of emphysema increases, patients may suffer from homogenously spread

disease throughout the entire lung volume. These cases cannot be classified as one specific type of emphysema.

Nonetheless, there exists some correlation between the disease type and the spatial distribution of the disease in the lung. In fact, radiologists utilize this correlation extensively during their visual assessments. Centrilobular emphysema, found predominantly in cigarette smokers, attacks the apical and posterior segments of the upper lobes; panlobular emphysema has usually lower lobe predominance, while the paraseptal type is present primarily in the lung periphery, adjacent to the visceral pleura and interlobular septa.

These spatial distribution properties are very useful in the automated assessment of the specific type of emphysema. The center of mass coordinates of the entire 3D low attenuation region provides spatial information about the areas in which emphysema are more preponderant. The formulae of these coordinates are given in section 7.3.1.3 as derivations from the computation of central moments. The most relevant coordinate will be the z_c coordinate which can relate to the upper, middle, or lower lobes of the lung.

We started with a database of fifty-three cases suffering from a different degree of emphysema (mild, moderate, severe).

For each case we gathered the following information:

z_{min}: the number of the first slice containing lung image

z_{max}: the number of the last slice containing lung image

z_c: the z coordinate of the center of mass of the emphysematous region

We define $z_c\%$ as:

(7.22)
$$z_c\% = \frac{z_c - z_{\min}}{z_{\max} - z_{\min}}$$

The metric $z_c\%$ measures how low, along the z-axis, the center of the mass is located inside the lung.

The CT-scan database has been partitioned into two sets: set_A (26 cases) and set_B (27 cases). Radiologists visually assessed the emphysema type first for set_A , then on set_B. In set_A, nine cases have been evaluated as *centrilobular*, one case as *pericicatricial*, one case as a co-existence of *centrilobular with panlobular* and fifteen cases have been classified as *indeterminate*. In the last category, for most of the cases, the low attenuation regions seem to be distributed relatively homogenously throughout the lung volume. Since the large majority of the cases with a determinate type are centrilobular, most of the analysis targeted this group.

Comparing the results of our computation with type assessments we observed that for the majority of the cases that have been classified as centrilobular type, the z-coordinate of the center of mass is located in the upper 25-35% of the lung.

However two cases, named C_1 and C_2, were an exception. Both cases have been classified as centrilobular, but $z_c\%$ value for C_1 was 56 and for C_2 was 66. We asked our radiologist to take a closer look at these two cases. After the second examination the radiologist pointed out in case C_1 artifacts due to metallic staples

embedded in the patient's lower lung parenchyma. These foreign objects generated elongated low attenuation areas. It is these areas that incorrectly influenced the value of z_c. The image of C_2 presented cardiac motion artifacts. These artifacts generated almost equally distanced semicircular darker shapes on the lung parenchyma adjacent to the heart in two of the slices. The presence of these artifacts makes us categorize the two mentioned cases as *anomalies*. Therefore, they have been eliminated from our statistical analysis.

As the next step we considered the cases of set_B. We picked eleven cases: seven cases with z_c in the *range of interest* (z_c% in 25 to 35 range) and four cases out of this range. We made the prediction that *if z_c is in the "range of interest" then the type of emphysema is centrilobular.*

For each selected case, we checked the emphysema-type evaluation done by the radiologist. Each case with z_c in the range of interest was already classified by the radiologist as centrilobular. Our predictions were correct in 100% of the picked cases in set_B.

Once we had the type classification completed for all the cases (set_A and set_B) we performed statistical analysis. A distribution of the cases by type done by the radiologists is shown in figure 7.7.

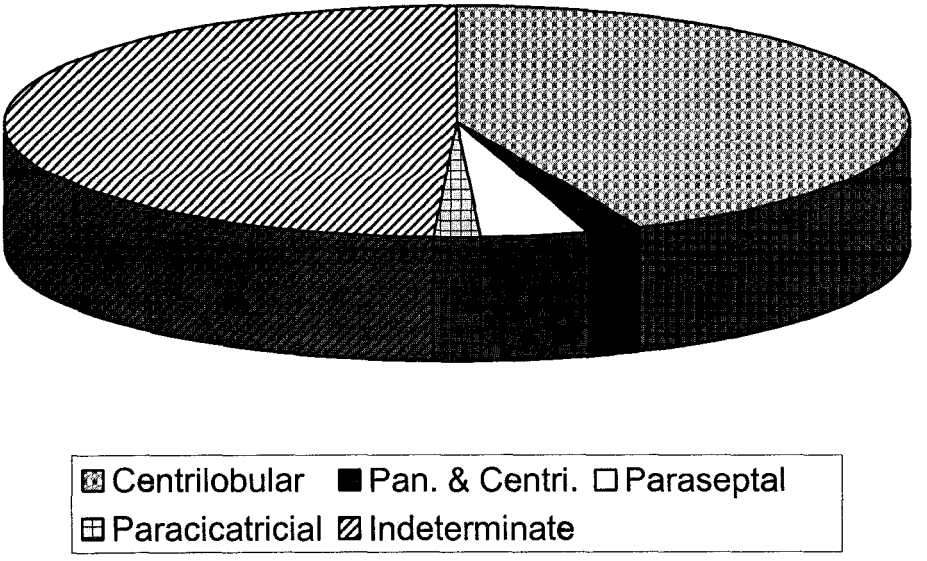

Figure 7.7: Distribution of cases by emphysema type.

The skewed distribution is an outcome of the images provenance. The Early Lung Cancer Action Project provides our database. One enrollment requirement is a heavy smoking history. Thus, many patients are expected to suffer from centrilobular emphysema. As the disease progresses it might develop panlobular components.

For the purpose of creating an emphysema type model we defined two main groups: *PositiveCentrilobular* and *NotPureCentrilobular*. The latter group includes all the indeterminate cases as well as the ones of different type or of coexisting emphysema types. The two anomaly cases have been excluded from our study. We ran an experiment to test if $z_c\%$ discriminates between different categories. The null hypothesis has been defined as:

(7.23) H_0: *mean* $z_c\%$ *PositiveCentrilobular =mean* $z_c\%$*NotPureCentrilobular*

The alternative hypothesis has been defined as:

(7.24) *H1: mean z_c% PositiveCentrilobular < mean z_c%NotPureCentrilobular*

meaning that in centrilobular type cases the center of mass is higher located in the lung compared to center of mass's location in cases that are not strictly centrilobular.

Table 7.5 displays the results of our statistical analysis.

Analysis / Category	N	mean zc%	st.dev. zc%	Stat. Sign.
PositiveCentrilobular	21	32.21	0.038	$p < 0.001$
NotPureCentrilobular	30	49.24	0.085	**YES**

Table 7.5: Statistical analysis on z_c% by categories of emphysema-type.

The statistical analysis shows that in terms of the location of the center of mass along the z-axis the two categories are significantly different ($p < 0.001$). In fact it appears that for pure centrilobular cases the z coordinate of the center of mass is located in the upper third of the lung and z_c% values are in the 25-35 range. The z_c% parameter can be considered a significant discriminator for detecting centrilobular emphysema.

The high correlation between z_c% values and location of the disease in the lung makes us believe that reliable results based on z_c% parameter can be obtained for detecting panlobular emphysema; it resides mostly in the lower half side of the lung. Unfortunately, during the time of our study we did not have the necessary data to test this hypothesis.

We also considered the possible utility of $y_c\%$ values, defined as:

(7.25) $$y_c\% = \frac{y_c - y_{\min}}{y_{\max} - y_{\min}}$$

It turns out that there are no significant differences in the value of $y_c\%$ between different types of emphysema. For the total number of cases the mean value of $y_c\%$ was 53.374+/- 7.757 (mean+/- std.dev). A distribution of $y_c\%$ on our database is pictured in figure 7.8.

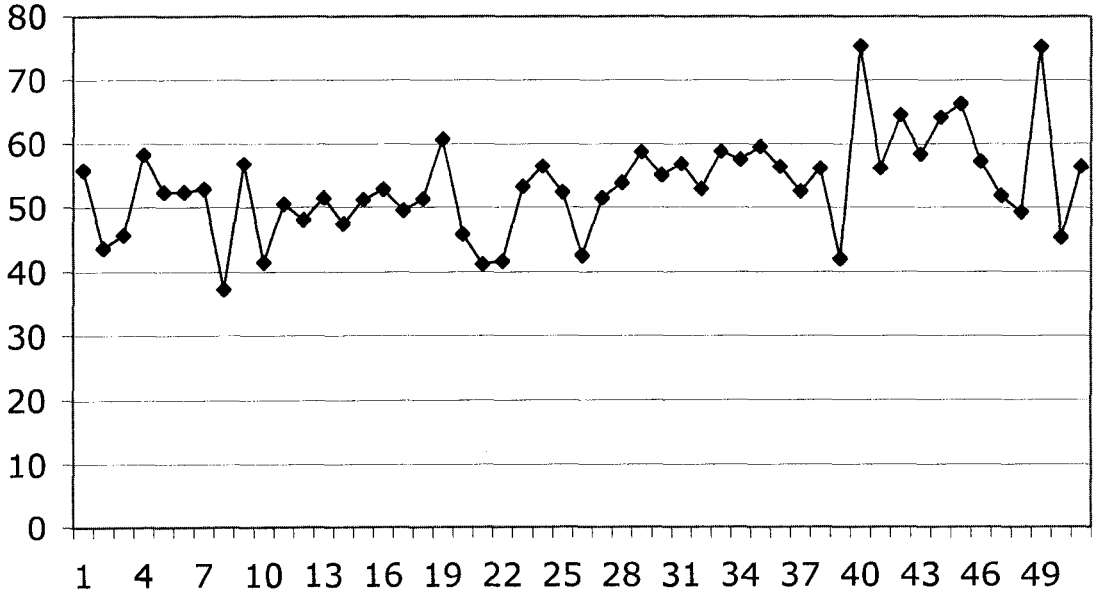

Figure 7.8: $y_c\%$ distribution in our low-dose CT scan images.

For most of the *Indeterminate* cases, the coordinates of the center of mass (y_c, z_c) are located in the middle of the lung. This implies a homogenous distribution of the disease across the entire lung volume. This fact also relates to

the findings described in section 6.2. Most of the graphical displays showed the emphysema homogenously distributed on the z-axis of the lung.

On the other hand, for types of emphysema that have a more concentrated spatial distribution, such as centrilobular or panlobular emphysema, the z_c% metric becomes a reliable parameter in describing an emphysema type model.

7.4.2 Analysis of 3D Connected Emphysematous Components

Since emphysema is a diffuse disease it might evenly destroy the lung parenchyma as it progresses. Most emphysematous areas do not show any visible margins or walls. Due to their irregular boundary and small size, many of the LAAs are hard to be identified separately. At first glance a view of the overall picture of the lung and its attenuation gives us a faster and more accurate understanding of the disease than the study of a particular small low attenuation region. Thus, our primary approach is to study pulmonary emphysema in a unified component.

However, it is important to know if information about distinctive components can assess the pulmonary disease. For future research it is also useful to know which descriptors are not significant in assessing emphysema and which ones are. This chapter presents work done in analyzing information provided by individual 3D emphysematous connected components.

7.4.2.1 The Average Size of Components: a Reliable Parameter

Chapter two presented research done in classifying emphysema based on the size of the emphysematous components. Sakai, et al[50], uses a four-point scale in defining the *severity* of emphysema as a function of the diameter of low attenuation regions (see table 2.2). Blechschmidt, et al[7], uses a combination of *severity* and *extent* (given by percentage of LAA) and classifies the disease into four categories: normal, suspicion of emphysema, emphysema, severe bullous emphysema (see table 2.3). In our study, *bullous* emphysema is not considered a main type of emphysema. The radiologist presented to us cases in which the size of the emphysematous area is above 5mm. He named these cases as *"emphysema cases with bullae changes"*; they are present in any of the severity groups of our database: mild, moderate and severe.

In our study we discussed quantification of emphysema based on the individual emphysematous component volume. We used as input the filtered segmented lung images of our screening database. For each case, using the automated information-gathering program (see section 7.3.4) we computed the size of each low attenuation 3D connected component. These components satisfied our "region of interest" criteria: their attenuation is lower than –950HU and their size (represented by the total number of voxels) are greater than 100 voxels. The rationale behind defining the region of interest is described in section 7.1.

For each case, the average component-size is defined as:

(7.26) $$comp\_S_{case} = \frac{\sum comp\_size}{n\_comps}$$

where

comp_size is the total number of voxels in a component

n_comps is number of components in a specific study case

We performed statistical analysis on the average component size by emphysema category. The results are shown in table 7.6.

Severity / comp_S	Normal	Mild	Moderate	Severe
N (cases)	15	28	15	17
mean	694.740	987.206	3389.638	10170.989
std.dev.	141.480	459.390	2601.873	3798.072

Table 7.6: Basic statistics on the average component size by category.

In order to test the accuracy of the *average component size* metric in classifying emphysema by severity, we performed an analysis of variance. We determined if difference between the average sizes of the components corresponding to different degrees of emphysema is statistically significant. The null hypothesis was defined as:

(7.27) H_{01}: *mean_compS_mild = mean_compS_normal*

H_{02}: *mean_compS_moderate = mean_compS_mild*

H_{03}: *mean_compS_severe = mean_compS_moderate*

where *mean_compS_category* represents the mean of the *average component size*$_{case}$ of the cases in *category*.

To determine if there is an increasing trend in the *mean component size* index with the increase of severity we defined the alternative hypothesis as:

(7.28) H_{01}: *mean_compS_mild* > *mean_compS_normal*

H_{02}: *mean_compS_moderate* > *mean_compS_mild*

H_{03}: *mean_compS_severe* > *mean_compS_moderate*

The results of the variance test are shown in table 7.7.

Categories / stat. results	Normal/Mild	Mild/Moderate	Moderate/Severe
z	4.210	4.559	5.449
p from z	< 0.00001	< 0.00001	< 0.00001
Stat. Sign.	**YES**	**YES**	**YES**

Table 7.7: Results in differentiating between severity degrees using average component size.

The statistical results indicate that the average component size very accurately differentiate between severity categories of emphysema (p <00001). Thus the average component size metric can be considered an accurate metric in quantifying emphysema.

As the disease develops, the individual components increase in size. As in the other severity quantifications performed, the gap between normal and mild

categories is the smallest one, compared to mild versus moderate and moderate versus severe. The statistics show that the average size grows with a ratio of 1.42 between mild and normal and with a more than double ratio for mild versus moderate or moderate versus severe, where the ratios are 3.43 and 3.00 respectively.

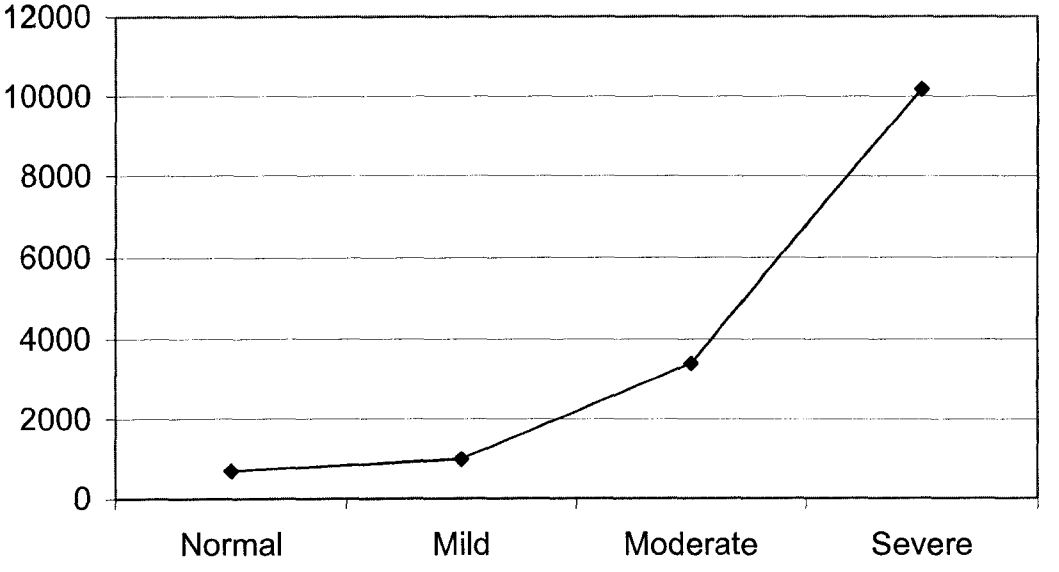

Figure 7.9: Severity of emphysema as a function of the average component size.

The average component size proves to be the metric that, compared to the emphysema index and the brightness index, differentiates the best between degrees of emphysema. The brightness index, as well as the average component size, provides statistical significance. However, the parameters that define these are very different. There are situations in which it might be easier to provide information about image attenuation than about individual component average size.

We can define an emphysema severity-model based on the average component size metric (table 7.8).

	Average component size
normal	695 +/- 142
mild	983 +/- 459
moderate	3390 +/- 2601
severe	10170 +/ 3798

Table 7.8: Emphysema case severity, based on average component size.

7.4.2.2 Additional Considerations

We have seen so far that there are spatial and densitometric parameters that can be used in classifying the degree of emphysema and even identifying special types of emphysema. Metrics, such as emphysema index (E), brightness of the image (B), coordinate of the center of mass (Z_c), and average component size (S) were able to differentiate between different emphysema categories with high statistical significance.

This section presents additional information we've obtained from our low dose lung CT scans. It is meant as a foundation for future research.

Number of Components by Severity of Emphysema

The first interesting parameter is the number of low attenuation connected components in each segmented lung image by emphysema category. A distribution of the number of components inside of each of the emphysema categories is shown in figure 7.10.

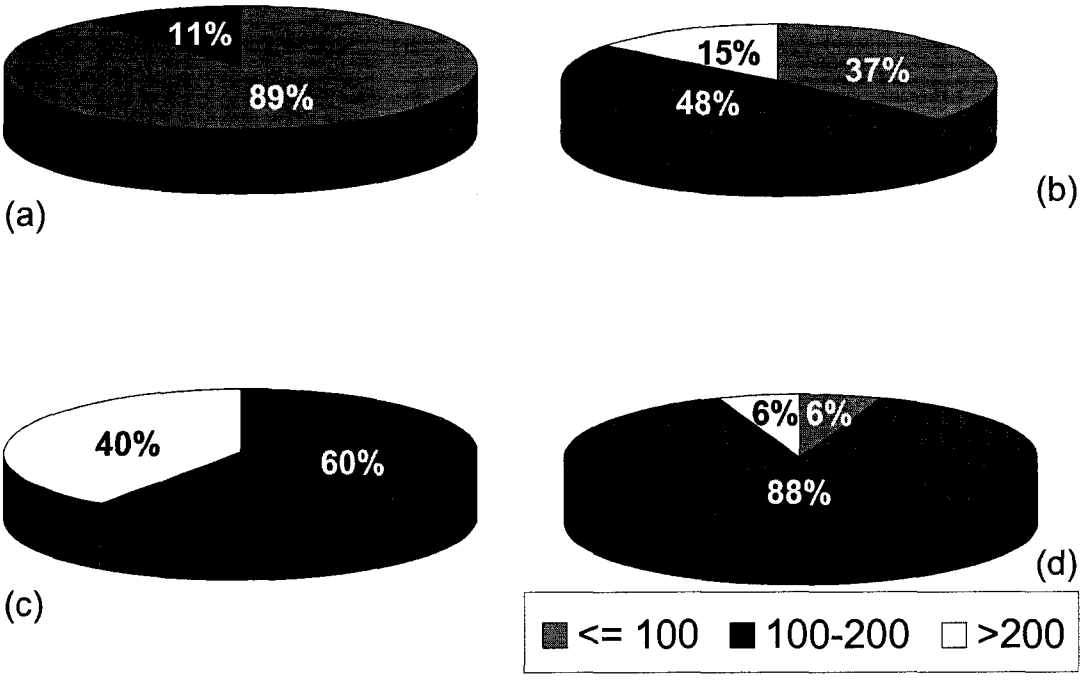

Figure 7.10: Distribution of number of components; normal *(a)*, mild *(b)*, moderate *(c)*, severe *(d)*.

Observe that even in normal cases still there are components in the low attenuation range. There appear to be a number of reasons for this: Some components might represent very small bronchi that merged into the lung. We stopped our airways segmentation when the size of the component was

approximately 30 pixels in 2D; over several slices, even the narrowest of airway may accumulate 100 pixels and thus be taken into consideration. Other components may be due to small motion artifacts or artifacts created by foreign objects in the body. Darker regions may be linked to other pulmonary diseases from which the patient might be suffering. The parenchymal tissue is not homogenous and there is no sharp boundary in intensity between what a healthy and emphysematous tissue is. Finally, variations from the real density of the tissue can be introduced by the partial volume effect. Despite that, our data set exhibited only two cases that exceeded 100 components. Both of these cases had less than 120 components each. With the increase of severity, there is an increasing trend of the percentage of cases with the number of components in the 100 to 200 range.

Figure 7.11 shows the average number of components for each of the categories.

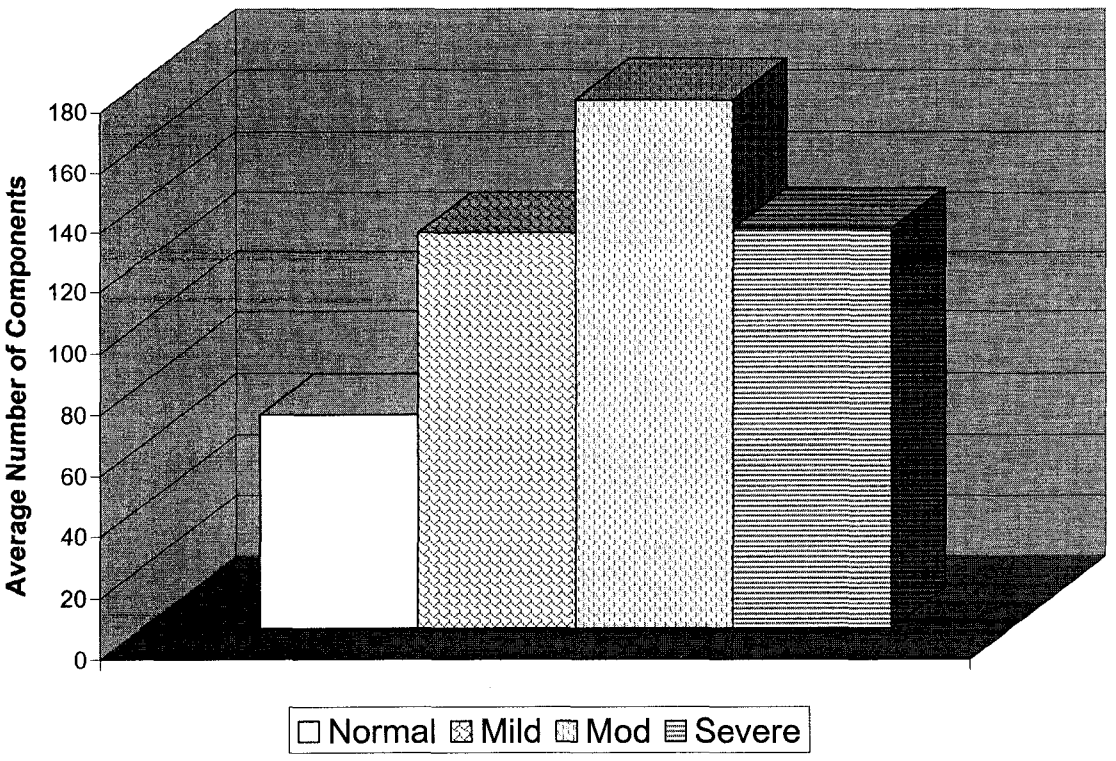

Figure 7.11: Average number of components for each category of severity.

It is interesting to note that the average number of components steadily increases from normal to mild to moderate, but then recedes when moving into the severe category. This can be attributed to the fact that in earlier stage of the disease close low attenuation regions grew to such an extent as to merge into one larger component. Once emphysema becomes extensive the number components radically decreases while the component size increase.

Right Lung vs. Left Lung

We wondered if the disease progresses differently in the right lung compared to the left lung. Reviewed medical literature doesn't describe emphysema in terms of which of the two lungs it resides.

For each case we analyzed the number of LAA components in the right lung versus the left lung. The average result, as seen in figure 7.12, shows that there is no significant difference between left and right or between any two severities.

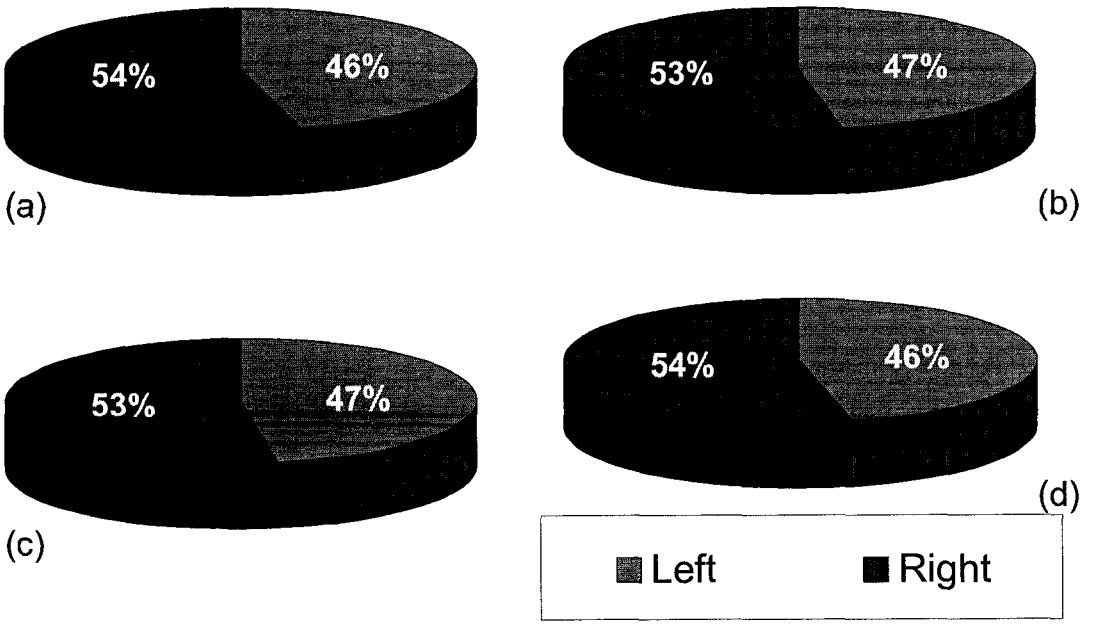

Figure 7.12: Comparative component count between left and right lungs for normal *(a)*, mild *(b)*, moderate *(c)*, severe *(d)* emphysema cases.

The number of components is slightly higher in the right lung than the left one reflecting the fact that the right lung is always larger than the left lung. This makes us believe that the disease destroys at an equal pace both lungs, at least for the type of cases in our database: centrilobular or uniformly distributed emphysema. There are exceptions, however. These can be found more often in paracicatricial caused by intra-pulmonary scars. In these cases, emphysema is localized around the scar.

8 CONCLUSION

Emphysema is a lung disease that affects millions of Americans. Until fairly recently its detection was done via visual assessments by thoracic radiologists and pulmonary functions tests. Over the past few years' automated computerized techniques have been introduced to aid in its diagnosis. These methods however, use high-dose CT scans. While these scans provide clear and accurate data, they expose patients to relatively high doses of x-ray radiation. In our work we show how the analysis can be done using *low-dose* screening scans. Such a system is quite desirable since they expose the patient to less radiation. Detection of the disease from a low-dose screening scan, done as a regular check-up, could result in an earlier emphysema detection and treatment.

Low-dose scans however are plagued by higher degree of noise; the quality of the image is much lower than that of a standard-dose clinical scan. Our work represents a significant step in overcoming this problem.

Our work focused on solving the following problems:

- Determine if existing quantification methods can be successfully used in detection and quantification of pulmonary emphysema from helical low-radiation CT scans. For rectifying the necessary low-dose lung images, this step included the development of an appropriate segmentation algorithm and filtering method.

- Develop better models for quantifying emphysema based on additional spatial and densitometric information.

8.1 Contributions

We now briefly review each of the major phases of our work.

8.1.1 Modular Segmentation Algorithm for Low-Dose CT-Scan Images

For the segmentation phase, a simple thresholding is not sufficient; emphysema has the same intensity as other parts of the lung, most notably the airways. Thus, we developed a fully-automated emphysema segmentation algorithm for low-dose images. The algorithm was modular, allowing for the removal of surrounding body tissue, vessels, and airways.

Through careful examination of a large case set we identified, enumerated and classified many morphological properties of lung airways. This was crucial in designing our algorithm and will be helpful to future work on airways segmentation. We adapted a number of computer-vision techniques to this realm. In the airways tracking process new developed techniques are burrowing, dynamic ancestor tracking, and airway split detection. The high level of noise increased the difficulty of the segmentation. It should be noted that the algorithm had not

altered the density information contained in the resulting segmented image; we specifically wanted to let the image to be filtered in a future phase of our work. Our segmentation algorithm was applied on a large database of CT-images. Its correctness has been validated by pulmonary radiologists for different noise-degree images.

Besides furthering the research presented in this paper, the segmentation algorithm can assist in efforts to classify other pulmonary diseases in the low-dose setting.

8.1.2 Sliding Window Method and Graphical Display

We studied whether automated computer analysis of low-dose CT scans based on two popular methods (four-slice and total volumetric method) could accurately estimate the degree of emphysema. These methods evaluate the disease through the computation of the emphysema index *E*. Generalizing these two methods, we created an umbrella method of evaluation based on a *sliding-window*. The new algorithm performs both the analysis and the graphical display of the emphysema as a function of the scan slice number.

The results showed promise in being able to quantify emphysema from low-dose images. This automated emphysema quantification is highly correlated with those obtained through visual assessments done by experienced pulmonary radiologists.

The *sliding-window* technique helps mitigate the signal-to-noise ratio (SNR) issues in the low-dose CT scans, particularly in upper region of the lung. This technique considers overlapping blocks of slices. We determined that examining five slices at a time gave us optimal information about emphysema index on the affected regions. Furthermore, the data produced from this technique can be easily represented as a graph of the emphysema index versus the location in the lung. Such depictions succinctly summarize the damage to the lung for radiologists. A better understanding of the emphysema spatial distribution can lead to the detection of various types of emphysema as well as characterize their degree.

8.1.3 Adaptive Filtering for Low-Dose CT-Scan Images

After the successful extraction of the lung's parenchyma, noise filtering was needed to clean up the data set and reconnect portions of contiguous emphysema regions that appear isolated due to noise. This was necessary for further study of densitometric and spatial properties of the emphysematous regions. The goal was to do this with the minimum loss of attenuation values.

Exploring our database allowed us to document that, in the context of low-dose scans, noise occurs mostly in the apices and posterior side of the lung. Knowing about noise concentration allowed us, to direct noise cleanup efforts on these regions. Our new spatial adaptive median filter satisfied our aforementioned goal.

8.1.4 Information Retrieval

With the clearer image in place, data collection was the next step. We developed software to calculate metrics, such as the area, volume, elongatedness, geometric moments and location. When dealing with location, a component associated with the right or left lung can then be referenced as a distance from the lung's center. Moreover, the component would be subsequently referenced as a distance from the center of the lung pair. Statistics were gathered on the emphysematous region both as a whole and broken up into individual 3D connected components.

8.1.5 Emphysema Models

After the data collection phase, we conducted analysis to correlate our metrics with severity and types of emphysema. We developed new metrics capable of better quantifying the severity of emphysema. Based on these new metrics we were also able to recognize cases with a special type of emphysema, centrilobular, and to differentiate between cases were pure centrilobular emphysema and cases that are not only centrilobular, and those of indeterminate type. Automated emphysema type identification had not been previously developed.

8.1.5.1 Brightness

A new parameter for the quantification of emphysema by severity has been introduced; the brightness index *B*. This parameter has proved to be superior to

the widely used parameter, the emphysema index *E*. Over the entire lung region, the brightness parameter does not require us to define a specific low attenuation range. This presents an advantage, since there is no common agreement as to what this range must be. Depending on the research goals, the upper limit might take various values. Severity quantification based on the brightness of a specific lung region showed high correlation with the assessments done by radiologists. A relative brightness index has also been introduced. It is based on the contrast between overall attenuation of the image and what is to be considered normal parenchyma (out of the emphysematous range). The newly introduced brightness metrics presented, provided for excellent differentiation between severity categories. These differences were more significant than those obtained using the emphysema index *E*. We proposed a new severity model based on the relative brightness index BR.

8.1.5.2 Emphysema Type Classification: the z_c Coordinate

Until now the type of emphysema has not been automatically determined. The coordinates of the center of mass of entire low attenuation region provides spatial information about the areas in which emphysema is concentrated. We defined a new parameter $z_c\%$ that can successfully differentiate between cases that are strictly centrilobular and the ones that are not. Our studies showed that for all centrilobular cases the z coordinate of the center of mass is in the upper 1/3 of the lung. For the other types it was not. In all fifty-three of the studied cases, the

range of z_c% could be narrowed even further: if z_c% values are in the 25-35 range then the disease is purely centrilobular. These results are indicative of the possibility of refining emphysema type classification for a larger number of categories, including panlobular.

8.1.5.3 Average Size of Emphysematous Component

We discussed quantification of emphysema based on the individual emphysematous component volume. As the disease progress the size of the emphysematous areas increases. The presence of large size (> 5mm) low attenuation areas, named bullae is not always a criterion in categorizing the severity of emphysema. In all our categories (mild, moderate and severe) the radiologist identified cases affected by *"emphysema with bullous changes"*. However, if there is an increase in the size of the majority of low attenuation regions throughout the entire lung volume, then the disease is more acute.

The new metric, the *component average size,* is a reliable index in classifying the severity of emphysema. Compared to other studied quantification methods, *component average size* index presented the highest statistical significance in differentiating between degrees of emphysema. We also suggested a severity model based on this parameter.

8.1.6 Other Findings

Additional studies were done on the relationship between the number of low attenuation components and the severity of the emphysema. Based on the number of components we arrange our cases in three groups: cases with less than 100 components, cases with a number of components between 100-200 and cases with more than 200 components. It should be noted that the percentage of cases with a number of components in the 100-200 range increases as the severity increases.

We compared the number of components in the left lung versus the right lung. There is no significant difference between left and right lung. The left lung always had slightly fewer components. This is explained by the fact that the left lung is always smaller than the right one.

8.2 Future Work

Research in the analysis of emphysema has just begun. The results of this work show promises for an accurate and early detection of pulmonary emphysema using a low dose CT scan.

New methods of analysis may be developed to help distinguish various types of emphysema. We would like to refine our type classification based on location of the center of mass as well as on the location of each component.

Additional cases in our database, cases affected by panlobular or paraseptal type, will give us the possibility to refine and continue our work in emphysema type classification.

The extensive experimentation yielded much more data then was needed for the current work. For example, a complete set of moments for each emphysematous component as well as for the entire emphysematous region, the coordinates of each component from the center of the lung and the center of each lung. This information will allow us to develop a 3D shape model of the emphysema.

For some of the patients we are collecting additional tests for the purpose of doing a longitudinal study to analyze what further trends may be discerned.

Many of the techniques that we developed can be also applied in the study of other pulmonary diseases. We are looking forward to extending our work in detection and quantification of pulmonary emphysema as well as extending the developed methods to other areas of biomedical research.

BIBLIOGRAPHY

Print Resources

[1] Arakawa, Akihiko, Yasuyuki Yamashitaa, Yoshiharu Nakayamaa, Masaki Kadotaa, Hirotsugu Korogib, Osamu Kawanob, Mitsuhiro Matsumotob and Mutsumasa Takahashia. "Assessment of lung volumes in pulmonary emphysema using multidetector helical CT: comparison with pulmonary function tests". Computerized Medical Imaging and Graphics, September 2001, pages 399-404.

[2] Archer, Derek C., C. L. Coblentz, R. A. deKemp, C. Nahmias and G. Norman. "Automated in Vivo Quantification of Emphysema". Radiology, Vol. 188, pp 835-838, 1993.

[3] Armato, S.G. III, M.L.Giger, K. Ashizawa and H. MacMahon. "Automated lung segmentation in digital lateral chest radiographs". Medical Physics, 25(8):1507 - 1520, August 1998.

[4] Baldi, Simonetta, Massimo Miniati, Calogero Riccardo Bellina, Luigi Battolla, Giosue Catapano, Enrico Begliomini, Davide Giustini and Carlo Giuntini. "Relationship between Extent of Pulmonary Emphysema by High-resolution Computed Tomography and Lung Elastic Recoil in Patients with Chronic Obstructive Pulmonary Disease". Am J Respir Crit Care Med Vol 164. pp 585-589, 2001.

[5] Bankier, Alexander, Viviane De Maertelaer, Caroline Keyzer and Pierre Alain Gevenois. "Pulmonary Emphysema: Subjective Visual Grading versus Objective Quantification with Macroscopic Morphometry and Thin-Section CT Densitometry". Radiology 1999. 211:851-858.

[6] Bankman, Isaak N.. *Handbook of Medical Imaging Processing and Analysis.* Academy Press, 2000.

[7] Blechschmidt, R. A., R. Werthschutzky and U. Lorcher. "Automated CT Image Evaluation of the Lung: A morphology-based concept" IEEE Transactions on Medical Imaging, Vol. 20, No. 5, May 2001.

[8] Brejl, M. and M. Sonka. "Object localization and border detection criteria design in edge-based image segmentation: automated learning from examples". IEEE:,Vol. 19, No, 10, Oct 2000: 973-985

[9] Brown, Matthew S., Michael F. McNitt-Gray, Lloyd E. Greaser, Amita Sapra, Kuo-Tung Li, James W. Sayre, Katherine Martin and Denise R. Aberle. "Knowledge-

based segmentation of thoracic computed tomography images for assessment of split lung function". Med. Phys. 27 (3), March 2000.

[10] ----------, Michael F. McNitt-Gray, Nicholas J. Mankovich, Jonathan G. Goldin, John Hiller, Laurence S. Wilson and Denise R. Aberle. "Method for Segmenting Chest CT Image Data Using an Anatomical Model: Preliminary Results". IEEE Transactions on Medical Imaging vol 16. No 6. December 1997

[11] Carvalho, B. M., Garduno, E., and Herman, G. T. "Multiseeded Fuzzy Segmentation on the Face Centered Cubic Grid".

[12] Chabat, F., Xiao-Peng Hu, D. M. Hansell and Guang-Zhong Yang. "ERS transform for the automated detection of bronchial abnormalities on CT of the lungs". Imperial Coll. of Sci., Technol. & Med., London, UK. Medical Imaging, IEEE Transactions on Volume 20, Issue 9, Sept. 2001, 942-952.

[13] Cleverley, Joanne R. MRCP, FRCR; Nestor L. Muller, MD, PhD. "Advances in Radiologic Assesment of Chronic Obstructive Pulmonary Disease Clinics". Chest Medicine, Vol. 21, Number 4, Dec 2000, pp. 653-663.

[14] ----------, Sujal R. Desai, Atholu. Wells, Hiroshi Koyama, Sian Eastick, Maria A. Schmidt, Clare L. Charrier, Peter D. Gatehouse, Peter Goldstraw, John R. Pepper. "Evaluation of Patients Undergoing Lung Volume Reduction Surgery: Ancillary Information Available from Computed Tomography". Clinical Radiology, Vol. 55, Issue 1, Jan. 2000, pp 45-50

[15] Coxson, Harvey O., Robert M. Rogers, Kenneth P. Whittall, Yulia D'Yachkova, Peter D. Pare, Frank C. Sciurba, James C. Hogg. "A Quantification of the Lung Surface Area in Emphysema Using Computed Tomography". Am J Respir Crit Care Med Vol 159, pp 851-856, 1999.

[16] Everhart, Jason, Michael Cannon, John Newell and David Lynch. "Image Segmentation Applied to CT Examination of Lymphangioleyomatosis (LAM)". PhD. Thesis.

[17] Gabor, Herman. *Image Reconstruction from Projections: The fundamentals of Computerized Tomography.* Elsevier Science & Technology Books, 1980.

[18] Gierada, David S., Roger Yusen, Thomas Pilgram, Lora Crouch, Richard M. Slone, Kyongtae T. Bae, Stephen S. Lefrak, Joel D. Cooper. "Repeatability of Quantitative CT Indexes of Emphysema in Patients Evaluated for Lungs Volume Reduction Surgery". Radiology 2001, 220: 448-454.

[19] Gonzales, R. C., R. E. Woods. *Digital Image Processing.* Addison-Wesley, 1992.

[20] Gould, G.A., W. Macnee, A. McLean, P.M. Warren, A. Redpath, J.J.K. Best, D. Lamb and D.C. Flenley. "CT Measurements of Lung Density in Life Can Quantitate Distal Airspace Enlargement -- An Essential Defining Feature of Human Emphysema". American Review of Respiratory Disease,1988; 137:380-392.

[21] Guenard, Herve, Mamadou Diallo, Francois Laurent and Jean Vergeret. "Lung Density and Lung Mass in Emphysema". Chest, Vol. 102, No. 1, pp. 198-203, 1992.

[22] Haralick, R. M., L. G. Shapiro. *Computer and Robot Vision.* Addison Wesley, 1992.

[23] ----------, S. R. Sternberg, X. Zhuang, "Image Analysis using mathematical morphology". IEEE Transactions on Pattern Analysis and Machine Intelligence, 4(9):532 -550, 1987.

[24] Hawa, Mamadou, Hann Diallo, Herve Guenard, Francois Laurent, Pierre Charles and Jacques Giron. "Distribution of Lung Density and Mass in Patients with Emphysema as Assessed by Quantitative Analysis of CT". Chest 2000, 118:1566-1575.

[25] Hayhurst, M. D., D. C. Flenley, A. McLean, A. J. Whigtman, and W. Macnee. Hedlund, Laurence W., R. Anderson, P. Goulding, J. Beck, E. Effman and C. Putman. "Two Methods for Isolating the Lung Area of a CT Scan for Density Information". Radiology, Vol. 144, pp. 353-357, July 1982.

[26] ----------, D. C. Flenley, A. McLean, A. J. Whigtman and W. Macnee. "Diagnosis of pulmonary emphysema by computerized tomography". Lancet 1984, 2:320-322. Am J Respir Crit Care Med Vol 161, pp 1264-1273, 2000.

[27] Hornak, Joseph P.. *Encyclopedia of Imaging Science and Technology.* 2 Volume Set, Wiley, 2002.

[28] Hounsfield, G. N. "Computed Medical Imaging: Nobel lecture, December 8, 1979". Journal of Computed Assisted Tomography, 4(5):665-674, October 1980.

[29] Hu, Shiying, Eric A. Hoffman and Joseph M. Reinhardt. "Automatic Lung Segmentation for Accurate Quantitation of Volumetric X-Ray CT Images". IEEE Transactions on Medical Imaging, Vol. 20, No. 6, June 2001.

[30] Jain, Ramesh, Rangachar Kasturi, Brian G. Schunck. *Machine Vision.* McGraw-Hill, Inc, 1995.

[31] Kalender, Willi A., Heinz Fichte, Werner Bautz and Martin Skalej. "Semiautomatic Evaluation Procedures for Quantitative CT of the Lungs". Journal of Computed Assisted Tomography, 15(2):248-255, March/April1991.

[32] ----------; Rainer Rienmuller, MD; Wolfgang Seissler; Jurgen Behr; Matthias Welke and Heinz Fichte. "Measurement of Pulmonary Parenchymal Attenuation: Use of Spirometric Gating with Quantitative CT". Radiology 1990:175, 265-268.

[33] Kemerink, Gerrit J., Rob J. S. Lamers, Bas J. Pellis, Han H. Kruize, J. M. A. van Engelshoven. "On segmentation of lung parenchyma on quantitative computed tomography of the lung". Med. Phys. 25 (12), December 1998.

[34] Kostis, William J., Simina C. Fluture, David F. Yankelevitz, Claudia I. Henschke. "Method for analysis and display of distribution of emphysema in CT scans". SPIE Conference on Image Processing, February 2003.

[35] ----------; Simina C. Fluture, Ali O. Farooqi, David F. Yankelevitz, Claudia I. Henschke. "Volumetric assessment of emphysema on low-dose screening CT scans". SPIE Conference on Image Processing, February 2003.

[36] Lei, T., W. Sewchand. "Statistical approach to X-ray CT imaging and its applications in image analysis -- Part 1: Statistical analysis of CT imaging". IEEE Trans. Med. Imag., Vol. 11, Feb. 1992, pp. 53-61.

[37] ----------. "Statistical approach to X-ray CT imaging and its applications in image analysis -- Part 2: A new stochastic model-based image segmentation technique for CT image". IEEE Trans. Med. Imag., Vol. 11, Feb. 1992, pp. 62-69.

[38] Luo, Jiebo and Chang Wen Chen. "Coherently three-dimensional wavelet-based approach to volumetric image compression". SPIE, Journal Of Electronic Imaging, Vol. 7, Issue 3, July 1998, pp. 474-485.

[39] Madsen, M.T., R. Uppaluri, E. A. Hoffman, G. McLennan. "Pulmonary CT image classification with evolutionary programming". Acad. Radiology, vol 6, no 12, pp 736-741, 1999.

[40] Mochizuki, Toshio, Hiroaki Nakajima, Fumio Kokubu, Tamio Kushishashi and Mitsuru Adachi. "Evaluation of Emphysema in Patients With Reversible Airway Obstruction Using High-Resolution CT". Chest 1997, 112:1522-26.

[41] Muller, Nestor, Catherine Staples, Roberta Miller and Raja Abboud. "Density Mask: An objective method to Quantitate Emphysema using Computed tomography". Chest 1988, 94:782-787.

[42] Nakano, Yasutaka, Shigeo Muro, Horoaki Sakai, Toyohiro Hirai, Kazuo Chin, Mitsuhiro Tsukino, Koichi Nishimura, Harumi Itoh, Peter D. Pare, James C. Hogg and Michiaki Mishima. "Computed Tomographic Measurements of Airway Dimensions and Emphysema in Smokers". Am J Respir Crit Care Med (www.atsjournals.org), Vol. 162, pp. 1102-1108, 2000.

[43] Park, Kyung J., Colleen J. Bergin, Jack Clausen. "Quantitation of Emphysema with Three-dimensional CT Densitometry: Comparison with Two-dimensional Analysis, Visual Emphysema Scores, and Pulmonary Function Test Results". Radiology 1999, 211:541-547

[44] Park, Wonkyu, Eric Hoffman, Milan Sonka, Matthew S. Brown, Michael F. McNitt-Gray, Nicholas J. Mankovich, Jonathan G. Goldin, John Hiller, Laurence S. Wilson and Denise R. Aberle. "Segmentation of Intrathoracic Airway Trees: a fuzzy logic approach". IEEE Transactions on Medical Imaging, Vol. 17, No. 4, August 1998.

[45] Reeves, A. P., R.J. Prokop, S.E.Andrews, and F. P.Kuhl. "Three-dimensional shape analysis using moments and Fourier descriptors". IEEE Transactions on Pattern Analysis and Machine Intelligence, 10(6):937-943, November 1988.

[46] Rogowitz, Bernice E., Thrasyvoulos N. Pappas, and Jan P. Allebach. Special Section on Human Vision and Electronic Imaging. SPIE, Journal of Electronic Imaging, Vol. 10, Issue 1, January 2001, pp. 8-9.

[47] ----------, Thrasyvoulos N. Pappas, and Jan P. Allebach. "Human vision and electronic imaging". SPIE, Journal of Electronic Imaging, vol 10, Issue 1, January 2001, pp. 10-19.

[48] Rosenblum, Lawrence, Richard Mauceri, David Wellenstein, "Density Patterns in the Normal Lung as Determined by Computed Tomography". Radiology, 137:409-416, November 1980.

[49] Sakai F., Fumikazu, Gordon Gamsu, Jung-Ji Im, Carolyn S. Ray. "Pulmonary Function Abnormalities in Patients with CT-Determined Emphysema". Journal of Computed Assisted Tomography, November/December 1987, 11(6):963-968.

[50] Sakai N., M. Mishima, K. Nishimura, H. Itoh and K. Kuno, "An automated method to assess the distribution of low attenuation areas on chest CT scans in chronic pulmonary emphysema patients," Chest, vol. 106, no 5, pp 1319-1325, 1994

[51] Salzman, Steve H.. "Can CT Measurements of Emphysema Severity Aid Patient Selection for LVRS?". Chest 2000, 118:1231-1232.

[52] Satoh, Katashi MD; Takuya Kobayashi, MD; Takahiko Misao, MD; Yoshimi Hitani, MD; Yuka Yamamoto, MD; Yoshihiro Nishiyama, MD and Motoomi Ohkawa, MD. "CT Assessment of Subtypes of Pulmonary Emphysema in Smokers". Chest 2001, 120:725-729.

[53] Shapiro, Steven D.. "Evolving Concepts in the Pathogenesis of Chronic Obstructive Pulmonary Disease". Clinics in Chest Medicine, Vol. 21, No. 4, pp. 621-630 December 2000.

[54] Soeijima, Kenzo, Kazuhiro Yamaguchi, Eiichi Kohda, Kei Takeshita, Yoko Ito, Hiroaki Mastubara, Tsuyoshi Oguma, Tkashi Inoue, Yasuyuki Okubo, Kazuhisa Amakawa, Hiroki Tateno and Tetsuya Shiomi. "Longitudinal Follow-up Study of Smoking-induced Lung Density Changes by High-resolution Computed Tomography". Am J Respir Crit Care Med Vol 161. pp 1264-1273, 2000

[55] Sonka, Milan, Vaclav Hlavac, Roger Boyle. *Image Processing, Analysis, and Machine Vision.* PWS Publishing, Second Edition, 1998.

[56] ----------, Wonkyu Park, and Eric A. Hoffman. "Rule-Based Detection of Intrathoracic Airway Trees". IEEE Transactions on Medical Imaging, Vol. 15, No. 3, June 1996.

[57] Uppaluri, Renuka, Eric A. Hoffman, Milan Sonka, Patrick G. Hartley, Garry W. Hunninghake and Geoffrey McLennan. "Computer Recognition of Regional Lung Disease Patterns". Am J Respir Crit Care Med Vol. 160, pp 648-654, 1999.

[58] ----------, Theophano Mitsa, Milan Sonka, Eric A. Hoffman and Geoffrey McLennan. "Quantification of Pulmonary Emphysema from Lung Computed Tomography Images". Am J Respir Crit Care Med 1997, 156:248-254.

[59] Van Belle, A. F., R. J. S. Lamers, G. P. M. Ten Velde and E. F. M. Wouters. "Diagnostic yield of computed tomography and densitometric measurements of the lung in thoracoscopically-defined idiopathic spontaneous pneumothorax". Respiratory Medicine, Vol. 95, Issue 4, April 2001, pp. 292-296.

[60] Wisser, Wilfried MD; Walter Klepetko, MD; Manfred Kontrus, MD; Alex Bankier, MD; Ömer Senbaklavaci, MD; Alexandra Kaider, MSc; Theo Wanke, MD; Edda Tschernko, MD and Ernst Wolner MD. "Morphologic Grading of the Emphysematous Lung and Its Relation to Improvement after Lung Volume Reduction Surgery". The Annals of Thoracic Surgery, Vol. 65, Issue 3, March 1998, pp. 793-799.

Web Resources

[61] http://www.britannica.com/nobel/micro

[62] "Lung Anatomy and Physiology", http://hcp.iressa.com/article/Article/11018.aspx, Last Accessed April 2004.

[63] Bock, Rudolf K., "Spherical Coordinates", http://rkb.home.cern.ch/rkb/AN16pp/node271.html#2, Last Accessed April 2004.

[64] "Amersham Health's Medcyclopaedia", http://www.amershamhealth.com/medcyclopaedia, Last Accessed April 2004.

[65] http://www.musc.edu/dc/icrebm/statisticalSignificance

[66] "P value calculator", http://www.graphpad.com/quickcalcs/Pvalue2.cfm, Last Accessed April 2004.

[67] "DICOM Homepage", http://medical.nema.org/dicom, Last Accessed April 2004.

[68] Reeves, A. P., "Computer Vision and Image Analysis Group: Cornell University", http://wonko.via.cornell.edu/visionx/, Last Accessed April 2004.